Substitution Effects and Electronic Structure Studies in Double Perovskites: How Crystal Structure Influences Physical Properties

Dissertation

zur Erlangung des Grades

„Doktor der Naturwissenschaften”

am Fachbereich Chemie, Pharmazie und Geowissenschaften

der Johannes Gutenberg-Universität Mainz

Haitao Gao

geboren in Hebei, China

Mainz, 2010

Contents

1 Introduction

Over the past half-century, the size of electronic components on silicon chips have been reduced dramatically along with more performance being packed into computers due to the booming development of semiconductor industry. The current technology runs into a bottle neck, because the further shrinkage of components size is hindered by fundamental physical laws. The recently emerged “spintronics” brings about a new perspective, as some predicted advantages of this new technology enables not only to break the deadlock but also to improve the speed of data processing, storage density and the energy consumption.

In contrast to conventional electronic devices requiring charge currents, spintronic devices demand spin currents.[1] Such devices should have faster switching times and lower power consumption, mainly because spins can be manipulated faster and at lower energy cost than charges. To understand what is meant by a spin current, consider an electron current that flows through a channel and contains only up-spin polarized electrons. Simultaneously, the movement of down-spin polarized electrons generates a similar current which flows in the opposite direction. This leads to a current of spins only, because there is no net particle transfer across any cross section of the channel (Figure 1.1).[2] The advantages of a spin current over a charge current consist in not only suppressing the ohmic resistivity due to no charges transported but also keeping the current invariant under time reversal. In other words, even if a clock ran backwards, the spin current would still keep flowing in the same direction.[3]

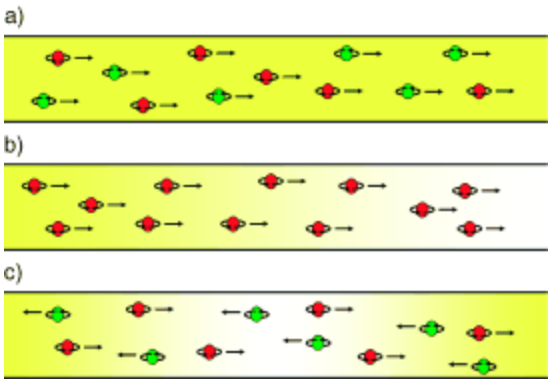

Figure 1.1 (a) regular charge current, (b) a spin and charge current, and (c) a pure spin current through a channel. The spin (red or green) and direction of movement of the electrons are indicated.[3]

Spin current requires new types of materials that are 100% spin-polarized. A half-metallic ferromagnet defined by de Groot *et al*. satisfies this requirement.[4] In half-metallic compounds, the valence band related to the electrons of one spin direction is fully filled and the other is partially filled with respect to the electrons of opposite spin direction (Figure 1.2). Therefore, only one type of electrons (either spin up or spin down) can pass through. This leads to a completely polarized current, which is related to the spin of electrons. In this sense, half-metallic ferromagnets make people associate them with magnetoresistance.

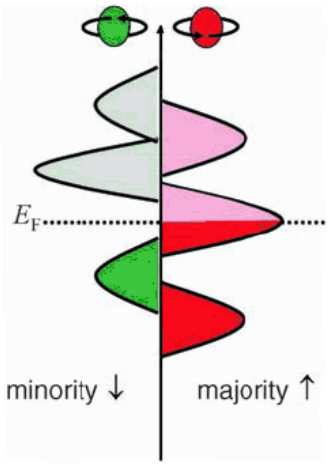

Figure 1.2 Schematic DOS curve for a half-metallic ferromagnet. In this case, the band gap occurs in the minority DOS (left).[3]

Magnetoresistance (MR) in general is the change of the electrical resistance upon application of a magnetic field. The effect was first discovered by William Thomson (more commonly known as Lord Kelvin) in 1856. It was later called ordinary magnetoresistance (OMR). In the experiment, Kelvin found out that MR was dependent on the angle between the direction of the electrical current and orientation of the magnetic field. The first MR effect was also known as "anisotropic magnetoresistance" (AMR).[5] However, Kelvin was unable to improve the electrical resistance of anything by more than 5%. Nevertheless, people applied the AMR effect for many years until 1980s, such as magnetic sensors and readout heads for magnetic hard disk.

A significant breakthrough to increase MR was the discovery of "giant magnetoresistance" (GMR) effect by Grünberg[6] and Fert.[7] GMR is ten times higher than AMR. The GMR effect was first observed in Fe/Cr multilayer systems.[7] The coupling of metallic ferromagnetic (Fe) layers across non-magnetic metallic (Cr) layers induces an antiferromagnetic coupling between

successive Fe layers. Depending on the thickness of Cr layers, the interlayer exchange coupling between the Fe layers changes from ferromagnetic to antiferromagnetic. As a result, the resistance of the whole system rests with the relative alignment of electron spins in different Fe layers to each other. As shown in Figure 1.3, without application of external magnetic field, the Fe layers are antiparallel arranged. The spin-oriented majority electrons of one Fe layer cross the Cr layer until they encounter a scattering center, where they would become minority electrons in the next Fe layer. When a magnetic field is applied, the resistivity drops dramatically, as the relative alignment of the magnetization in neighboring Fe layers switches from antiparallel to parallel. In this case, the electrons from one Fe layer with their initial spin orientation are able to enter the adjacent Fe layer, since their spin orientation is consistent with that of the adjacent Fe layer.

Figure 1.3 Scattering paths of electrons in simple GMR multilayers, FM1 and FM2 represents the two ferromagnetic layers. NM refers to the non-magnetic layer.[8]

Usually, MR is mathematically defined in literature as:

$\Delta R/R = (R_{\uparrow\uparrow} - R_{\uparrow\downarrow}) / R_{\uparrow\uparrow}$, where $R_{\uparrow\uparrow}$ and $R_{\uparrow\downarrow}$ are the resistance for antiparallel and parallel alignments of the magnetizations in two adjacent magnetic layers. The GMR of an Fe/Cr multilayer can reach 79% at 4 K and small fields, and is still 20% at room temperature.[7]

The record for GMR effect was not broken until the discovery of "colossal magnetoresistance" (CMR) by von Helmot[9] in 1993. He and his co-workers found that MR in manganese perovskite is by orders of magnitude, which is even larger than GMR by a few percent. The two end members (x = 0, 1) of $La_{1-x}Ca_xMnO_3$, are all antiferromagnetic insulators, however, when x = 0.2 – 0.4, the solid solution becomes metallic, mixed-valent (Mn^{3+}/Mn^{4+}), ferromagnetic, and exhibit a sharp drop in resistance. Later people found that this sharp drop in resistance was ascribed to a unique type of metal(low temperature) - insulator(high temperature) transition. Although CMR in the manganese perovskite is so impressive, CMR system remains still far from real applications

with respect to two crucial factors: sensitivity (MR in low fields) and the temperature dependence (small MR at room temperature).[3]

An insulating layer, commonly Al_2O_3, instead of a metal layer (such as Cr layer) between two Fe layers in GMR multilayered systems, was adopted to separate the ferromagnetic metal layers. This design to construct the high density "random access memory" (RAM) is able to read out information at low working current. This improvement is not given in GMR based RAM, as the metallic GMR devices exhibit a low absolute resistivity. If this sandwiched insulating layer is sufficiently thin (1 – 2 nm), electrons of the ferromagnetic metal layers can tunnel through the insulating layers. Therefore this effect is named tunnel magnetoresistance (TMR).[10] Likewise, tunneling probability and the current flow is determined by the relative orientation of the spins to each other in the magnetic layers. Due to the spin polarized band structure of the conduction band of the ferromagnetic metal layers, the spin direction of the conduction band depends on the external magnetic field. In Figure 1.4, when the magnetic layers have parallel spin alignment, the spin states at the Fermi level (E_F) are the same in both layers e.g. spin down. In this case, a spin down electron of the ferromagnetic layer 1 (FM1) can tunnel into the ferromagnetic layer 2 (FM2), as FM2 provides empty spin-down states at E_F. It is the other way round in case of antiparallel alignment, where the spin down electron of FM1 is hardly able to tunnel into FM2 since the FM2 spin down band is completely filled with electrons. Consequently, the TMR is related to the spin polarization of the two magnetic layers (P1 and P2). Quantitatively, the TMR effect ($\Delta R/R$) is expressed by:

$$\frac{\Delta R}{R} = \frac{P_1 P_2}{1 - P_1 P_2}$$

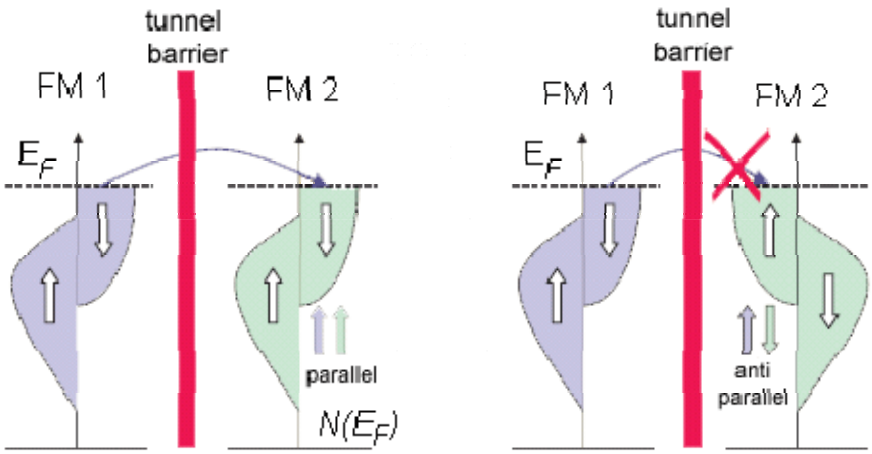

Figure 1.4 Scattering paths of electrons in simple GMR multilayers, FM1 and FM2 represents the two ferromagnetic layers. NM refers to the non-magnetic layer.[8]

The discovery of TMR enables faster non-volatile magnetic data storage devices with higher density. Significantly, this type of devices possesses easy distinguishability even at a low working current. However the main drawback of the TMR devices is still the multilayered structure, which is limited by the physical boundary conditions of the thin film technology. This problem may be overcome by another type of materials in possession of "powder magnetoresistance" effect (PMR). The PMR effect is a variant of TMR. In PMR point contacts are made between the powder grains of a half-metallic material. The PMR effect originates from the spin dependent tunneling of the charge carriers from one grain to the adjacent one across the grain boundary. Without magnetization, the magnetic orientation of the grains is random. Thus, electrons cannot tunnel through the boundary between grains, as the adjacent grains do not offer empty states at E_F, and the resistance is high. When sufficiently magnetized, the magnetic domains of the grains orient themselves along the direction of the field. In this case, spin direction of empty states near E_F is the same in every grain, and charge carriers have the opportunity to tunnel from one to the other. As a result, the resistance is decreased compared to the non-magnetized state. The PMR effect could be improved by introducing insulating particles into the grain boundaries of PMR materials. A famous experiment was to dilute ferromagnetic CrO_2 particles with insulating Cr_2O_3, where the MR effect was increased from 29% to 50% at 5 K (Figure. 1.5).[11, 12] Larger contact resistances between grains generally lead to a larger MR ratio in PMR materials.

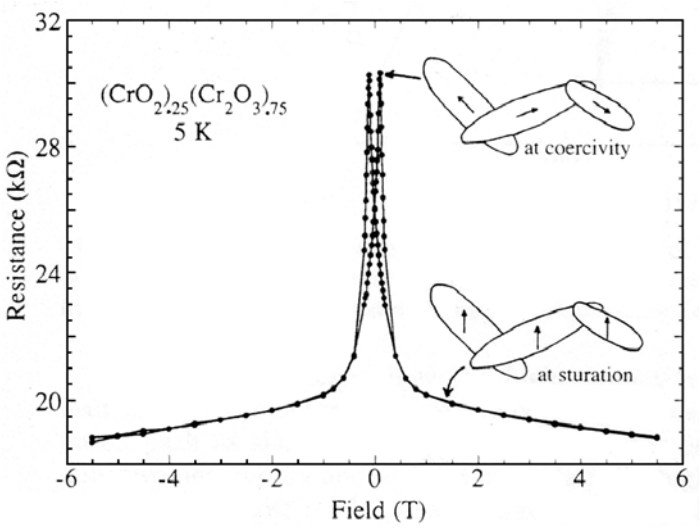

Figure 1.5 PMR effect at the example of $(CrO_2)_{0.25}(Cr_2O_3)_{0.75}$.[8, 11]

The PMR materials entail two factors at least: a spin polarized half-metallic band structure and a broad temperature range over which a ferromagnetic phase exists until at least two times above working temperature. In the PMR materials studied heretofore, the MR effect is strongly dependent on the temperature and the maximum of MR is far below the Curie temperature (Tc), usually several hundred K below.

Double perovskite compounds, Sr_2FeMoO_6, Sr_2FeReO_6 and Sr_2CrReO_6, after intensive studies, are considered to be the potential candidate.[13-16] The MR effect in these compounds at room temperature and low magnetic fields is technically attractive for spintronic application. In addition, the extreme flexibility of the perovskite structure with respect to symmetry as well as elements involved enables the substitution of almost every ion by a variety of candidates without the risk of a phase separation.[17-22]

Double perovskites have the general formula $A_2MM'X_6$, where A is a large electropositive ion, M and M' represents relatively smaller transition metal or main group metal and X is usually an oxide or a halide ion. Double perovskites have ideally a rock-salt configuration of MO_6 and $M'O_6$ octahedra between which the A cations are situated in the 12-coordinated voids, and the octahedra are connected by sharing a corner oxygen atom (Figure 1.6). The tolerance factor t is usually used to estimate their symmetries,[23] because structural distortions occur in many perovskites when the A and(or) M/M' atoms have not exactly the right size to fit the sites generated by the remainders of the structure. For perovskites (AMX_3), t is described as

$$t = \frac{r(A) + r(X)}{\sqrt{2}\left[r(M) + r(X)\right]}.$$

For double perovskites ($A_2MM'X_6$), t is altered to

$$t = \frac{r(A) + r(O)}{\sqrt{2}\left[\frac{r(M) + r(M')}{2} + r(O)\right]}.$$

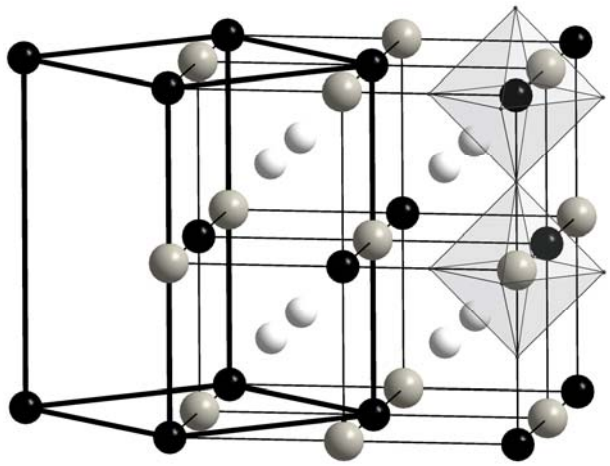

Figure 1.6 Crystal structure of the double perovskite $A_2MM'O_6$; M (black), M' (dark grey), A (light grey), and O (corners of the octahedra); the cubic unit cell is drawn in thin black lines, the tetragonal unit cell in thick black lines.

In practice, there is some flexibility and usually, a cubic perovskite forms with t in the range $0.9 < t < 1.0$.

For $t > 1$, the M/M' site is larger than required. If t is slightly larger than 1.0, the structure distorts but is still basically a perovskite; for the larger departures from $t = 1.0$, the M/M' ion demands a smaller site, of lower coordination number and the structure changes completely, as in $BaSiO_3$, which has tetrahedrally coordinated Si. The tolerance factor indicates a cubic symmetry when $0.89 \leq t \leq 1$, tetragonal or monoclinic distortion when $0.8 \leq t \leq 0.89$. When $t < 0.8$, an ilmenite structure is expected.

In the ideal double perovskites, the oxygen atoms are situated on the connection line of the M and M' cations. This situation requires a high symmetry, either cubic or partially tetragonal. The

continuously reduced symmetry (tetragonal or monoclinic) decreases the *M*–O–*M′* bond angle by tilting of MO_6 and $M'O_6$ octahedra. The oxygen atoms are not any more located on the direct connection line between *M* and *M′*. Actually, symmetry reduction and tilting of MO_6 and $M'O_6$ octahedra has a significant impact on the electronic interaction between *M*, *M′* and O orbitals along *M*–O–*M*–O–*M*.

In the double perovskite family, Sr_2FeMoO_6 was the first one found to display a large low-field MR effect at room temperature arising from its half-metallic nature.[13] Formally, Fe and Mo sites bear valence of +8. The high spin magnetic ion Fe^{3+} bears a magnetic moment of 5 μ_B. Due to the double exchange mechanism, Fe^{3+} induces on its neighboring Mo^{5+} ($4d^1$) a magnetic moment of -1 μ_B (minus representing an opposite spin to that of Fe^{3+}). In contrast to the ferromagnetic coupling of Mn in manganese perovskites, Fe^{3+} and Mo^{5+} couple antiferromagnetically to form a ferrimagnet. The antiferromagnetic coupling leads to an overall 4 μ_B/f.u. (f.u: formula unit) in Sr_2FeMoO_6. Sarma *et al*.[24] analyzed the unusual electronic structure of Sr_2FeMoO_6 (Figure 1.7) and found that in the absence of any hopping interaction, the Fe^{3+} has a larger exchange splitting compared to the crystal field splitting, while the situation is reversed for the Mo site; in the presence of hopping interactions, there is finite coupling between states of same symmetry at Fe and the Mo sites, leading to perturbations of the bare energy levels. The Mo $t_{2g}\uparrow$ state will be pushed up and the Mo $t_{2g}\downarrow$ state will drop further down due to hybridize with the corresponding Fe states. These opposite movements between these two states increase the energy separation between these two states, thereby substantially increasing the effective exchange splitting at the Mo site, which was usually expected Mo as a nonmagnetic nature in other surroundings.

As a consequence of the hopping interaction, the charge distribution between Fe and Mo is difficult to determine. The valence states of Fe are reported between 2+ and 3+, arising from the magnetic values $\mu_{Fe} = 4.1\ \mu_B \leftrightarrow \mu_{Mo} = 0\ \mu_B$ and $\mu_{Fe} = 4.6\ \mu_B \leftrightarrow \mu_{Mo} = -0.6\ \mu_B$.[25-29] Yet, any charge distribution between $Fe^{3+} \leftrightarrow Mo^{5+}$ and $Fe^{2+} \leftrightarrow Mo^{6+}$ gives rise to a theoretical saturation magnetization of 4 μ_B/f.u. Since Fe/Mo disorder leads to an antiferromagnetic alignment of the neighboring Fe atoms in a form of Fe–O–Fe, the saturation magnetization (Ms) is usually reduced up to Ms = 2.7 μ_B/f.u.[30-34] Additionally, the Curie temperature (Tc) is also reduced due to this disorder effect ($Tc(Sr_2FeMoO_6) = 420$ K).[33-35]

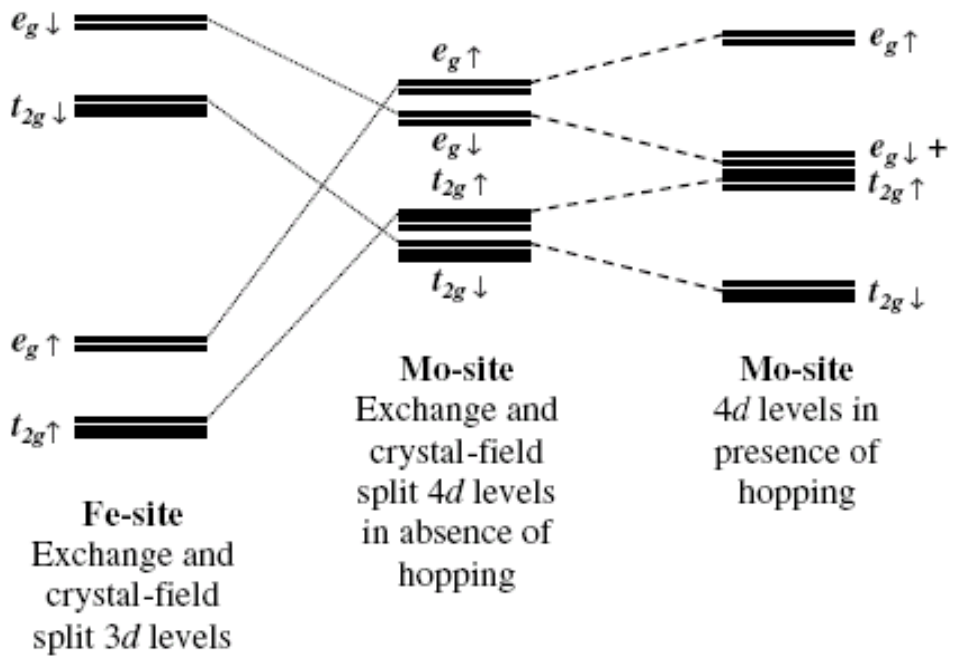

Figure 1.7 Energy level diagram expected at the Fe (left panel) and Mo (central panel) sites from an ionic picture. The energy level at Mo are modified in the presence of Fe–Mo hopping interactions as show in the right panel.[24]

With respect to crystallography, Sr_2FeMoO_6 is cubic ($Fm\bar{3}m$) above 400 K, and it is distorted to a tetragonal phase ($I4/m$) below 400 K.[25-27, 30-32] The perovskite tolerance factor predicts this structural phase transition pretty well and perovskites with $t = 0.899$ are expected to undergo such a transition. Due to similar ionic size of Fe^{3+} and Mo^{5+},[36] anti-site disorder Fe/Mo was found in this compound, which has a significant impact on structural, electrical, and magnetic properties on Sr_2FeMoO_6. Despite a reduced anti-site disorder under carefully controlled synthesis conditions, the disorder usually amounts to 30%.[33, 37, 38]

There is a diverse chemistry attempted to improve the MR effect in the parent compound of Sr_2FeMoO_6. Yuan *et al.* enhanced MR by reducing the grain size to 29–45 nm using a sol-gel synthesis method.[39] Niebieskikwiat *et al.* found the oxygen-induced boundary effects by oxygenation of the sample, thereby improving MR by more than two orders of magnitude.[30] The strategy of electron-doping has often been tested. Usually, electron-doping is achieved by replacing divalent cations with trivalent rare earth cations at the A site. This kind of doping was effective to increase Tc in $Sr_{2-}xLa_xFeMoO_6$ (Tc = 425 K and 490 K for x = 0 and x = 1

respectively).[40] The opposite effect has been observed in hole doped $Sr_{2-x}A'_xFeMoO_6$ (A′ = K or Na).[41, 42] The size of different alkali earth cations (Ca, Sr and Ba) has different steric effects. The phase diagram was established to show how the monotonic decrease of *M*–*M*′ distances strengthens the magnetic interaction and increase Tc in the $Sr_{2-x}Ba_xFeMoO_6$ series ($0 < x < 2$). The further reducing r_A leads to a continuous bending of the Fe–O–Mo angle due to the gradual symmetry reduction. The effect has a more significant impact on the magnetic interaction than the $d_{m(m')–O}$ decrease. In general, the overall Tc reduction takes place when $r_A < r_{Sr} = 1.44$ Å.[16] Among the alkali earth substitution, the highly ordered cubic solid solution $Ba_{1.6}Sr_{0.4}FeMoO_6$ was selected to preserve the symmetry while doping with La^{3+}. The symmetry and anti-site disorder remained indeed unchanged upon the doping.[43]

The second member of double perovskite family was Sr_2FeReO_6, which shows a large PMR effect at room temperature as well. Kobayashi *et al.* calculated for the first time the half-metallic property of this compound.[14] If the electronic structure of Sr_2FeMoO_6 and that of Sr_2FeReO_6 are put together for a comparison, one will find that both compounds have qualitatively equivalent configurations. The DOS of Sr_2FeReO_6 indicated that eight electrons from both Fe and Re sites are distributed within Re and Fe states. In spin up band, the Fe 3*d* states are filled with five electrons and the corresponding Re 5*d* states are empty (Figure 1.8). In contrast to the spin up band, the spin down band reveals a metallic nature. The hybridized Fe/Re band accommodates the rest two delocalized electrons. This arrangement is mediated by a Zener double exchange[44] along the –Fe–O–Re–O– line, forming an overall ferrimagnetic half-metal. Despite of difficulties to determine the valance state of Fe, NMR and Mössbauer spectra imply that the valance state of Fe is between 2.5+ and 3+.[28, 45, 46] The experimental magnetometry shows that Ms = 2.7 μ_B/f.u., which is in good agreement to the expected value deduced from the ferrimagnetic model.

For the series of A_2FeReO_6 (A = Ca, Sr and Ba), the wide range of r_A variation will, like its Mo-based analogue, simultaneously impact on lattice effects, magnetic and magneto-transport properties. From Ba to Ca, the ground state changes from a cubic system showing metallic behavior to a monoclinic compound showing insulating behavior, anomalously high Curie temperature, and huge coercivity.[47] The tolerance factor for Ba_2FeReO_6 is $t = 0.965$, predicting a cubic structure, consistent with the experimental results ($Fm\bar{3}m$, $c = 8.054$ Å).[45, 48] Hence, Fe–O–Re band angle is 180°. Because of the larger A cation, anti-site disorder in Ba_2FeReO_6 is reduced to 2%. The band structure of Ba_2FeReO_6 resembles that of Sr_2FeReO_6, a half metallic

ferrimagnet. The experimental transport properties and magnetic properties are in good agreement to the prediction: a metal nature, Ms = 3.04 μ_B/f.u. with a Curie temperature of Tc = 315 K, low compared to its other two sister compounds, (Tc(Ca_2FeReO_6) = 520 K). The low field MR was reported to be 3% at 10 K and 2 KOe.[45, 48-50]

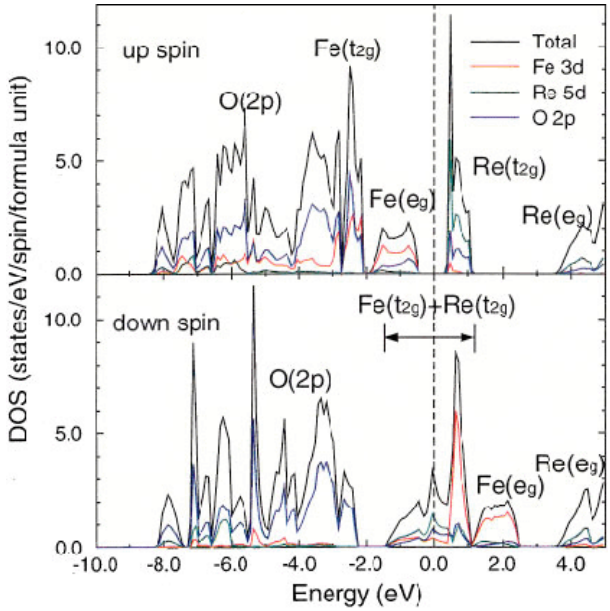

Figure 1.8 DOS of Sr_2FeReO_6.[14]

In contrast, Ca_2FeReO_6 represents an anomaly in the Re and Mo based double perovskite family. Ca_2FeReO_6, with a tolerance factor 0.842, is monoclinic. Above Tc (520 K), this material is monoclinic phase M1 with space group of $P2_1/n$. Below 300 K, it is comprised of two monoclinic phases M1 (90%) and M2 (10%). Below 150 K, the relative weight of these two phases changes dramatically, along with a formation of a new monoclinic phase (M1 ≈ 35%, M2 ≈ 60% and M3 ≈ 5%). The Fe–O–Re average angle is 156°. Despite the bending, the antiferromagnetic alignment between Fe and Re is preserved. However, the two itinerant spin down electrons in its sister compounds are localized at the Re sites in Ca_2FeReO_6. As a result, the valences of Fe and Re are 3+ and 5+ respectively. Another remarkable feature of Ca_2FeReO_6 is the metal-insulator transition around 100–150 K. Ca_2FeReO_6 is a metal at room temperature, and does not show an MR effect.[45, 48-52] The symmetry, lattice constants, and magnetism of $Ba_{2-x}Sr_xFeReO_6$ ($0 < x < 2$) as well as $Sr_{2-x}Ca_xFeReO_6$ ($0 < x < 2$) change linearly with the

substitution level. The lattice constants decreases from Ba^{2+} via Sr^{2+} to Ca^{2+} as expected from their ionic radii.[36] Due to the tilting of the FeO_6 and ReO_6 the shrinking of the lattices constants is much faster than that of the ionic radii. The gradual increase of Tc can be rationalized by thinking of the influence of the lattice parameters and MO_6 tilt angles on the electronic band. A reduced cation size causes a decrease of the Fe–O–Re bond length which increases the electronic band width and eventually Tc, so that in Ca_2FeReO_6 the reduction of the bond angle enables Re–Fe to interact. This additional effect plays an important role to enhance Tc. [15, 20, 47, 53, 54]

Like the chemistry of electron/hole-doping to improve the MR effect for Sr_2FeMoO_6, some of the doping experiments were performed at different sites in Sr_2FeReO_6, especially at Fe and Re sites. Kim *et al*. replaced Re partly with Fe ($Sr_2FeRe_{2/3}Fe_{1/3}O_6$), and found that stoichiometry forces the valence states of Fe and Re to be 3+ and 6+, and that the expected saturation magnetization is approximately 2.6 μ_B/f.u., which is not verified by the experimental results (Ms = 0.9 μ_B/f.u.). Upon doping, the metallic nature in the parent compound is preserved, and Tc is even increased to 475 K. Unfortunately the MR effect is decreased compared to the parent compound.[55]

When Re is substituted by W, the metallic nature of Sr_2FeReO_6 is bleached, and a magnetic transition was observed from ferrimagnetism to antiferromagnetism. This result is not surprising, because the end member of the substitution, Sr_2FeWO_6 is an antiferromagnetic insulator, in which adjacent Fe^{2+} ions couple antiferromagnetically through $W^{6+}(5d^0)$.[56]

Substitution of Re by a small amount (~0.1) of Nb and Ta causes a remarkable increase of the anti-site disorder even up to 25%. If the anti-site disorder is taken into account, the measured Ms could be rationalized by thinking of the normal antiferromagnetic arrangement of localized and itinerant electrons. Although the degree of disorder impacts on the magnetic and electronic properties in the doped materials, the small substitution by these ions does not greatly affect Tc.[57, 58]

Concerning substitution of Re by Mo, there is no investigation on Sr_2FeReO_6 reported yet, but a similar study was performed in Ba_2FeReO_6.[59] $Ba_2FeMo_{1-x}Re_xO_6$ ($0 < x < 1$) does not show any phase separation, and all the member of the solid solutions are cubic phases. The highest Tc appears at $x = 0.5$, but the saturation and saturation magnetization do not vary linearly with the substitution level. In addition, all members are semiconducting and the maximum of the MR

effect is just 1.34% at 70 KOe and low temperature. This result is certainly far from the practical application.

Jung *et al.* investigated the main group metal doping effect by using Sb to substitute Re. Due to the similar radii between Sb^{5+} and Re^{5+}, the role of 5*d* element Re in the parent compound could be well studied by gradually replacing it with the valence rigid metal. The solid solutions, $Ba_2FeRe_{1-x}Sb_xO_6$, undergo a magnetic transition upon Sb substitution from magnetic to antiferromagnetic. ^{57}Fe and ^{121}Sb Mössbauer spectroscopy confirms that Fe serves as the role of charge buffer. The doping by the main group metal blocks the super-exchange pathways Fe–O–Re(Sb)–O–Fe and destroys the itinerant magnetism of the parent compound.[60]

Besides the doping on the Re site, the doping on the Fe site is intensively investigated as well. Kato and co-workers performed a systematic study on Sr_2MReO_6 (*M* = Mg, Sc, Cr, Mn, Fe, Co, Ni and Zn). They found that Re in the ordered double perovskite is essentially penta-valent for *M* = Sc, Cr and Fe and hexa-valent for *M* = Mg, Mn, Co, Ni and Zn. Structurally, most of the Sr-based compounds have tetragonal symmetry except for some monoclinic compounds (*M* = Sc, Mn, and Zn). Ferromagnetic properties were observed for *M* = Cr, Mn, Fe and Ni, whereas, antiferromagnetic features were observed for *M* = Sc and Co compounds. Compounds containing Mg and Sc were considered spin-glass materials. Except for metallic Sr_2FeReO_6 and Sr_2FeReO_6, the other compounds are either semiconducting or insulating. They also pointed out the mixed valence nature of Re for *M* = Cr and Fe compounds by the bond-valence sum method. Sr_2CrReO_6 is found to be the highest Tc compound (635 K).[19]

Recently, Jung *et al.* investigated the doping effect on the Fe site respectively by Zn and Cr. In contrast to a electron model by Zn, a hole-doping by Cr was demonstrated to be valid in terms of both experiment and theoretical calculation, despite of a slight increase of the anti-site disorder due to this kind of doping.[61] Besides substitutions by transition metals, people also selected Ga, a main group metal with rigid valence, to perform substitution at the Fe site. The solid solutions, $Sr_2Fe_{1-x}Ga_xReO_6$, underwent phase separation (tetragonal/cubic) when $x \geq 0.4$, accompanied by a magnetically ordered and a paramagnetic phase detected by Mössbauer spectroscopy. A non-anticipated finding is that Ga not only occupied the Fe but also the Re site. The end member of the solid solutions, Sr_2GaReO_6, was theoretically predicted to be a half-metallic ferromagnet although this compound does not contain any magnetic 3*d* transition elements.[62]

In this PhD work, Sr_2FeReO_6 is selected as a parent compound. The work is divided into three main parts. The first part is about two chapters of solid solutions, $Sr_2FeRe_{1-x}M'_xO_6$ (M' = Ga/Fe, $0 \leq x \leq 0.5$). The second part presents two chapters of discussions on compounds derived from replacing Fe with In and Ga. The final part consists of two chapters of theoretical discussions dealing with some special double perovskite oxides. These insulating/semiconducting double perovskites are easily predicted as half metals without special treatment. A general approach is found to be useful to overcome the pitfalls for the band structure calculations of these "pseudo-half metals".

Reference

[1]I. Zutic, J. Fabian, S. Das Sarma, Rev. Mod. Phys. **76**, 323 (2004).

[2]P. Sharma, Science **307**, 531 (2005).

[3]C. F. Felser, G.; Balke,B., Angew. Chem., Int. Ed. Engl. **46**, 668 (2007).

[4]R. A. de Groot, F. M. Mueller, P. G. v. Engen, K. H. J. Buschow, Phys. Rev. Lett. **50**, 2024 (1983).

[5]W. Thomson, Proc. R. Soc. London Ser. A **8**, 546 (1857).

[6]G. Binasch, P. Grünberg, F. Saurenbach, W. Zinn, Phys. Rev. B **39**, 4828 (1989).

[7]M. N. Baibich, J. M. Broto, A. Fert, F. N. Van Dau, F. Petroff, P. Etienne, G. Creuzet, A. Friederich, J. Chazelas, Phys. Rev. Lett. **61**, 2472 (1988).

[8]J. Wecker, R. Kinder, R. Richter, PhiuZ **5**, 210 (2002).

[9]R. von Helmolt, J. Wecker, B. Holzapfel, L. Schultz, K. Samwer, Phys. Rev. Lett. **71**, 2331 (1993).

[10]J. S. Moodera, J. Nassar, G. Mathon, Annu. Rev. Mater. Sci. **29**, 381 (1999).

[11]J. M. D. Coey, T. Venkatesan, A. J. Millis, J. R. Cooper, P. C. Riedi, P. B. Littlewood, D. M. Edwards, J. Z. Sun, J. Inoue, Philos. Trans. R. Soc. Lond. A **356**, 1519 (1998).

[12]H. Y. Hwang, S. W. Cheong, Science **278**, 1607 (1997).

[13]K. I. Kobayashi, T. Kimura, H. Sawada, K. Terakura, Y. Tokura, Nature **395**, 677 (1998).

[14]K. I. Kobayashi, T. Kimura, Y. Tomioka, H. Sawada, K. Terakura, Y. Tokura, Phys. Rev. B **59**, 11159 (1999).

[15]H. Kato, T. Okuda, Y. Okimoto, Y. Tomioka, Y. Takenoya, A. Ohkubo, M. Kawasaki, Y. Tokura, Appl. Phys. Lett. **81**, 328 (2002).

[16]D. Serrate, J.Phys.:Condense.Matter **19**, 023201 (2007).

[17]A. W. Sleight, J. Longo, R. Ward, Inorg. Chem. **1**, 245 (1962).

[18]F. K. Patterson, C. W. Moeller, R. Ward, Inorg. Chem. **2**, 196 (1963).

[19]H. Kato, T. Okuda, Y. Okimoto, Y. Tomioka, K. Oikawa, T. Kamiyama, Y. Tokura, Phys. Rev. B **69**, 184412 (2004).

[20]H. Kato, T. Okuda, Y. Okimoto, Y. Tomioka, K. Oikawa, T. Kamiyama, Y. Tokura, Phys. Rev. B **65**, 144404 (2002).

[21]Y.-I. Kim, P. M. Woodward, J. Solid State Chem. **180**, 3224 (2007).

[22]D. Logvinovich, R. Aguiar, R. Robert, M. Trottmann, S. G. Ebbinghaus, A. Reller, A. Weidenkaff, J. Solid State Chem. **180**, 2649 (2007).

[23]A. West, *Basic Solid State Chemistry (Second Edition)* (JOHN WILEY & SONS, LTD, 1999).

[24]D. D. Sarma, P. Mahadevan, T. Saha-Dasgupta, S. Ray, A. Kumar, Phys. Rev. Lett. **85**, 2549 (2000).

[25]B. Garcia-Landa, C. Ritter, M. R. Ibarra, J. Blasco, P. A. Algarabel, R. Mahendiran, J. Garcia, Solid State Commun. **110**, 435 (1999).

[26]O. Chmaissem, R. Kruk, B. Dabrowski, D. E. Brown, X. Xiong, S. Kolesnik, J. D. Jorgensen, C. W. Kimball, Phys. Rev. B **62**, 14197 (2000).

[27]B. Fisher, K. B. Chashka, L. Patlagan, G. M. Reisner, J. Magn. Magn. Mater. **272-276**, 1790 (2004).

[28]C. C. Kapusta, D. Zajac, P. C. Riedi, M. Sikora, C. J. Oates, J. Blasco, M. R. Ibarra, J. Magn. Magn. Mater. **272-276**, E1619 (2004).

[29]M. S. Moreno, J. E. Gayone, M. Abbate, A. Caneiro, D. Niebieskikwiat, R. D. Sanchez, A. de Siervo, R. Landers, G. Zampieri, Solid State Commun. **120**, 161 (2001).

[30]D. Niebieskikwiat, A. Caneiro, R. D. Sánchez, J. Fontcuberta, Phys. Rev. B **64**, 180406 (2001).

[31]D. Niebieskikwiat, A. Caneiro, R. D. Sánchez, J. Fontcuberta, Physica B: Condensed Matter **320**, 107 (2002).

[32]K. Wang, Y. Sui, Physica B: Condensed Matter **344**, 423 (2004).

[33]D. Sánchez, M. García-Hernández, J. L. Martínez, J. A. Alonso, M. J. Martínez-Lope, M. T. Casais, A. Mellergård, J. Magn. Magn. Mater. **242-245**, 729 (2002).

[34]T.-Y. Cai, Z.-Y. Li, J. Phys.: Condens. Matter **16**, 3737 (2004).

[35]B. Martinez, J. Navarro, L. Balcells, J. Fontcuberta, J. Phys.: Condens. Matter **12**, 10515 (2000).

[36]R. Shannon, Acta Crystallographica Section A **32**, 751 (1976).

[37]A. Sharma, A. Berenov, J. Rager, W. Branford, Y. Bugoslavsky, L. F. Cohen, J. L. MacManus-Driscoll, Appl. Phys. Lett. **83**, 2384 (2003).

[38]D. D. Sarma, E. V. Sampathkumaran, S. Ray, R. Nagarajan, S. Majumdar, A. Kumar, G. Nalini, T. N. Guru Row, Solid State Commun. **114**, 465 (2000).

[39]C. L. Yuan, S. G. Wang, W. H. Song, T. Yu, J. M. Dai, S. L. Ye, Y. P. Sun, Appl. Phys. Lett. **75**, 3853 (1999).

[40]J. Navarro, C. Frontera, L. Balcells, B. Martínez, J. Fontcuberta, Phys. Rev. B **64**, 092411 (2001).

[41]K. Yoshida, Y. Fujii, H. Shimizu, J. Appl. Phys. **98**, 103901 (2005).

[42]G. Kim, S. S. Lee, S. C. Wi, J. S. Kang, S. W. Han, J. Y. Kim, B. W. Lee, J. Y. Kim, H. J. Shin, B. G. Parr, J. H. Park, B. I. Min, J. Appl. Phys. **99**, 08Q309 (2006).

[43]D. Serrate, J. M. De Teresa, J. Blasco, M. R. Ibarra, L. Morellon, C. Ritter, Appl. Phys. Lett. **80**, 4573 (2002).

[44]C. Zener, Phys. Rev. **82**, 403 (1951).

[45]J. Gopalakrishnan, A. Chattopadhyay, S. B. Ogale, T. Venkatesan, R. L. Greene, A. J. Millis, K. Ramesha, B. Hannoyer, G. Marest, Phys. Rev. B **62**, 9538 (2000).

[46]J. J. Blanco, T. Hernandez, L. M. Rodriguez-Martinez, M. Insausti, J. M. Barandiaran, J.-M. Greneche, T. Rojo, J. Mater. Chem. **11**, 253 (2001).

[47]J. M. D. Teresa, D. Serrate, J. Blasco, M. R. Ibarra, L. Morellon, Phys. Rev. B **69**, 144401 (2004).

[48]W. Prellier, V. Smolyaninova, A. Biswas, C. Galley, R. L. Greene, K. Ramesha, J. Gopalakrishnan, J. Phys.: Condens. Matter **12**, 965 (2000).

[49]N. Auth, G. Jakob, W. Westerburg, C. Ritter, I. Bonn, C. Felser, W. Tremel, J. Magn. Magn. Mater. **272-276**, E607 (2004).

[50]J. Herrero-Martin, G. Subias, J. Blasco, J. Garcia, M. C. Sanchez, J. Phys.: Condens. Matter **17**, 4963 (2005).

[51]W. Westerburg, O. Lang, C. Ritter, C. Felser, W. Tremel, G. Jakob, Solid State Commun. **122**, 201 (2002).

[52]E. Granado, Q. Huang, J. W. Lynn, J. Gopalakrishnan, R. L. Greene, K. Ramesha, Phys. Rev. B **66**, 064409 (2002).

[53]D. Serrate, J. M. De Teresa, P. A. Algarabel, C. Marquina, L. Morellon, J. Blasco, M. R. Ibarra, J. Magn. Magn. Mater. **290-291**, 843 (2005).

[54]T. Alamelu, U. V. Varadaraju, M. Venkatesan, A. P. Douvalis, J. M. D. Coey, J. Appl. Phys. **91**, 8909 (2002).

[55]T. H. Kim, M. Uehara, S. W. Cheong, S. Lee, Appl. Phys. Lett. **74**, 1737 (1999).

[56]A. Poddar, S. Das, Physica B: Condensed Matter **344**, 325 (2004).

[57]J. J. Blanco, M. Insausti, L. Lezama, J. P. Chapman, I. Gil de Muro, T. Rojo, J. Solid State Chem. **177**, 2749 (2004).

[58]T. H. Jose Julio Blanco, Lide M. Rodriguez-Martinez, Maite Insausti, Jose Manuel Barandiaran, Jean-Marc Greneche and Teofilo Rojo, J. Mater. Chem. **11**, 253 (2001).

[59]F. Sriti, N. Nguyen, C. Martin, A. Ducouret, B. Raveau, J. Magn. Magn. Mater. **250**, 123 (2002).

[60]A. Jung, V. Ksenofontov, S. Reiman, H. Therese, U. Kolb, C. Felser, W. Tremel, Phys. Rev. B **73**, 144414 (2006).

[61]A. Jung, I. Bonn, V. Ksenofontov, G. Melnyk, J. Ensling, C. Felser, W. Tremel, J. Mater. Chem. **15**, 1760 (2005).

[62]A. Jung, I. Bonn, V. Ksenofontov, M. Panthofer, S. Reiman, C. Felser, W. Tremel, Phys. Rev. B **75**, 184409 (2007).

2 $Sr_2FeRe_{1-x}Ga_xO_6$: How Cations Distributed over the *M* and *M´* Sites due to Substitution Effect

2.1 Introduction

The double perovskites Sr_2FeMoO_6[1] and Sr_2FeReO_6[2] reveal half-metallic ferrimagnetic behavior at room temperature, and have recently attracted much attention due to the discovery of tunnelling magnetoresistance (TMR). These two materials exhibit relatively high Curie temperatures (401 K and 415 K, respectively). The high Curie temperature is an important condition for a high degree of spin polarization at room temperature. In the idealized cubic modification (the elpasolite structure type), double perovskites have a general formula $A_2MM'O_6$ (A = alkali earth metal, M/M' = 3*d* transition metal). Double perovskites may be derived from a rock salt arrangement of corner-sharing of MO_6 and $M'O_6$ octahedra (Figure 1.6).

The Zener double exchange mechanism[3, 4] mediates the electron interaction along the axes of the cubic unit cell along the Fe–O–*M′* units via oxygen bridges, forming double exchange pathways Fe–O–*M′*–O–Fe. Thereby, the long-range interaction Fe–Fe and *M′*–*M′* is ferromagnetic, whereas the short-range interaction between Fe and *M′* atoms is antiferromagnetic. This leads to ferromagnetic, ferrimagnetic, or antiferromagnetic behaviour depending on the electron count of the participating elements.[5] Another interesting aspect of Fe–*M′* interactions is that when either Fe or *M′* is substituted by metals with invariant valence, the other one starts to take the part of redox-buffer upon alteration of the overall charge balance and magnetic property of the whole compound.[6-8] The solid solution $Sr_2Fe_{1-x}Ga_xReO_6$ reveals an interesting cation disorder effect. Ga was actually expected to substitute Fe due to its similar ionic size and charge. However the experimental finding was that the Fe substitution took place on the Re site as well. Since Ga appears to occupy the Re sites in $Sr_2Fe_{1-x}Ga_xReO_6$ as well, the following question arises: will the substitution of Re with Ga also lead to a pronounced cations disorder effect? Therefore, a series of samples of $Sr_2FeRe_{1-x}Ga_xO_6$ ($0 \leq x \leq 0.5$) were prepared and characterized with respect to X-ray diffraction refinement, magnetism, and Mössbauer spectra.

2.2 Experimental

Synthesis: Starting materials were reagent grade SrO (Aldrich, 99.9% purity), Fe_2O_3 (Alfa Aesar, 99.99% purity), Ga_2O_3 (Aldrich, 99.99% purity), Re metal, Re_2O_7 (Alfa Aesar, 99.9% purity). All starting materials were stored under Argon in a glovebox (Braun Labmaster) and were examined by X-ray powder diffraction prior to use. The solid solution samples were prepared by high temperature solid state reactions. Because of the strongly hygroscopic behavior of SrO and the high vapor pressure of Re_2O_7, the samples were prepared under inert gas atmosphere in a glove box. Stoichiometric amounts of starting materials were ground in an agate mortar and pressed into pellets. In order to avoid SrO from attacking the quartz tubes, these pellets were transferred into corundum containers and finally sealed in evacuated quartz glass ampoules. The samples for $x \leq 0.4$ were heated at 1273 K (1373 K for $x = 0.5$) for seven days. The quartz ampoules were rapidly cooled to room temperature by quenching in ice bath.

Characterizations: X-ray powder diffraction measurement was performed using a Siemens D5000 with monochromatized Cu$K_{\alpha 1}$ radiation [Ge(220) monochromator] and a Braun M50 PSD. Lattice constants (relative to Si, which was used as internal standard) were obtained by Rietveld refinements applying the fundamental parameter approach (TOPAS Academic).[9]

The variable-temperature magnetic susceptibility measurement of $Sr_2FeRe_{1-x}Ga_xO_6$ was carried out using a Quantum Design MPMS-XL superconducting quantum interference device (SQUID) magnetometer, equipped with a high-temperature furnace.

Mössbauer spectroscopy measurement of powder samples was performed in transmission geometry using a constant-acceleration spectrometer. ^{57}Fe Mössbauer spectra were recorded at room temperature using a 50mCi ^{57}Co(Rh) source. The RECOIL 1.03 Mössbauer Analysis Software was used to fit the experimental spectra [10]. Isomer shift values are quoted relative to α-Fe at 295 K.

2.3 Results and discussion

2.3.1 Structural characterization

The crystal structures of $Sr_2FeRe_{1-x}Ga_xO_6$ were analyzed by X-ray powder diffraction and Rietveld refinements. The Sr_2CuWO_6 structure type (space group *I*4/*m*) was explored to perform

the Rietveld refinements. The corresponding X-ray diffraction patterns are presented in Figure 2.1. The intensities of the (101) and (002) reflection are decreasing as a function of the Ga content. In analogy to the Sr_2FeMoO_6,[11] these two reflections imply the feature of Fe/Re disorder in parent compound Sr_2FeReO_6. The x = 0.5 sample contain some impurities. These impurities are just of slight amount (less than 5%), and they are analyzed to be $SrFe_{12}O_{19}$, ReO_3, and Ga_2O_3.

Table 2.1 Lattice parameters obtained based on tetragonal structure model in space group of *I*4/*m*.

Parameters	**0**	**0.1**	**0.2**	**0.3**	**0.4**	**0.5**
a/Å	*5.56741(8)*	*5.5622 (1)*	*5.5605(2)*	*5.5656(2)*	*5.5740(3)*	*5.56641(8)*
c/Å	*7.9010(2)*	*7.8931(2)*	*7.8871(4)*	*7.8911(3)*	*7.8992(5)*	*7.8858(2)*
(a/c)²	*2.01855(7)*	*2.0119(2)*	*2.0119(2)*	*2.0119(2)*	*2.0119(2)*	*2.0069(1)*
M(Fe)	*0.9742(8)*	*0.812(2)*	*0.804(3)*	*0.553(3)*	*0.665(5)*	*0.613(3)*
M(Re)	*0.0257(2)*	*0.078(1)*	*0.135(9)*	*0.1425(9)*	*0.284(2)*	*0.245(1)*
M(Ga)	*0*	*0.106(1)*	*0.061(2)*	*0.3011(2)*	*0.053(4)*	*0.141(3)*
M'(Fe)	*0*	*0.145(2)*	*0.196(3)*	*0.347(3)*	*0.055(5)*	*0.381(3)*
M'(Re)	*1*	*0.874(3)*	*0.803(1)*	*0.6537(9)*	*0.600(2)*	*0.258(1)*
M'(Ga)		*0.000(1)*	*0.000(3)*	*0.000(9)*	*0.347(4)*	*0.358(3)*
d(M–O1)/Å	*2.06(1)*	*2.05(1)*	*1.87(2)*	*1.841(2)*	*2.070(4)*	
d(M–O2)/Å	*2.08(1)*	*1.99(7)*	*2.07(1)*	*2.075(1)*	*2.677(6)* *2.900(6)*	
d(M'–O1)/Å	*1.87(1)*	*1.90(1)*	*2.07(2)*	*2.104(2)*	*1.880(4)*	
d(M'–O2)/Å	*1.90(1)*	*1.97(7)*	*1.88(1)*	*1.890(1)*	*2.699(8)* *2.879(8)*	

Structural data obtained from the refinements based on a tetragonal model are listed in Table 2.1, and cation distribution is displayed in Figure 2.2. In the parent compound, Sr_2FeReO_6, Fe and Re occupy the *M* and *M′* sites in an ordered fashion. Upon substitution, Fe and Re start to be statistically distributed on the *M* and *M′* sites. Ga initially prefers to occupy the *M* site at low substitution level. With increasing substitution, Ga starts to occupy the *M′* site above x = 0.4. Although Ga is distributed preferably at the *M* site at a low level of substitution, Ga is forced to enter the *M′* sites above x = 0.4 due to the inter-charge repulsion pressure. The cationic radius of Ga^{3+} (62 pm) is intermediate between that of Fe^{3+} (64.5 pm) and that of Re^{5+} (58 pm). Therefore, Ga^{3+} might act as a "bridge" cation, which catalytically causes a disorder between Fe/Re, eventually leading to a statistic distribution of Fe and Re on the *M* and *M′* sites.

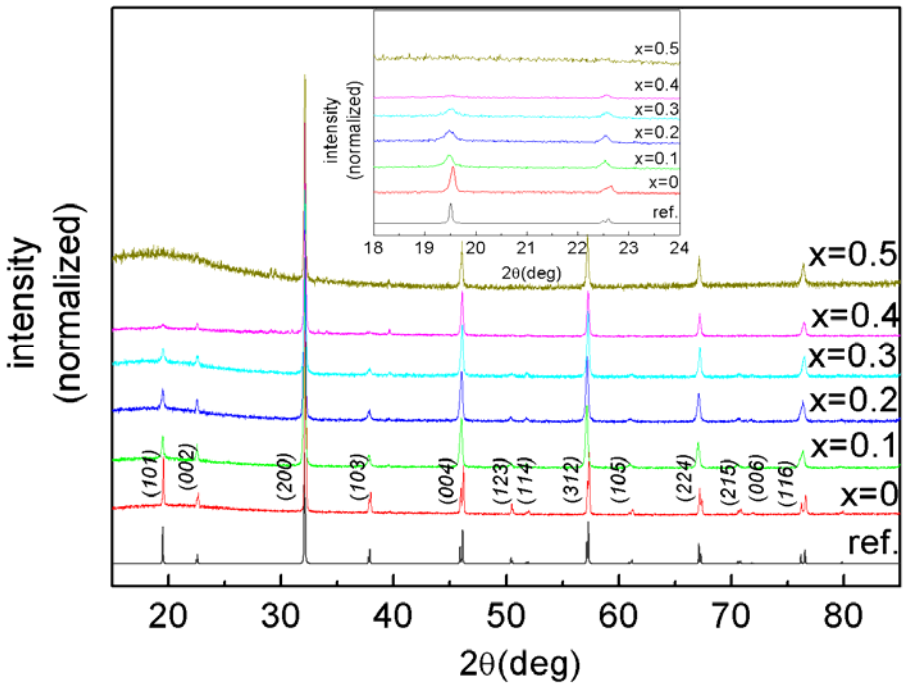

Figure 2.1 X-ray diffraction patterns of $Sr_2FeRe_{1-x}Ga_xO_6$; "reference" is Sr_2FeReO_6 (*I*4/*m*, fully ordered).[2]

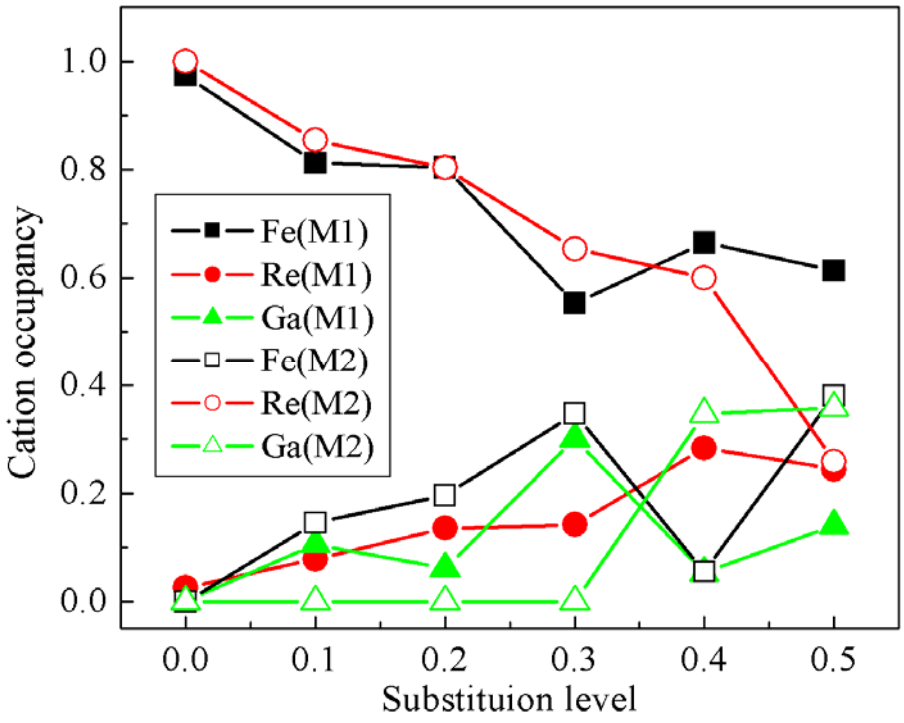

Figure 2.2 Cation distribution in $Sr_2Fe_{1-x}Ga_xReO_6$ versus substitution level x. M1 corresponds to *M* site and M2 corresponds to *M′* site.

2.3.2 Magnetic measurement

The field dependence of the magnetization at 5 K was measured in order to determine the saturation magnetization of the samples. Figure 2.3 indicates that the saturation magnetization is decreased with the Ga content increasing. The x = 0.5 sample finally exhibits nearly linear dependence on the applied magnetic field, indicative of either a paramagnetic or an antiferromagnetic behavior. Based on the hysteresis loops with small coercive fields, the parent compound Sr_2FeReO_6 can be classified as soft magnetic. Upon increasing the Ga content, the hysteresis loop is widened and the coercive field becomes larger. However, the overall area of the hysteresis loop is generally decreased due to the lower "saturation magnetization", until the hysteresis loop is almost closed for $Sr_2FeRe_{0.5}Ga_{0.5}O_6$. The sharp decrease of the saturation magnetization for the x = 0.1 sample compared to the parent compound is remarkable. The impurities in the x = 0.5 sample are less than 5%. The impurities were found to be non-ferromagnetic. Therefore, one can consider that there are no magnetic contributions of these impurities.

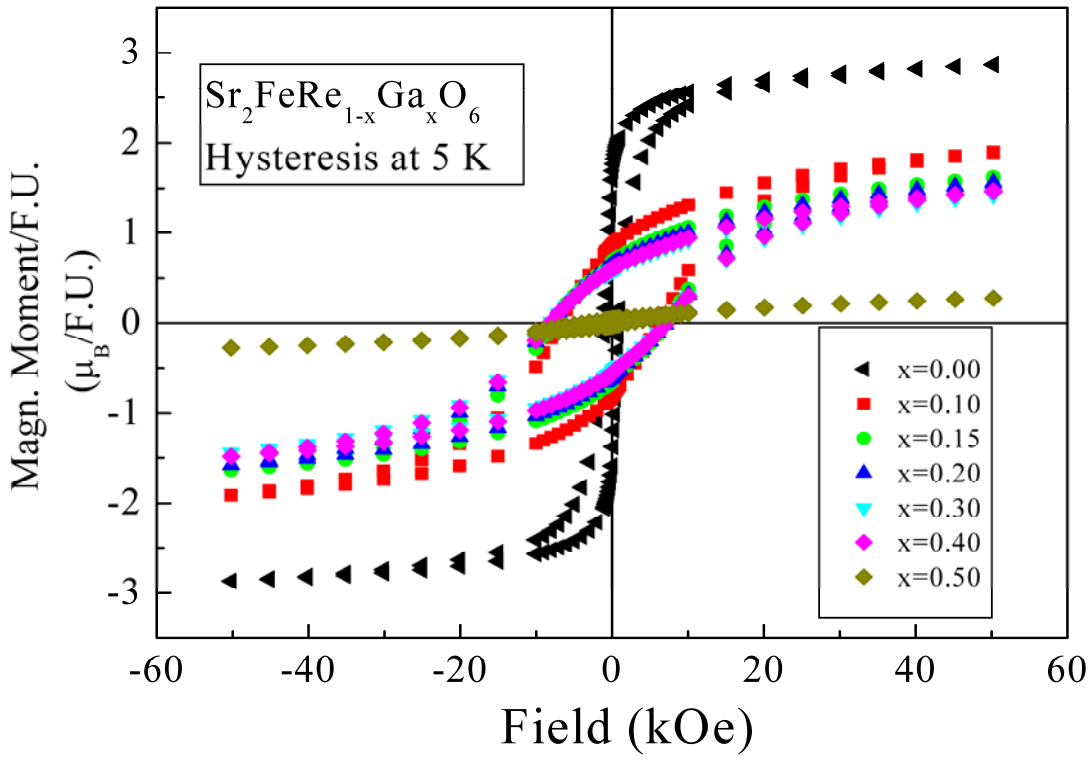

Figure 2.3 Magnetic hysteresis loops of $Sr_2FeRe_{1-x}Ga_xO_6$ measured at 5 K.

Susceptibility versus temperature data are shown in Figure 2.4. The parent compound has a Curie temperature (T_c) around 401 K, which is nearly the same to the one reported (see above). With increasing Ga content, the Curie temperatures are lowered but still above room temperatures until x = 0.4. When the Ga substitution increases to x = 0.5, the susceptibility exhibits an *S*-like shape, indicating an antiferromagnetic type of ordering in this material. The similar phenomenon was also observed in $Sr_2FeRe_{1-x}Sb_xO_6$ for x = 0.6[7] and in $Sr_2FeRe_{1-x}Fe_xO_6$ for x = 0.3 and x = 0.4.[12] The antiferromagnetic ordering at x = 0.5, may be attributed to the formation of Fe–O–Fe–O–Fe clusters, where Fe ions are coupling antiferromagnetically. On the other hand, Fe–O–Ga/Re(d^0)–O–Fe can also give rise to long-range Fe–Fe antiferromagnetic ordering.[13]

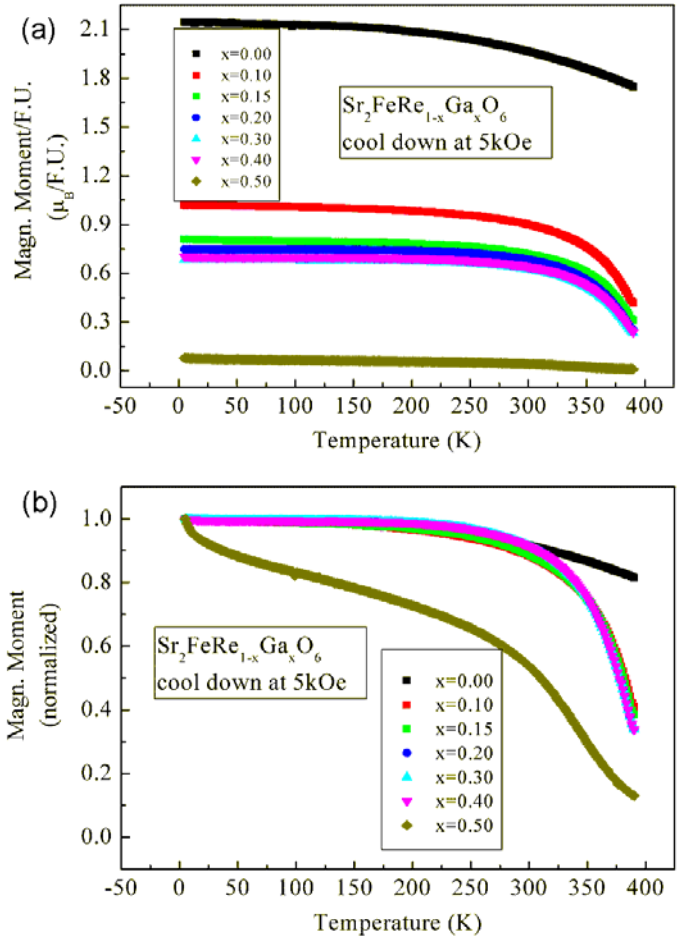

Figure 2.4 Magnetic susceptibility of $Sr_2FeRe_{1-x}Ga_xO_6$ versus temperature cooled down at 5000 Oe: (a) non-normalized, (b) normalized.

2.3.3 Mössbauer spectroscopy

^{57}Fe Mössbauer experiments give deeper insight into chemical composition and the magnetic structure of $Sr_2FeRe_{1-x}Ga_xO_6$. Figure 2.5 shows the room temperature spectra of the measured samples. The parameters from the data evaluation are summarized in Table 2.2. All spectra exhibit mainly magnetic hyperfine patterns in addition to weak paramagnetic signals. The 6-line patterns are typical for magnetically ordered materials. A minor paramagnetic quadrupole doublet even for Sr_2FeReO_6 was observed also in previous preparations of this compound[6] and may be associated either with an impurity phase or a certain Fe/Re anti-site disorder. The latter is obvious from the presence of two hyperfine sextets in Sr_2FeReO_6 differing in their isomer shifts as well as in their internal magnetic field strengths. The sharp 6-line pattern of the majority component with IS = 0.58 mm/s and H_{hf} = 336.0 KOe (84.2%) is due to the well ordered Sr_2FeReO_6 phase, the crystal structure of which is characterized by only one Fe site with six Re neighbors. The minor component with IS = 0.51 mm/s and H_{hf} = 380.8 KOe, (10.8%) corresponds to Fe sites with distorted coordination geometry. These results are consistent with the structural refinement. The isomer shift value of 0.58 mm/s for Sr_2FeReO_6 in the previous work was attributed to an Fe charge state of +2.7.[6] A decrease in the isomer shift with a concomitant increase in hyperfine field points to an increase in the charge state. The Fe/Re disorder disturbs the charge transfer from the t_{2g} minority spin states of Re into those of Fe which explains the reduced IS value for the second component.

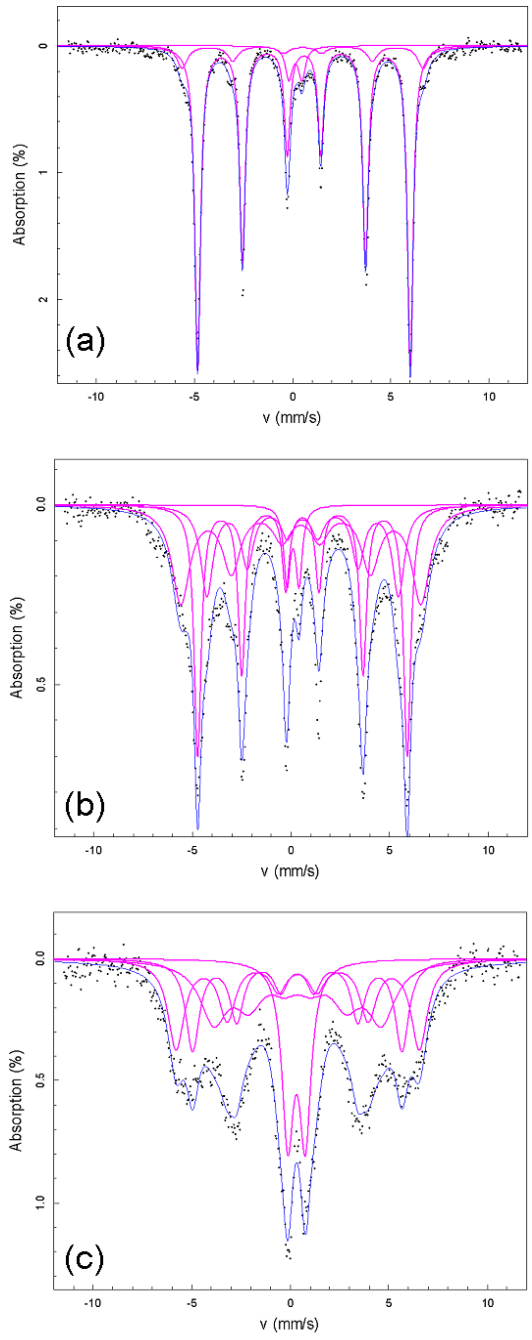

Figure 2.5 ^{57}Fe Mössbauer spectroscopy at room temperature of (a) Sr_2FeReO_6, (b) $Sr_2FeRe_{0.9}Ga_{0.1}O_6$, and (c) $Sr_2FeRe_{0.5}Ga_{0.5}O_6$.

The spectra of substituted samples were analyzed by three hyperfine sextets in addition to a quadrupole doublet. In the previous study for $Sr_2Fe_{1-x}M_xReO_6$ (*M* = Cr, Zn), the relation between isomer shift, hyperfine field and Fe valence states was elucidated. It was found out that a higher

iron valence state corresponds to a lower isomer shift and an appropriately larger hyperfine field compared to the non-substituted parent phase.[6] The sharp sextet which corresponds to well ordered regions of the materials with intact Re–O–Fe charge transfer paths persists in the spectrum of $Sr_2FeRe_{1-x}Ga_xO_6$ for x = 0.1. Its IS and H_{hf} values remain unchanged from those of Sr_2FeReO_6. Also the IS of a second sextet is nearly unchanged, only its H_{hf} is somewhat reduced. A pronounced third feature with a smaller IS = 0.50 mm/s and a larger H_{hf} = 378 KOe indicates the substitution of iron sites with Gallium and as a result of disorder, the number of charge transfer paths is reduced. Its IS, however, is still larger than the typical IS ~ 0.36 mm/s of Fe^{3+} [6, 14], indicating that these sites are still partly involved in Fe–Re charge transfer processes.

This is in contrast to the sample with x = 0.5. The sharp 6-line pattern corresponding to Fe–Re ordered regions has completely disappeared and three sextets with very similar isomer shifts typical of Fe^{3+} sites (0.36 – 0.38 mm/s) can be seen in the data (Table 2.2). Their absorption lines are broadened due to a distribution of hyperfine parameters, a variable coordination environment and the vicinity of the magnetic ordering temperature. This compares well with the X-ray data, which suggest an essentially disordered perovskite structure $Sr_2FeRe_{0.5}Ga_{0.5}O_6$. It is reasonable to describe the material as an antiferromagnet due to exchange interactions between the $3d^5$ high spin configurations of Fe^{3+} sites, no matter whether the Fe-sites are separated by Ga/Re(d^0) or not. In fact, substituting the Re ions on the *M'* sites in $Sr_2[Fe]_M[Re_{1-x}Ga_x]_{M'}O_6$ by Ga ions disrupts the Re–O–Fe charge transfer paths and introduces Fe sites which, due to disorder, are partially surrounded by Fe ions or by Ga ions as next nearest neighbors. Thanks to the strong on-site electronic correlations associated with the $3d^5$ shell of Fe^{3+} sites these areas become electronically localized and the magnetism in these regions is essentially determined by pronounced antiferromagnetic super-exchange interactions between the half-filled $t_2^3e^2$ shells of Fe^{3+}. This view is supported by the magnetization (see above) and conductivity measurement, where the conductivity of the substituted samples was too large to be measured by PPMS.

In such a context the question arises what is the charge state of Re in this material. From the Mössbauer spectrum the presence of Fe^{4+} sites can be ruled out as they should result in spectral components with IS ~ 0 mm/s.[14] Accordingly, the x = 0.5 sample may correspond to $Sr_2Fe(III)Re_{0.5}(VII)Ga_{0.5}(III)O_6$, or alternatively, an oxygen deficiency could be introduced for charge compensation. For instance, assuming the presence of Re(VI) the chemical composition would be $Sr_2Fe(III)Re_{0.5}(VI)Ga_{0.5}(III)O_{5.75}$.

Table 2.2 Selected parameters of Mössbauer spectra for the $Sr_2FeRe_{1-x}Ga_xO_6$ at room temperature (IS: isomer shift, B_{hf}: hyperfine field, ε: quadrupole interaction parameter, ΔE_Q: quadrupole splitting).

x	IS (mm s^{-1})	Percentage (%)	B_{hf} (KOe)	ε or ΔE_Q (mm s^{-1})
0	0.14(3)	5.1(5)		0.67(4)
	0.51(3)	10.8(2)	380.8(3)	
	0.582(2)	84.2(1)	336.0(1)	
0.1	0.10(2)	5.0(4)		0.20(3)
	0.50(2)	35.7(4)	377.5(3)	
	0.575(5)	36.6(4)	329.7(6)	
	0.59(2)	22.7(4)	301.3(3)	
0.5	0.32(2)	19.0(9)		0.36(3)
	0.38(3)	27.4(5)	382.7(3)	
	0.36(3)	23.2(8)	329.4(3)	
	0.37(7)	30.3(7)	264.0(9)	

2.4 Conclusion

In the solid solutions of $Sr_2FeRe_{1-x}Ga_xO_6$, the compounds start to be subject to anti-site disorder upon substitution of Re by Ga. Ga^{3+} is intermediate in size between Fe^{3+} and Re^{5+}. This effect breaks the site ordering in Sr_2FeReO_6. All cations on *M/M′* sites (Fe, Ga and Re) are distributed statistically over the *M/M′* sites. Generally, the *M* site is favourite for Fe, and the *M′* site favourite for Re. Ga prefers to occupy the *M* site at low level substitution but is forced to enter the *M′* sites above x = 0.4 due to the inter-charge repulsion pressure, making the *M′* site slightly more favourite for Ga. Along with the striking anti-site disorder, a magnetic transition takes place from ferromagnetism to antiferromagnetism. The Mössbauer spectra suggest that the valence of Fe increases from initial +2.7 to final +3 and remains stable. And then, Re acts as the redox buffer to compensate the charge deficiency (over the *M/M′* sites) due to hole-doping effect.

References

[1]K. I. Kobayashi, T. Kimura, H. Sawada, K. Terakura, Y. Tokura, Nature **395**, 677 (1998).

[2]K. I. Kobayashi, T. Kimura, Y. Tomioka, H. Sawada, K. Terakura, Y. Tokura, Phys. Rev. B **59**, 11159 (1999).

[3]C. Zener, Phys. Rev. **82**, 403 (1951).

[4]F. Sher, A. Venimadhav, M. G. Blamire, B. Dabrowski, S. Kolesnik, J. P. Attfield, Solid State Sci. **7**, 912 (2005).

[5]J. B. Goodenough, (Interscience, New York, 1966).

[6]A. Jung, I. Bonn, V. Ksenofontov, G. Melnyk, J. Ensling, C. Felser, W. Tremel, J. Mater. Chem. **15**, 1760 (2005).

[7]A. Jung, V. Ksenofontov, S. Reiman, H. Therese, U. Kolb, C. Felser, W. Tremel, Phys. Rev. B **73**, 144414 (2006).

[8]A. Jung, I. Bonn, V. Ksenofontov, M. Panthofer, S. Reiman, C. Felser, W. Tremel, Phys. Rev. B **75**, 184409 (2007).

[9]R. W. Cheary, A. Coelho, J. Appl. Crystallogr. **25**, 109 (1992).

[10]K. Lagarec, D. G. Rancourt, Nuclear Instruments and Methods in Physics Research Section B: Beam Interactions with Materials and Atoms **129**, 266 (1997).

[11]L. Balcells, J. Navarro, M. Bibes, A. Roig, B. Martinez, J. Fontcuberta, Appl. Phys. Lett. **78**, 781 (2001).

[12]H. Gao, V. Ksenofontov, J. Barth, M. Panthoefer, P. Adler, C. Felser, W. Tremel, (to be submitted).

[13]H. Kawanaka, I. Hase, S. Toyama, Y. Nishihara, Physica B: Condensed Matter **281-282**, 518 (2000).

3 $Sr_2FeRe_{1-x}Fe_xO_6$: How Crystal Structure Influences Physical Properties

3.1 Introduction

The double perovskites Sr_2FeMoO_6[1] and Sr_2FeReO_6[2] reveal half-metallic ferrimagnetic behavior at room temperature, and have recently attracted much attention due to the discovery of a tunnelling magnetoresistance (TMR). Double perovskites are presented with a general formula $A_2MM'O_6$ (A = alkali earth metal, M/M' = 3d transition metal). Double perovskites may be derived from a rock salt arrangement of corner-sharing of MO_6 and $M'O_6$ octahedra (Figure 1.6). Sr_2FeMoO_6 and Sr_2FeReO_6 exhibit relatively high Curie temperatures (401 K and 415 K, respectively). The Curie temperature is an important condition for a high degree of spin polarization at room temperature.

The Zener double exchange[3, 4] mediates the electron interaction along the Fe–O–M' units via oxygen bridges, forming double exchange pathways Fe–O–M'–O–Fe. Thereby, the long-range interaction Fe–Fe and M'–M' is ferromagnetic, whereas the short-range interaction between Fe and M' atoms is antiferromagnetic. This leads to ferromagnetic, ferrimagnetic, or antiferromagnetic behavior depending on the electron count of the participating elements.[5] Another interesting aspect of Fe–M' interactions is that when either Fe or M' is substituted by closed shell elements with invariant valence, the other one starts to take the part of a redox-buffer. Thus, the buffer effect balances the overall charge and changes the magnetic property of the whole compound.[6-8] Among double perovskite rhenates series substituted by closed shell elements, the solid solution $Sr_2Fe_{1-x}Ga_xReO_6$ reveals an interesting cation disorder effect. Ga was actually expected to substitute Fe due to the size and charge similarities, however the experimental fact indicated the Fe substitution took place on Re site as well. In this report, a systematic study is extended to substitute Re with Fe ($Sr_2FeRe_{1-x}Fe_xO_6$, $0 \leq x \leq 0.5$). At the first glance at $Sr_2FeRe_{1-x}Fe_xO_6$, one might intuitively expect a phase separation upon substitution of Re by Fe in Sr_2FeReO_6, because $Sr_2FeRe_{1-x}Fe_xO_6$ could separate into a mixture of $SrFeO_3$ and Sr_2FeReO_6 [$Sr_2FeRe_{1-x}Fe_xO_6 = (1 - x) \cdot Sr_2FeReO_6 + x \cdot SrFeO_3$].

$Sr_2FeRe_{1-x}Fe_xO_6$ was reported by a couple of work groups.[9-12] However, there is still an open gap with respect to a systematic and well-combined characterization for $Sr_2FeRe_{1-x}Fe_xO_6$. Therefore, the synthesis and characterizations of these compounds are presented herein.

3.2 Experimental

Synthesis: Starting materials were reagent grade SrO (Aldrich, 99.9% purity), Fe_2O_3 (Alfa Aesar, 99.99% purity), Re metal, Re_2O_7 (Alfa Aesar, 99.9% purity). All starting materials were stored under argon in a glovebox (Braun Labmaster) and were examined by X-ray powder diffraction prior to use. The solid solution samples were prepared by high temperature solid state reactions. Because of the strongly hygroscopic behavior of SrO and the high vapor pressure of Re_2O_7 the samples were prepared under inert gas atmosphere in a glovebox. Stoichiometric amounts of starting materials were ground in an agate mortar and pressed into pellets. In order to avoid SrO from attacking the quartz tubes, these pellets were transferred into corundum containers and finally sealed in evacuated quartz glass ampoules. The samples for $x \leq 0.4$ were heated at 1273 K (1373 K for $x = 0.5$) for seven days. The quartz ampoules were rapidly cooled to room temperature by quenching in ice bath.

Characterizations: X-ray powder diffraction measurement was performed using a Siemens D5000 with monochromatized $CuK\alpha_1$ radiation [Ge(220) monochromator] and a Braun M50 PSD. Lattice constants (relative to Si, which was used as internal standard) were obtained by Rietveld refinements applying the fundamental parameter approach (TOPAS Academic[9]).

The variable-temperature magnetic susceptibility measurement of $Sr_2FeRe_{1-x}Fe_xO_6$ was carried out using a Quantum Design MPMS-XL superconducting quantum interference device (SQUID) magnetometer, equipped with a high-temperature furnace.

The electrical resistivity (ρ) measurement was carried out by using a PPMS (Quantum Design) device. For the measurement, a pressed pellet contacted with silver epoxy paste was used.

High resolution transmission electron microscopy (HRTEM) and selected area electron diffraction (SAED) analyses were performed by a FEI Tecnai F30 ST microscope, operating at an extraction voltage of 300 kV and equipped with an energy dispersive X-ray (EDX) EDAX spectrometer. After milling for 90 minutes, the sample was dispersed in ethanol in an ultrasonic bath and sprayed on a copper grid coated with a carbon film. Simulated HRTEM images were performed multislice method [10, 11] using CERIUS program suit.[12]

Mössbauer measurement of powder samples were performed in transmission geometry using a constant-acceleration spectrometer. ^{57}Fe Mössbauer spectra were record at room temperature

using a 50mCi ^{57}Co (Rh) source. The RECOIL 1.03 Mössbauer Analysis Software was used to fit the experimental spectra [13]. Isomer shift values are quoted relative to α-Fe at 295 K.

Calculations: Band structure calculations were performed using the generalized gradient approximation (*GGA*) as well as local density approximation plus Hubbard *U* within the linear augmented plane-wave (LAPW)[14] framework. The crystal structure of the end member of the series of solid solutions, $Sr_2FeRe_{0.5}Fe_{0.5}O_6 \equiv Sr_4Fe_3ReO_{12}$, was adopted as an ideal ordered phase with a = 7.8707 Å derived from an ideally ordered $Ba_4Sb_3LiO_{12}$ type of structure (*Im*-3*m*). A "cubic primitive (*Im*-3*m*)" model was explored, because the previous structure refinements indicates that the tetragonal structure is very close to a cubic structure and tetragonal structure. In the cubic structure, two Fe atoms were differentiated by $Fe_{\mathbf{I}}$ and $Fe_{\mathbf{II}}$ respectively. Thus, the Fe atoms occupy two different positions, in a similar way that one arranges the Mn atoms in the calculation of $Mn_{3-x}Ga$.[15] The first ($Fe_{\mathbf{I}}$), with multiplicity 1, is located at Wyckoff position (0, 1/2, 1/2) and the second position ($Fe_{\mathbf{II}}$), with multiplicity 2, is at (1/2, 0, 0). Accordingly the nearest neighbor Re atoms are also differentiated to $Re_{\mathbf{I}}$, with multiplicity 1, at 1*a* (0, 0, 0) and $Re_{\mathbf{II}}$, with multiplicity 2, at 1*b* (1/2, 1/2, 1/2). The atomic configurations of $Fe_{\mathbf{I}}$ and $Fe_{\mathbf{II}}$ are arranged manually to realize their antiferromagnetic coupling by changing the 3*d*-shell electrons state of $Fe_{\mathbf{I}}$. After this modification, the initial body centered structure finally was transformed to a cubic primitive structure with space group of *Pm*-3*m*. The number of k points in the irreducible Brillouin zone was 20. The convergence criterion was fixed to 0.0001 Ry.

3.3 Results and discussion

3.3.1 Structural characterization

The crystal structures of $Sr_2FeRe_{1-x}Fe_xO_6$ were analyzed by X-ray powder diffraction (XRD) and Rietveld refinements. The Sr_2CuWO_6 structure type (space group *I*4/*m*) was adopted to perform the Rietveld refinements. The corresponding X-ray diffraction patterns are presented in Figure 3.1. The intensities of the (101) and (002) reflections decrease as a function of the Fe content (Figure 3.2). These two reflections imply a feature of Fe/Re disorder in the parent compound Sr_2FeReO_6, which was well-studied in the case of Sr_2FeMoO_6.[16] The reflections profile of the end member, $Sr_2FeRe_{0.5}Fe_{0.5}O_6$, appears to be a simple perovskite as reported by Gopalakrishnan *et al*.[17]

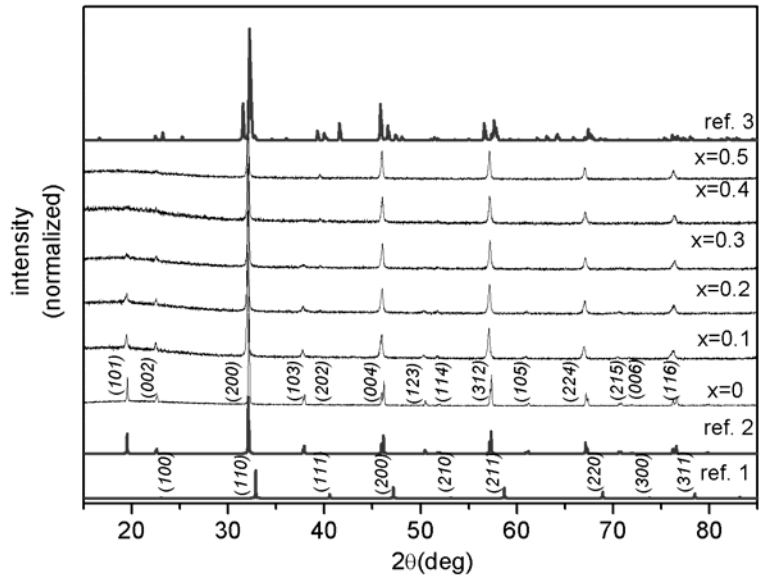

Figure 3.1 X-ray diffraction patterns of $Sr_2FeRe_{1-x}Fe_xO_6$; "ref.1" is $SrFeO_3$, "ref.2" is Sr_2FeReO_6 ($I4/m$, fully ordered)[2] , and ref.3 is $SrFeO_{2.5}$.

When one takes a close look at the PXRD patterns of $Sr_2FeRe_{1-x}Fe_xO_6$ and compares them with those of the references, $SrFeO_3$, Sr_2FeReO_6 and $SrFeO_{2.5}$, one finds that the patterns of $Sr_2FeRe_{1-x}Fe_xO_6$ resemble the pattern of Sr_2FeReO_6, but there is no superposition of $SrFeO_3$ and Sr_2FeReO_6. Although Sr_2FeReO_6 could be formally thought as $SrFeO_3$ + $SrReO_3$, in fact, the valences of Fe and Re are different in $Sr_2Fe^{+2.7}Re^{+5.3}O_6$[6] from $SrFe^{+4}O_3$. The Fe valence difference between Sr_2FeReO_6 and $SrFeO_3$ and the smaller ionic radii shift the pattern of $SrFeO_3$ to higher scattering angles, and therefore $SrFeO_3$ and Sr_2FeReO_6 are not superimposed in terms of PXRD. $SrFeO_{2.5}$ exhibits additional reflections compared to the solid solutions, which are not found in any of the solid solutions. All of these facts suggest that $Sr_2FeRe_{1-x}Fe_xO_6$ are solid solutions but not mixtures of $SrFeO_3$/$SrFeO_{2.5}$ and Sr_2FeReO_6, and that $Sr_2FeRe_{1-x}Fe_xO_6$ compound remains single phase but becomes highly disordered with increasing Fe content.

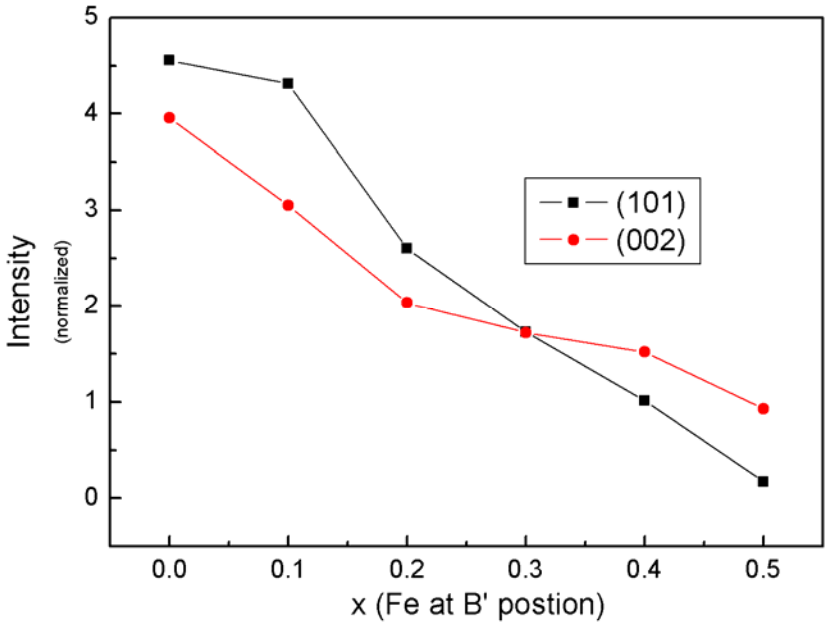

Figure 3.2 Intensities of (101) and (002) versus Fe content according to $Sr_2FeRe_{1-x}Fe_xO_6$.

On the other hand, when the synthesis procedures to prepare $Sr_2FeRe_{1-x}Fe_xO_6$ is considered, to anneal the samples at 1273 K in evacuated tubes (3.0×10^{-3} atm), the existence of $SrFeO_3$ can be ruled out under such conditions, because $SrFeO_3$ is obtained at 1033 K and O_2 partial pressure 3.33 atm[18] and the conditions for the other related phases are 1673 K (in air) for $SrFeO_{2.86}$ and 1157 K (in air) for $SrFeO_{2.86}$. Consequently, the O_2 partial pressure in the synthesis is too low to allow the formation of $SrFeO_3$. However one can also exclude the mixture of $SrFeO_{2.5}$ (I*bm*2) ,[19] now that the latter shows quite different PXRD pattern in contrast to the solid solutions.

The lattice parameters are listed in Table 3.1. Some parameters are analyzed in Figure 3.3. The parameters *a* and *c* approximately comply with Vegard's rule below $x \leq 0.3$ (Figure 3.3 (a)). The parameter of *c/a* is gradually approaching to $\sqrt{2}$, indicative of structural tendency to be a cubic phase. The XRD refinement for end member (x = 0.5) suggests that there is virtually no difference between the tetragonal and the cubic model (*Pm*-3*m*). The values of the Fe and Re contents are basically consistent with the nominal composition except for a slight difference. The Fe content is increasing linearly, while the Re content drops (Figure 3.3 (b)). With substitution, Fe and Re are distributed over the *M* and *M'* sites (Figure 3.3 (c)), indicating that the substitution causes a significant anti-site disorder. In particular, in $Sr_2FeRe_{0.5}Fe_{0.5}O_6$, Fe and Re are almost

evenly distributed on the *M* and *M′* sites. This result implies that a disordered perovskite is formed, suggesting a structural transition from initial ordered double perovskite (x = 0) to a final highly disordered perovskite (x = 0.5). Thus, a large amount of Fe–O–Fe is expected due to the significant anti-site disorder. The bond length shows that the Fe–O bond length decreases with substitution while the Re–O length increases with substitution (Figure 3.3 (d)). The overall lattice volume is reduced with substitution, suggesting that the decrease of the Re–O distance has an advantage over the increase of the Fe–O distance. It is worth noting that both the Fe–O and Re–O curves are oppositely bent at the turning point around x = 0.3, i.e., the Fe–O curve is bent up while the Re–O is bent down. This phenomenon suggests that below x = 0.3, Fe buffers the "hole-doping" effect; above 0.3, Re starts to buffer this effect.

Table 3.1 Lattice parameters based on tetragonal structure model in space group of *I*4/*m*. (*asd*: anti-site disorder).

Parameters	0	0.1	0.2	0.3	0.4	0.5
a/Å	*5.56741(8)*	*5.5705 (1)*	*5.5684(1)*	*5.5612(1)*	*5.5611 (2)*	*5.5751(1)*
c/Å	*7.9010(2)*	*7.9038(2)*	*7.8981(2)*	*7.886(3)*	*7.8838(3)*	*7.8981(4)*
(a/c)²	*2.01855(7)*	*2.0131(6)*	*2.0117(9)*	*2.0107(7)*	*2.009(7)*	*2.0069(4)*
asd1	*0.0257(35)*	*0.1217(32)*	*0.1350(37)*	*0.1655(38)*	*0.1914(44)*	*0.220(10)*
asd2	*0*	*0.1262(54)*	*0.2440(57)*	*0.4055(53)*	*0.5205(56)*	*0.690(12)*
M(Fe)	*0.9742(8)*	*0.8783(2)*	*0.8649(8)*	*0.834(5)*	*0.8086(1)*	*0.7804(8)*
M(Re)	*0.0257(2)*	*0.1216(8)*	*0.1350(2)*	*0.165(5)*	*0.1913(9)*	*0.2195(2)*
M'(Fe)	*0*	*0.1261(7)*	*0.2440(1)*	*0.4055(1)*	*0.5204(9)*	*0.6904(5)*
M'(Re)	*1*	*0.8738(3)*	*0.7559(9)*	*0.5944(9)*	*0.4795(1)*	*0.3095(5)*
Fe(content)	*0.9743(74)*	*1.0045(62)*	*1.1090(68)*	*1.2400(65)*	*1.3291(71)*	*1.471(16)*
Re(content)	*1.0257(74)*	*0.9955(62)*	*0.8910(68)*	*0.7600(65)*	*0.671(71)*	*0.529(16)*
d(Fe–O1)/Å	*2.057(14)*	*1.988(10)*	*1.974(12)*	*1.963(13)*	*1.975(15)*	*2.003(39)*
d(Fe–O2)/Å	*2.084(13)*	*2.0333(83)*	*2.0128(93)*	*2.009(97)*	*2.011(11)*	*2.022(20)*
d(Re–O1)/Å	*1.866(13)*	*1.9439(79)*	*1.9603(88)*	*1.9611(91)*	*1.954(11)*	*1.946(39)*
d(Re–O2)/Å	*1.898(14)*	*1.964(10)*	*1.975(12)*	*1.980(13)*	*1.967(15)*	*1.948(19)*

The EDX results are approximately close to the nominal composition of $Sr_4Fe_3ReO_{12}$. TEM images show that the sample consists of strongly agglomerated nano-domains of 5 to 50 nm in diameter. The heavy agglomeration often results in the superposition of different domains and the consequent formation of moiré patterns. The sample was therefore milled in order to reduce the

size and the thickness of the aggregates. After milling, it was possible to get HRTEM from single non-overlapping nano-domains lying on the thin borders of the aggregates.

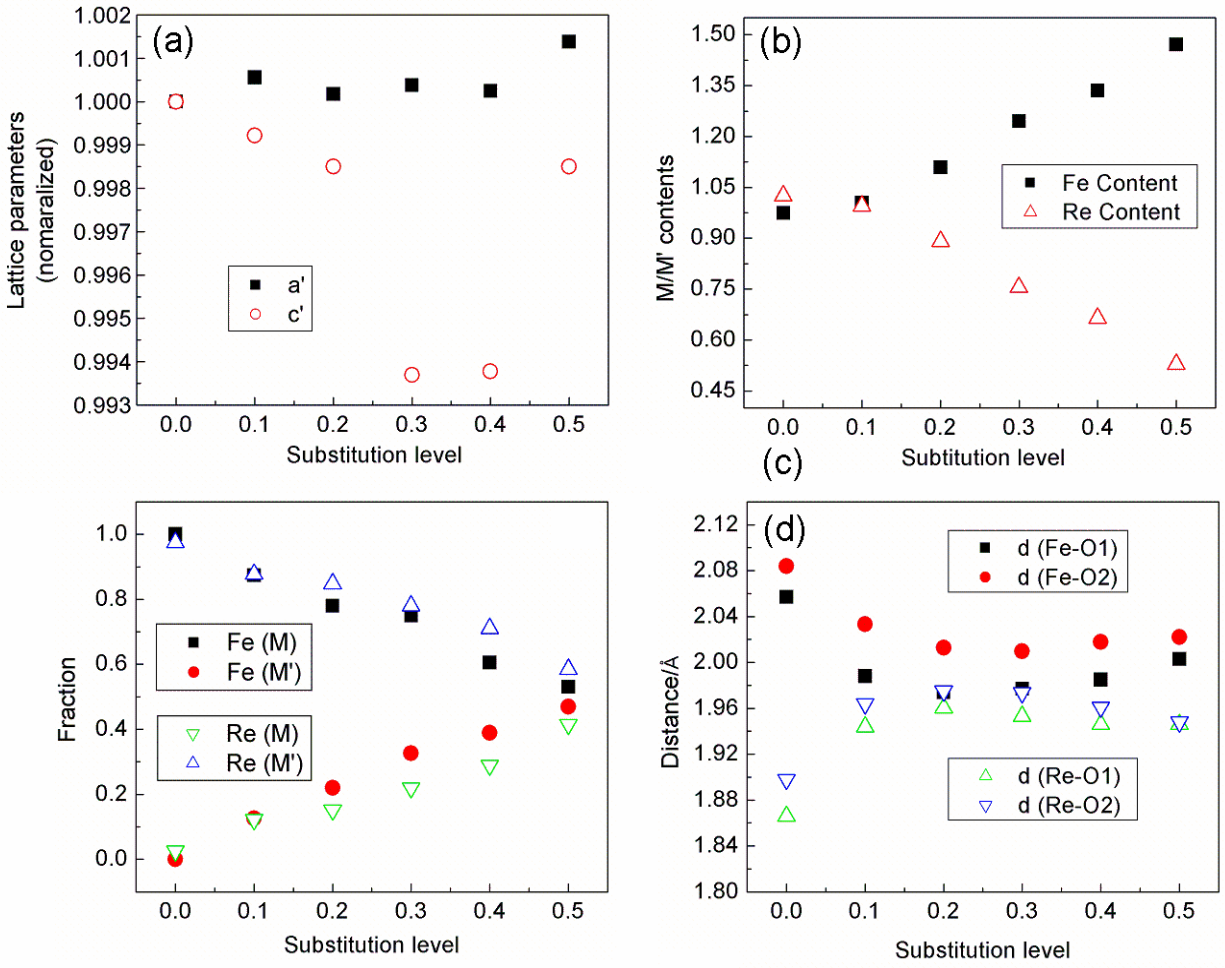

Figure 3.3 (a) lattice parameters *a* and *c*, (b) overall Fe and Re content in $Sr_2FeRe_{1-x}Fe_xO_6$, (c) distribution fractions of Fe and Re at *M* and *M'* sites, (d) bond length of d (*Fe/Re–O*1/*O*2).

Figure 3.4 shows an experimental HRTEM image of $Sr_2FeRe_{0.5}Fe_{0.5}O_6$ in the [2 0 -1] projection, and a relative Fourier transform and simulated high resolution transmission electron micrographs. The image shows a pseudo-hexagonal pattern with interplanar distances of 2.80(3) Å. The lattice spacings are in good agreement with the expected 2.79 Å for d_{020} and a d_{112} of the proposed tetragonal cell of $Sr_2FeRe_{0.5}Fe_{0.5}O_6$.

The [2 0 -1] projection in the tetragonal setting is equivalent to the [1 1 1] projection in cubic setting. The heavy atom (Sr, Fe and Re) arrangement of $Sr_4Fe_3ReO_{12}$ in the cubic elpasolite and in the tetragonal Sr_2CuWO_6 structures is identical and the partial structure of oxygen does not differ too much as well. Both $[1\ 1\ 1]_{cubic}$ and $[2\ 0\ -1]_{tetragonal}$ look hexagonal, and only the oxygen atoms break this symmetry slightly. Imposing defocus 0 nm and a reasonable thickness of 7 nm, an image very close to the experimental one was obtained.

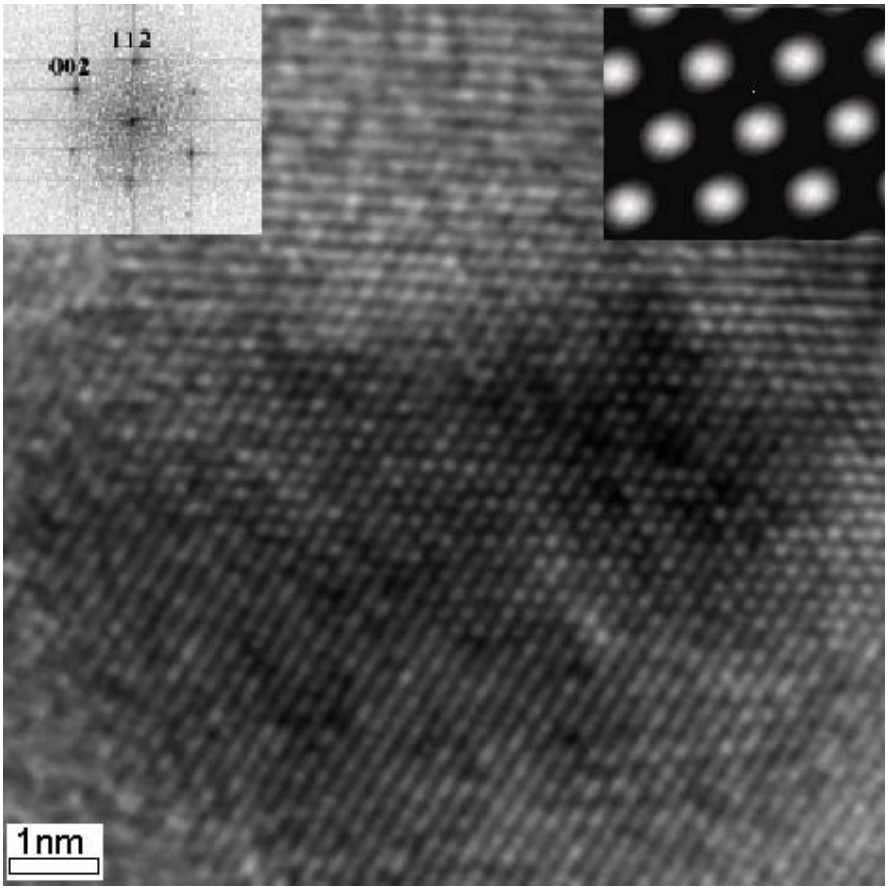

Figure 3.4 Experimental HRTEM of a $Sr_2FeRe_{0.5}Fe0._5O_6$ nanoparticle in [2 0 -1] projection. Upper-left inset: corresponding fast Fourier transform (FFT) showing the pseudo-hexagonal symmetry. Upper-right inset: relative simulated image obtained with defocus 0 nm and thickness 7 nm is shown.

3.3.2 Magnetic measurement

The field dependence of the magnetization at 5 K was measured in order to determine the saturation magnetization of the samples. Figure 3.5 indicates that the saturation magnetization decreases with increasing the Fe content, and it is very difficult to reach the saturation magnetization. Based on the hysteresis loops with small coercive fields, the parent compound Sr_2FeReO_6 can be classified as soft magnetic. Upon increasing the Fe content, the hysteresis loop is widened and the coercive field becomes larger. However, the overall area of the hysteresis loop is decreased due to the lower "saturation magnetization", until the hysteresis loop is almost closed for $Sr_2FeRe_{0.5}Fe_{0.5}O_6$. The sharp decrease of the saturation magnetization for the x = 0.1 sample (1.5 μ_B) compared to the parent compound (2.9 μ_B) is remarkable.

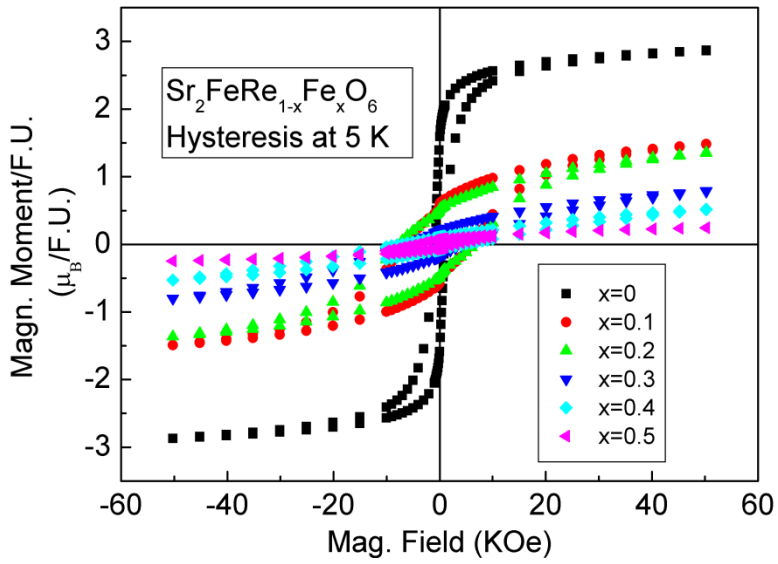

Figure 3.5 Magnetic hysteresis loops of $Sr_2FeRe_{1-x}Fe_xO_6$ measured at 5 K.

The magnetic susceptibility versus temperature was measured in two steps. In the first step, the measurement was performed at 5000 Oe from 5 K to 390 K, and the second step was carried out at 100 Oe from 300 K to 780 K. Due to the large difference of the magnetic moments between the samples, the data were normalized to the values at 5 K in Figure 3.6 (a). However, to make a better illustration, non-normalized data is presented in Figure 3.6 (b). The data for the high temperature susceptibility are shown in the inset of Figure 3.6 (a). The parent compound has a Curie temperature (T_c) around 401 K, which is nearly the same to the one reported previously.[2]

With increasing Fe content, the Curie temperatures remain almost unaffected. As the Fe substitution increases to x = 0.3 and x = 0.4, the susceptibility curves show a maximum corresponding to an antiferromagnetic type of ordering. The similar phenomenon was also observed in $Sr_2FeRe_{1-x}Sb_xO_6$ for x = 0.6. At a maximum Fe content of x = 0.5, the curve becomes smooth again. The antiferromagnetic ordering with increasing x may be attributed to the formation of Fe–O–Fe–O–Fe clusters, where the Fe ions couple antiferromagnetically.

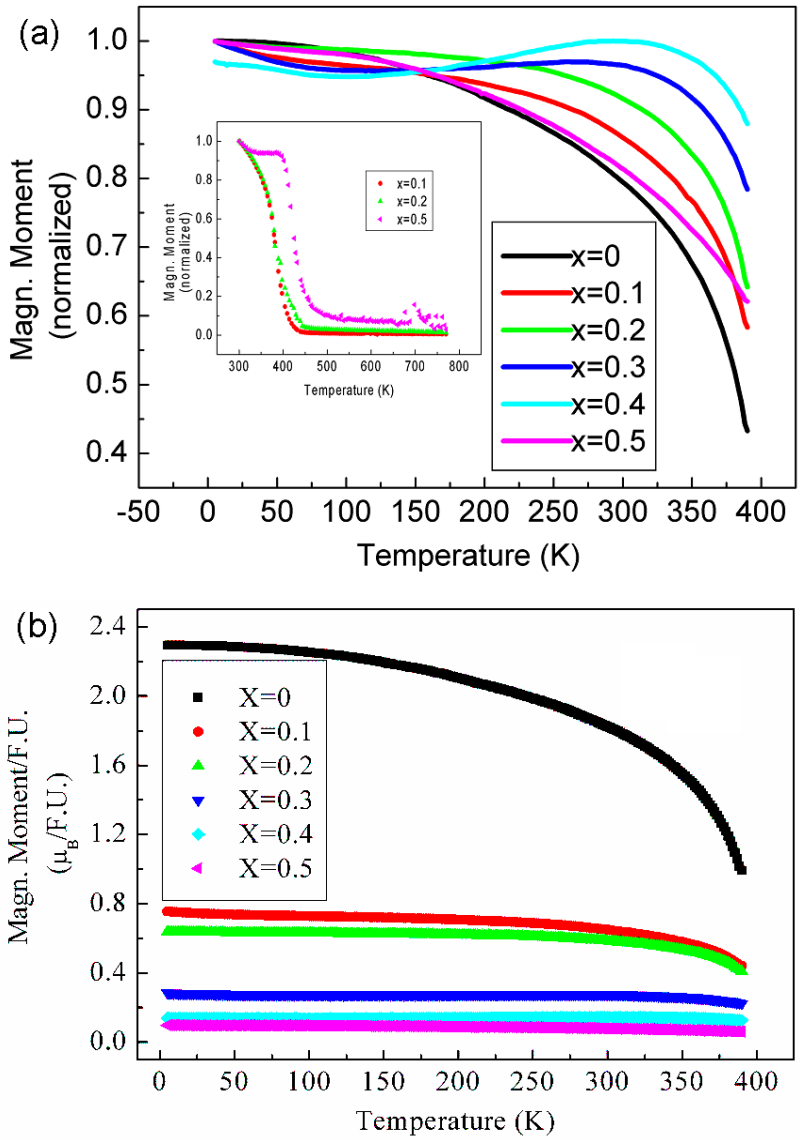

Figure 3.6 Magnetic susceptibility vs. temperature, inset is the temperature range between 300 K and 780 K. The measurement was performed by cooling under magnetic field of 5000 Oe: (a) normalized, (b) not normalized.

3.3.3 Conductivity measurement

The results of the resistivity measurement of five selected samples (x=0, 0.1, 0.2, 0.3 and 0.5) are presented in Figure 3.7. In accordance with the previous results,[2] the unsubstituted parent compound reveals a metallic behavior in the whole temperature range. In contrast, Fe substituted samples are all semiconducting. The room temperature resistance of the sample with x = 0.3 substitution level is several orders of magnitude higher than that of the unsubstituted parent compound. Among the samples, only the x = 0.5 compound shows an Arrhenius-like behavior in terms of temperature dependence of the resistivity. The activation energy E_a is determined as 0.18 eV.

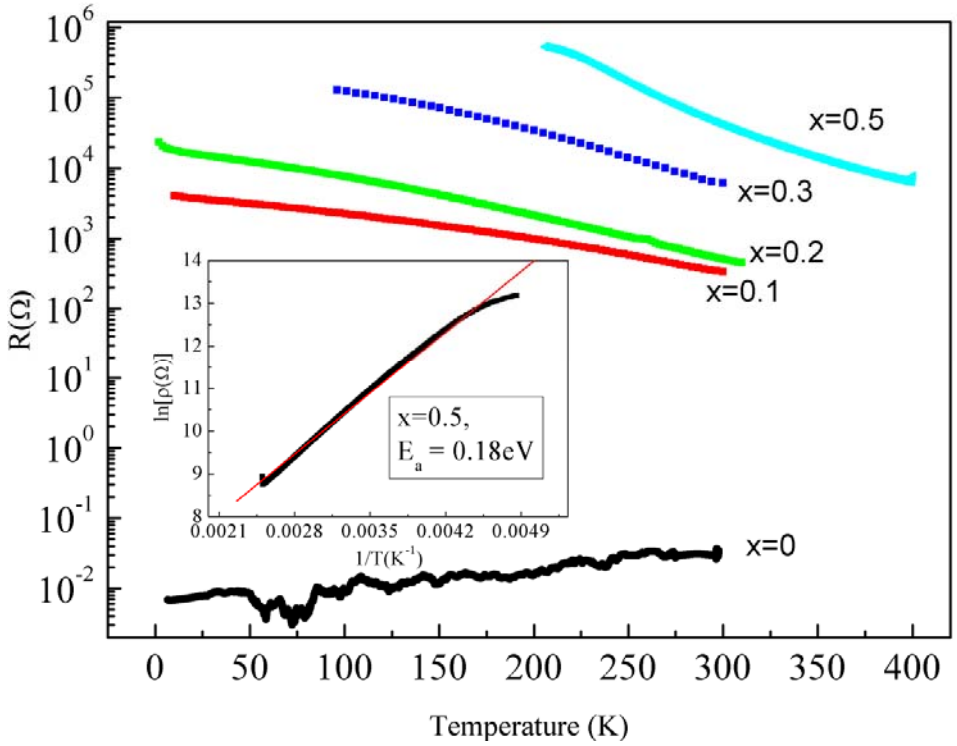

Figure 3.7 Conductivity measurement without application of an external magnetic field; inset is Arrhenius-fit.

3.3.4 Mössbauer spectroscopy

^{57}Fe Mössbauer experiments give deeper insight into the chemical composition and the magnetic structure of $Sr_2FeRe_{1-x}Fe_xO_6$. Figure 3.8 shows the room temperature spectra of the

materials. All spectra exhibit mainly magnetic hyperfine patterns in addition to weak paramagnetic signals. The 6-line patterns are typical for magnetically ordered materials. A minor paramagnetic quadrupole doublet even for Sr_2FeReO_6 has also been observed in previous preparations of this compound[6] and may be associated either with an impurity phase or a certain Fe/Re anti-site disorder. The latter is obvious from the presence of two hyperfine sextets in Sr_2FeReO_6 differing in their isomer shifts as well as in their internal magnetic field strengths. The sharp 6-line pattern of the majority component with IS = 0.58 mm/s and H_{hf} = 336.0 KOe (84.2%) is due to the well ordered Sr_2FeReO_6 phase, the crystal structure of which is characterized by only one Fe site with six Re neighbors. The minor component with IS = 0.51 mm/s and H_{hf} = 380.8 KOe, (10.8%) corresponds to Fe sites with distorted coordination geometry. These results are consistent with the structural refinement. The isomer shift value of 0.58 mm/s for Sr_2FeReO_6 in the previous work was attributed to an Fe charge state of +2.7.[6] A decrease in the isomer shift with a concomitant increase in hyperfine field points to an increase in the charge state. The Fe/Re disorder disturbs the charge transfer from the t_{2g} minority spin states of Re into those of Fe which explains the reduced IS value for the second component.

The sharp sextet which corresponds to well ordered regions of the materials with intact Re–O–Fe charge transfer paths persists in the spectra of the iron rich series $Sr_2FeRe_{1-x}Fe_xO_6$ up to x = 0.3. Its IS and H_{hf} values remain unchanged compared to those of Sr_2FeReO_6. However, additional features show up in the spectra with increasing x. Their absorption lines are broadened due to a distribution of hyperfine parameters, variable coordination environment and possibly due to the vicinity of the magnetic ordering temperature. The spectra up to x = 0.3 were analyzed by three hyperfine sextets in addition to a quadrupole doublet. The parameters from the data evaluation are summarized in Table 3.2. With increasing x a broad component appears with IS and H_{hf} values that are considerably smaller and larger than for the parent compound, respectively. In the previous study for $Sr_2Fe_{1-x}M_xReO_6$ (M = Cr, Zn), the relation was elucidated between the isomer shift, the hyperfine field, and the Fe valence states. A higher iron valence state corresponds to a lower isomer shift and an appropriately larger hyperfine field compared to the unsubstituted parent phase.[6] Actually, IS = 0.36 mm/s in the spectrum of x = 0.3 can be considered typical for Fe^{3+} at room temperature.[6, 20] In fact, substituting the Re ions on the M' sites in $Sr_2[Fe]_M[Re_{1-x}Fe_x]_{M'}O_6$ by Fe ions disrupts the Re–O–Fe charge transfer paths and introduces Fe sites which are entirely surrounded by other Fe ions as next near neighbors. Due to the strong on-site electronic correlations associated with $3d^5$ shell of Fe^{3+} sites, these areas

become electronically localized and the magnetism in these regions is essentially determined by pronounced antiferromagnetic super-exchange interactions between the half-filled $3d^5$ shells of Fe^{3+}. This view is supported by the magnetization measurement and transport measurement (see above).

The area fraction of this spectral component increases with x which means that the fraction of the localized antiferromagnetic regions increases at the expense of the more delocalized ferrimagnetic regions. Introducing additional Fe^{3+} on the *M'* sites also changes the coordination environment of Fe ions on the *M* sites. Accordingly, the third sextet may be attributed to Fe ions on the *M* site having Fe neighbors, which are still involved in Fe-Re charge transfer. This is in agreement with the IS values which suggest a gradual increase of the charges states of these Fe species with increasing x.

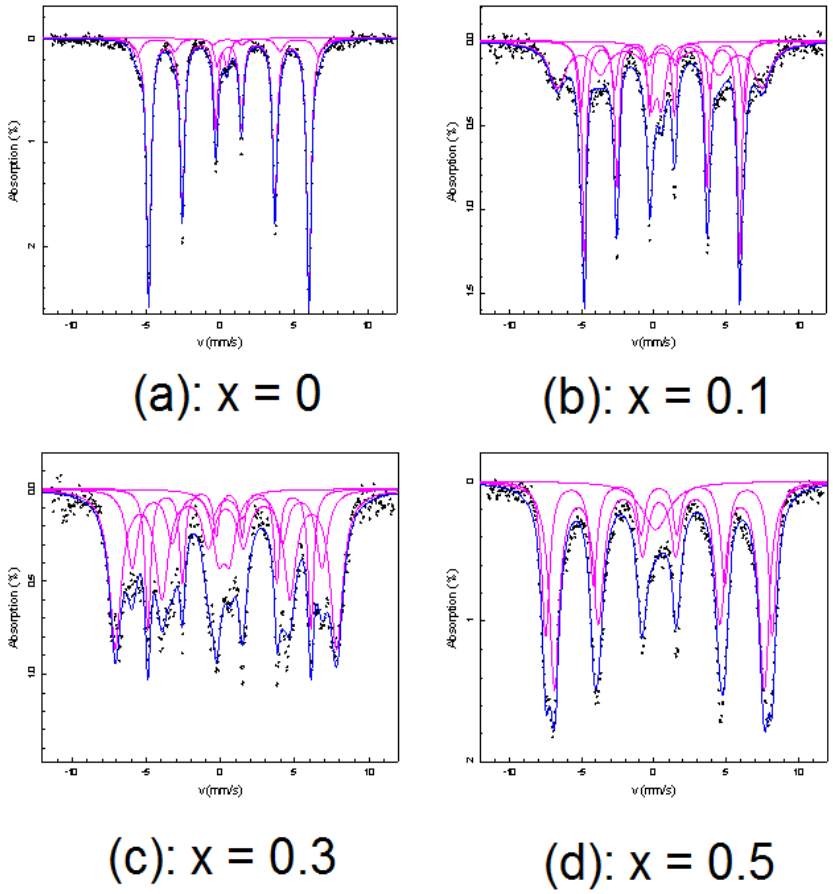

Figure 3.8 ^{57}Fe Mössbauer spectroscopy at room temperature of (a) Sr_2FeReO_6, (b) $Sr_2FeRe_{0.9}Fe_{0.1}O_6$,(c) $Sr_2FeRe_{0.7}Fe_{0.3}O_6$, and (d) $Sr_2FeRe_{0.5}Fe_{0.5}O_6$.

The sharp 6-line pattern corresponding to Fe–Re ordered regions has completely disappeared in the spectrum of the material with x = 0.5, and only two sextets with very similar isomer shifts typical of Fe^{3+} sites have been included in the data analysis. This compares well with the X-ray data which suggest an essentially disordered perovskite structure favoring the formulation of $SrFe_{0.75}Re_{0.25}O_3$. It is reasonable to describe the material as an antiferromagnet due to exchange interactions between the Fe^{3+} sites with a nearly statistical distribution of Re sites. In this context the question arises what is the charge state of Re in this material. From the Mössbauer spectrum the presence of Fe^{4+} sites can be ruled out as they should result in spectral components with IS ~ 0 mm/s. Accordingly, the x = 0.5 sample may correspond to $SrFe_{0.75}(III)Re_{0.25}(VII)O_3$, or alternatively, oxygen deficiency could be introduced for charge compensation. For instance, assuming the presence of Re(VI) the chemical composition would be $SrFe_{0.75}(III)Re_{0.25}(VI)O_{2.875}$.

Table 3.2 Selected Mössbauer parameters for the $Sr_2FeRe_{1-x}Fe_xO_6$ at room temperature (IS: isomer shift, H_{hf}: hyperfine field, ε: quadrupole interaction parameter, ΔE_Q: quadrupole splitting).

x	IS (mm s^{-1})	Percentage (%)	H_{hf} (KOe)	ε or ΔE_Q (mm s^{-1})
0	0.14	5.1		0.68
	0.51	10.8	380.8	
	0.58	84.2	336.0	
0.1	0.20	10.4		0.70
	0.43	33.1	439.7	
	0.59	17.1	351.1	
	0.58	39.5	333.5	
0.2	0.34	17.1		0.61
	0.40	36.1	460.5	
	0.58	31.8	339.2	
	0.52	15.3	393.0	
0.3	0.24	9.08		0.77
	0.36	49.6	461.9	
	0.44	21.9	395.8	
	0.59	19.3	340.5	
0.5	0.23	8.31		
	0.35	36.4	485.3	
	0.36	55.3	450.8	

Considering the complicated Mössbauer spectra of the $Sr_2FeRe_{1-x}Fe_xO_6$ series, one may ask whether they really arise from a solid solution or whether there are indications for a phase separation into Sr_2FeReO_6 and $SrFeO_{3-\delta}$. In the system $SrFeO_{3-\delta}$, four phases are known, namely, $Sr_2Fe_2O_5$ ($SrFeO_{2.5}$), $Sr_4Fe_4O_{11}$ ($SrFeO_{2.75}$), $Sr_8Fe_8O_{23}$ ($SrFeO_{2.875}$), and $SrFeO_3$. Each of these phases has a very typical Mössbauer spectrum which is useful for identifying these materials even in phase mixtures.[20] Under the synthesis conditions employed for $Sr_2FeRe_{1-x}Fe_xO_6$, one could expect the presence of brownmillerite-type $Sr_2Fe_2O_5$ (only Fe^{3+}). This compound shows an antiferromagnet ordering above room temperature. It should give rise to two sextets of similar area fraction in the Mössbauer spectra, but with considerable different isomer shifts and hyperfine fields as the two sites are coordinated octahedrally and tetrahedrally, respectively. Such a feature is not found in any of the present spectra. The more oxidized phases contain Fe^{4+} which should result in a quadrupole doublet or single line with IS ~ 0 mm/s. Such a feature is also not observed. Accordingly, one can exclude the formation of any of the phases in the $SrFeO_{3-\delta}$ system which supports the view that the system of $Sr_2FeRe_{1-x}Fe_xO_6$ is indeed a solid solution system. Again this is in full agreement with the X-ray data.

In order to obtain further insight into the origin of the complex Mössbauer spectra, I have calculated the probability of the various coordination environments of a given iron *M* site in the series $Sr_2[Fe]_M[Re_{1-x}Fe_x]_{M'}O_6$ (Figure 3.9). In an ordered elpasolite $A_2MM'O_6$ structure, *M* is surrounded by 6 third-coordinated *M′* (first coordinated atom of *M* is Oxygen, and second coordinated is *A*). A partial substitution of *M′* by *M* will change the second coordination of *M*. If *M* replaces *M′* randomly, one expects that *M* atom can be surrounded by *0M + 6M′*, *1M + 5M′*, *2M + 4M′*, *3M + 3M′*, *4M + 2M′*, *5M + 1M′*, and *6M + 0M′* third nearest neighbors, leading to 7 different possibilities for different surroundings of a *M* atom if restricting to the third shell.

The probability *P(n*, x*)* for a particular surrounding of the form *nM* atoms + (6 - n) *M′* atoms in a certain shell of the original M_0 atoms is given by a binomial distribution which depends on the concentration x of doped *M*. If applied to this particular probability to find *n* Re and (6 - *n*) Fe on the 6 positions of the third neighbor shell of the Fe_0 original ion is given by[21]

$$P(n,x) = \frac{N!}{(N-n)!}(1-x)^{N-n}x^n .$$

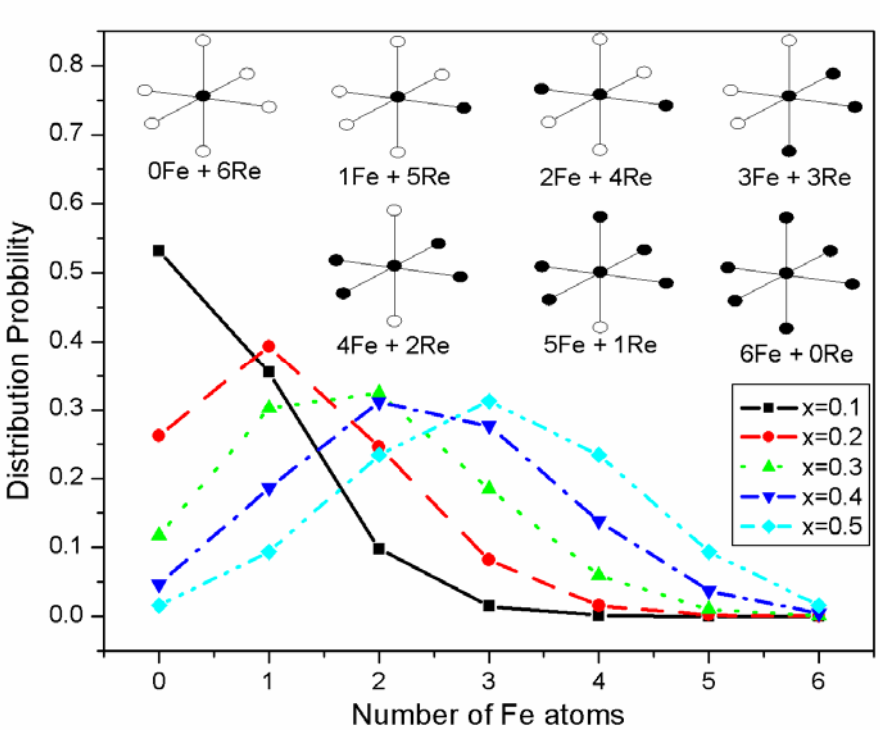

Figure 3.9 Probabilities cation distribution around original Fe in $Sr_2FeRe_{1-x}Fe_xO_6$.

For small x, more than 50% Fe sites are still entirely surrounded by Re sites. The fraction of these unperturbed iron sites decreases rapidly with x and for x = 0.5 they have totally disappeared. This trend is in qualitative agreement with the Mössbauer spectra, in particular with the disappearance of the signal of the well ordered phase in the spectrum of x = 0.5 sample. On the other hand, the probability of finding iron *M* sites with one or more Fe neighbors increases with x.

3.3.5 Electronic structure

In order to understand the electrical transport behaviour of the solid solutions, band structure calculations was performed for $Sr_2FeRe_{0.5}Fe_{0.5}O_6$. *GGA* + *U* was tested using the primitive cubic model. When *U* is increased to 4 eV, the partial DOS of Re is shifted to a higher energy and a gap around E_F is almost to open up. When *U* was further increased to 6 eV, a gap was opened (Figure 3.10). Ultimately, the calculation in *GGA* + *U*(6eV) manifests the insulating nature in $Sr_2FeRe_{0.5}Fe_{0.5}O_6$. In this band structure, the valence band of Fe is well below that of oxygen, which is separated from the hybridized 5*d*(Re)–2*p*(O) conduction band (upper Hubbard band).

The charge transfer energy Δ, the gap between oxygen *p* band and upper Hubbard band, is smaller than the on-site Coulomb energy *U*, energy difference between upper Hubbard band and lower Hubbard band, which leaves a charge-transfer gap ~(Δ-W^*).[22] This electronic configuration satisfies the criteria of a charge-transfer insulator. Therefore, the end member of $Sr_2FeRe_{1-x}Fe_xO_6$, $Sr_2FeRe_{0.5}Fe_{0.5}O_6$, can be defined as weak magnetic charge-transfer-type insulator.

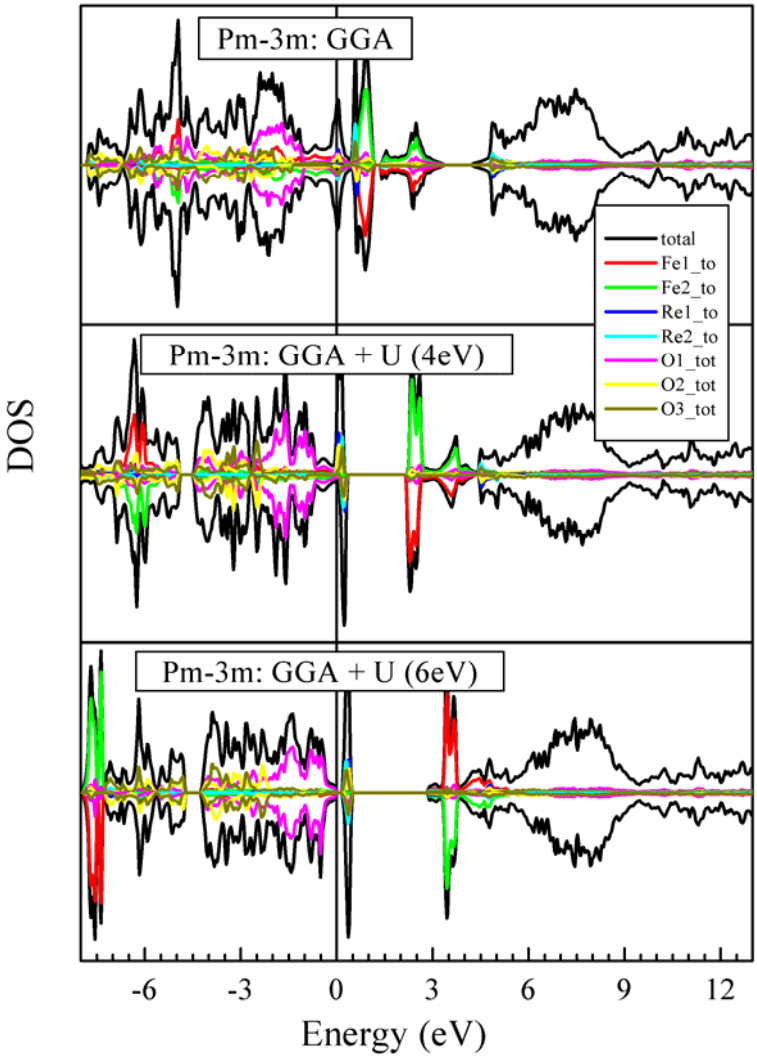

Figure 3.10 Density of State of $Sr_2FeRe_{0.5}Fe_{0.5}O_6$, based on primitive cubic model with respect to different methods

* band width

3.4 Conclusion

The series of compounds, with formula of $Sr_2FeRe_{1-x}Fe_xO_6$, are solid solutions rather than mixtures of Sr_2FeReO_6 and $SrFeO_{3-\delta}$. Upon substitution, the initial parent phase becomes disordered, and the whole series undergoes transition from ordered double perovskite to perovskite. With increasing substitution level, Fe and Re cations are distributed randomly at sites of *M* and *M′*. This leads to a great amount of local Fe–O–Fe clusters. Due to these local clusters, a magnetic transition is found from ferro(i)magnetism to antiferromagnetism. The disorder also arouses an electronic evolution from a metal (x = 0) to a semiconductor (above x = 0.1). The Mössbauer analysis, along with crystal refinements, suggests that Fe servers as buffer initially (valence changed from 2.7+ to 3+), and then its valence remains constant at 3+, when Re starts taking over the buffer role to balance the hole-doping effect. The band structure of $Sr_2FeRe_{0.5}Fe_{0.5}O_6$, the end member of the solid solutions, suggests that this material is a charge-transfer insulator.

References

[1]K. I. Kobayashi, T. Kimura, H. Sawada, K. Terakura, Y. Tokura, Nature **395**, 677 (1998).

[2]K. I. Kobayashi, T. Kimura, Y. Tomioka, H. Sawada, K. Terakura, Y. Tokura, Phys. Rev. B **59**, 11159 (1999).

[3]C. Zener, Phys. Rev. **82**, 403 (1951).

[4]F. Sher, A. Venimadhav, M. G. Blamire, B. Dabrowski, S. Kolesnik, J. P. Attfield, Solid State Sci. **7**, 912 (2005).

[5]J. B. Goodenough, (Interscience, New York, 1966).

[6]A. Jung, I. Bonn, V. Ksenofontov, G. Melnyk, J. Ensling, C. Felser, W. Tremel, J. Mater. Chem. **15**, 1760 (2005).

[7]A. Jung, V. Ksenofontov, S. Reiman, H. Therese, U. Kolb, C. Felser, W. Tremel, Phys. Rev. B **73**, 144414 (2006).

[8]A. Jung, I. Bonn, V. Ksenofontov, M. Panthofer, S. Reiman, C. Felser, W. Tremel, Phys. Rev. B **75**, 184409 (2007).

[9]R. W. Cheary, A. Coelho, Journal of Applied Crystallography **25**, 109 (1992).

[10]J. M. Cowley, A. F. Moodie, Acta Crystallogr. **10**, 609 (1957).

[11]W. O. Saxton, M. A. O'Keefe, D. J. H. Cockayne, M. Wilkens, Ultramicroscopy **12**, 75 (1983).

[12]*CERIUS2 version 4.6MS* 9685 Scranton Road, San Diego.

[13]K. Lagarec, D. G. Rancourt, Nuclear Instruments and Methods in Physics Research Section B: Beam Interactions with Materials and Atoms **129**, 266 (1997).

[14]P. Blaha, K. Schwartz, G. K. H. Madsen, D. Kvasnicka, J. Luitz, *Wien2K,An Augmented Plane Wave+Local Orbitals Program for Calculating Crystal Properties* ((Techn. Universität Wien, Austria,2001).

[15]J. Winterlik, B. Balke, G. H. Fecher, C. Felser, M. C. M. Alves, F. Bernardi, J. Morais, Phys. Rev. B **77**, 054406 (2008).

[16]L. Balcells, J. Navarro, M. Bibes, A. Roig, B. Martinez, J. Fontcuberta, Appl. Phys. Lett. **78**, 781 (2001).

[17]A. Nag, J. Manjanna, R. M. Tiwari, J. Gopalakrishnan, Chem. Mater. **20**, 4420 (2008).

[18]P. K. Gallagher, J. B. MacChesney, D. N. E. Buchanan, The Journal of Chemical Physics **41**, 2429 (1964).

[19]M. Schmidt, S. J. Campbell, J. Solid State Chem. **156**, 292 (2001).

[20]P. Adler, A. Lebon, V. Damljanovic, C. Ulrich, C. Bernhard, A. V. Boris, A. Maljuk, C. T. Lin, B. Keimer, Phys. Rev. B **73**, 094451 (2006).

[21]S. Wurmehl, J. T. Kohlhepp, H. J. M. Swagten, B. Koopmans, M. Wojcik, B. Balke, C. G. F. Blum, V. Ksenofontov, G. H. Fecher, C. Felser, Appl. Phys. Lett. **91**, 052506 (2007).

[22]J. Zaanen, G. A. Sawatzky, J. W. Allen, Phys. Rev. Lett. **55**, 418 (1985).

4 Sr_2InReO_6: Effect of Tilted Octahedra in Double Perovskites

4.1 Introduction

Oxides of the double perovskite type of $A_2MM'O_6$ (A = divalent cation or rare earth, *M/M'* = transition metal) have attracted much attention recently due to their intriguing physical properties and potential technological applications.[1-3] The two most prominent examples are Sr_2FeMoO_6[4] and Sr_2FeReO_6[5] with half-metallic ferrimagnetic behavior at room temperature, which makes them prospective magnetoelectronic compounds. For such polycrystalline materials, low-field intergrain tunneling magnetoresistance (TMR) at room temperature was reported. The conceptual basis for the observed half-metallic ferromagnetism is a large density of states of one spin direction at the Fermi level, while the other spin direction is insulating. Both compounds have a high Curie temperature ($T_c \approx 401$ K and 415 K, respectively) which is an important condition for a high degree of spin polarization at room temperature. Within the double perovskite family, the highest T_c have been reported for Sr_2CrReO_6 ($T_c \approx 635$ K) [6-8] and Sr_2CrOsO_6 ($T_c \approx 725$ K).[9-11]

Recently Re-based double perovskites have been intensively studied due to a high T_c and a complex exchange mechanism arising from spin-orbit coupling in Re.[12-16] Some efforts were made to replace the variable-valence transition metal atoms with fixed-valence elements, e.g. substitution of Fe with Zn or Ga and Re with Sb in Sr_2FeReO_6.[17-19] Jung *et al.* recently reported the effect of disorder in $Sr_2Fe_{(1-x)}Ga_xReO_6$.[17] Surprisingly, although Sr_2GaReO_6 contains only a $5d^2$ element Re, band structure calculations (*GGA*) predicted it to be a half-metal with highly spin-polarized *d*(Re)–*p*(O) states and Ga *p* states situated above the Fermi-level.[17] This finding is interesting, because the magnetism of 4*d* and 5*d* elements is rare in perovskite structures when in the absence of 3*d* elements. In contrast to three dimensional Re connections in ReO_3, the adjacent Re ions in Sr_2GaReO_6 are isolated by Ga, leading to no direct connectivity of Re. Whereas, Jung's band structure calculations showed that the conductivity in spin up state was found to arise from Re–Re interactions along the face diagonal. It is of interest whether or not the predicted band structure calculations agree with experimental data. Unfortunately, Sr_2GaReO_6 is difficult to be prepared as an ordered and stoichiometrically pure compound. Because Ga is chemically very similar to its heavier homologue In, In is selected to replace Ga to pursue this study through investigation of Sr_2InReO_6. Additionally, the larger ionic radius of In^{3+} may prevent the

appearance of anti-site disorder as found in $Sr_2Fe_{1-x}Ga_xReO_6$ due to the similarity of cationic radii of Fe^{3+}, Ga^{3+} and Re^{+5}.[17]

An early study by Sleight *et al.* reported Sr_2InReO_6 to be cubic (elpasolite type, *cF*40).[20] However, there are no detailed property studies available for this material. Herein, the systematic investigations on Sr_2InReO_6 are presented including its structural determination, band structure calculations based on different types structures as well as physical characterizations such as conductivity measurement, magnetic properties, and heat capacity.

4.2 Experimental

Synthesis: Sr_2InReO_6 was synthesized by high temperature solid state reactions. The starting compounds of SrO, In_2O_3, Re and Re_2O_7 (all purities above 99.9%) were weighed and mixed thoroughly inside a glovebox. In order to prevent an attack of SrO on the quartz tube, the material was pressed into pellets that were transferred subsequently into corundum containers and finally sealed in evacuated quartz tubes. The samples were annealed for six days at 1173 K. Thereafter, the ampoules containing the samples were rapidly cooled to room temperature by quenching in an ice bath.

Characterizations: Powder X-ray diffraction (PXRD) measurement was performed on a Siemens D5000 powder diffractometer with a Braun M50 position sensitive detector and CuKα_1 radiation [Ge(220) monochromator]. Lattice constants were obtained by Rietveld refinement with TOPAS Academic V4.1[21] applying the fundamental parameter approach.

Neutron powder diffraction patterns were obtained on the high intensity powder diffractometer at the Lujan Neutron Scattering Center at the Los Alamos Neutron Science Center LANSCE. The refinement of the crystal structure was performed by the Rietveld method, using the GSAS refinement program for joint refinement of the X-ray- and the neutron- diffraction data.

Magnetometry was performed using Quantum Design MPMS-XL SQUID magnetometer.

The electrical resistivity (ρ) measurement was carried out on sintered polycrystalline pellet by ordinary four probe method. For the measurement, a pressed pellet was used which was contacted with silver epoxy paste.

The specific heat in zero field and 0.1 T of the pellet-shaped sample was measured in the

temperature range 2 – 35 K using a PPMS (Quantum Design) device.

Band structure calculations: The band structure calculations were performed using the full-potential augmented plane-wave (FLAPW) within framework of the generalized gradient approximation (*GGA*) through the WIEN2k software package. The calculations were carried out by using the structural parameters obtained from the Rietveld refinements. The number of *k* points in the irreducible Brillouin Zone was 20, and the convergence criterion was fixed to 0.0001 Ry.

4.3 Results and discussion

4.3.1 Structural characterization

Sr_2InReO_6 was previously reported to crystallize in the cubic elpasolite structure type (*cF*40, *Fm*-3*m*).[20] However, X-ray powder diffraction pattern at ambient conditions (c.f. Figure 4.1) exhibited weak but significant Bragg intensities according to reflections which are systematically extinct in the elpasolite type (*Fm*-3*m*) as well as in the Sr_2CuWO_6 (*I*4/*m*) and the Ba_2PrIrO_6 (*P*4/*mnc*) structure type. Full pattern profile analyses showed the best fit according to the cryolite structure type. Thus, a structure model for Sr_2InReO_6 in the cryolite structure type was constructed using SPuDS[22] and adopted as the starting model in Rietveld refinements. All positional parameters were refined as well as the occupation factors of the In- and the Re-site according to an anti-site disorder model and one global isotropic displacement parameter. Due to the relatively low scattering power, the refinement of the positional parameters of the O-atoms was critical. Therefore, bond length restraints ($d_{Re–O}$ = 193 pm, $d_{In–O}$ = 216 pm, $d_{O–O}$ = 260 pm) using a GRS series (TOPAS) were applied. The final structure refinement converges at R_{wp} = 0.054 (c.f. Table 4.1). Refined Bond lengths and their variations are plausible (c.f. Table 4.3). The ratio Re/In is 1:1 within the 3σ confidence interval, the anti-site disorder accounts to less than 5%. Ambient temperature neutron powder diffraction data confirm the cryolite structure type (c.f. Figure 4.2). The final crystal structure model from joint refinement of the X-ray and neutron-diffraction data (Table 4.2) exhibit a clear contrast of the Re–O and In–O bond lengths of ⟨*d* (Re–O)⟩ = 1.97 Å and ⟨*d* (In–O)⟩ = 2.13 Å, which is slightly smaller than the value expected from the difference of Shannon radii of Re^{5+} (0.58 Å) and In^{3+} (0.80 Å) in octahedral coordination. The Re–O bond lengths themselves are split into two groups, i.e. Re–O1 (1.9778(2) Å) and Re–O2 (1.992(1) Å, both oriented in the *ab*-plane), and Re–O3 (1.942(3) Å, oriented

along the *c*-axis). The slight (but significant) difference in the Re–O bond lengths points towards Jahn–Teller distortion along the t_{2g} normal coordinate as expected for a transition metal cation with d^2 electron configuration in octahedral coordination.

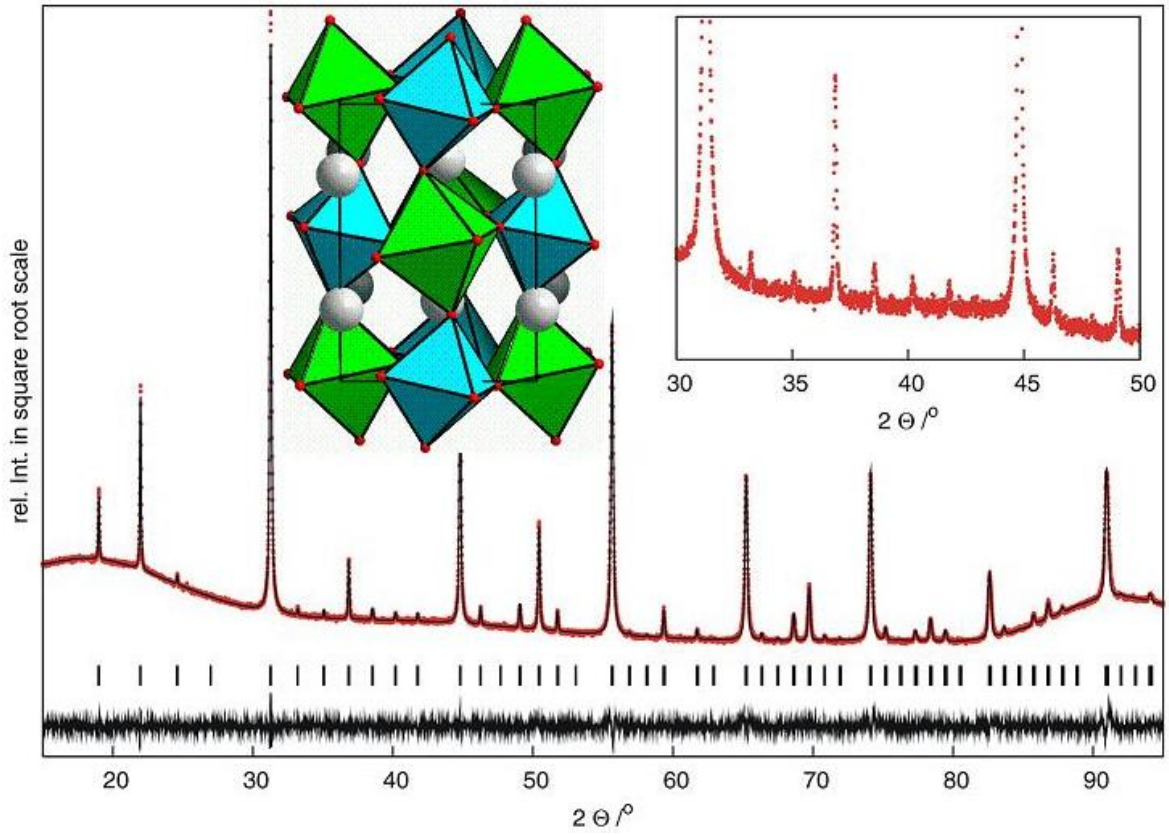

Figure 4.1 X-ray powder diffraction pattern of Sr_2InReO_6 at ambient conditions (black: experiment, red: fit from Rietveld-refinement, black below: difference curve). Inset left shows the crystal structure of Sr_2InReO_6 (white spheres: Sr; red spheres: O; green octahedra: In; blue octahedra: Re); inset right shows some highlighted weak reflections.

Table 4.1 Measurement data and refinement parameters of Sr_2InReO_6

Experiment	RT X-ray diffraction	RT neutron diffraction
Device	Siemens D5000	HIPD (LANSCE, LANL)
Formula sum	$Sr_2In_{0.97}Re_{1.03}O_6$	$Sr_2In_{0.98}Re_{1.02}O_6$
Crystal system	monoclinic	
radiation	$CuK\alpha_1$	pulsed neutrons
Space-group	$P2_1/n$ (14)	
Cell parameters	a =5.7157(4) Å, b =5.7199(3) Å, c =8.0837(6) Å, β =89.921(3)°	a = 5.70274(7) Å, b = 5.70343(7) Å, c = 8.06103(8) Å, β = 89.9029(5)°
Rwp, gof	5.38, 2.23	3.09, 2.88 for joint refinement

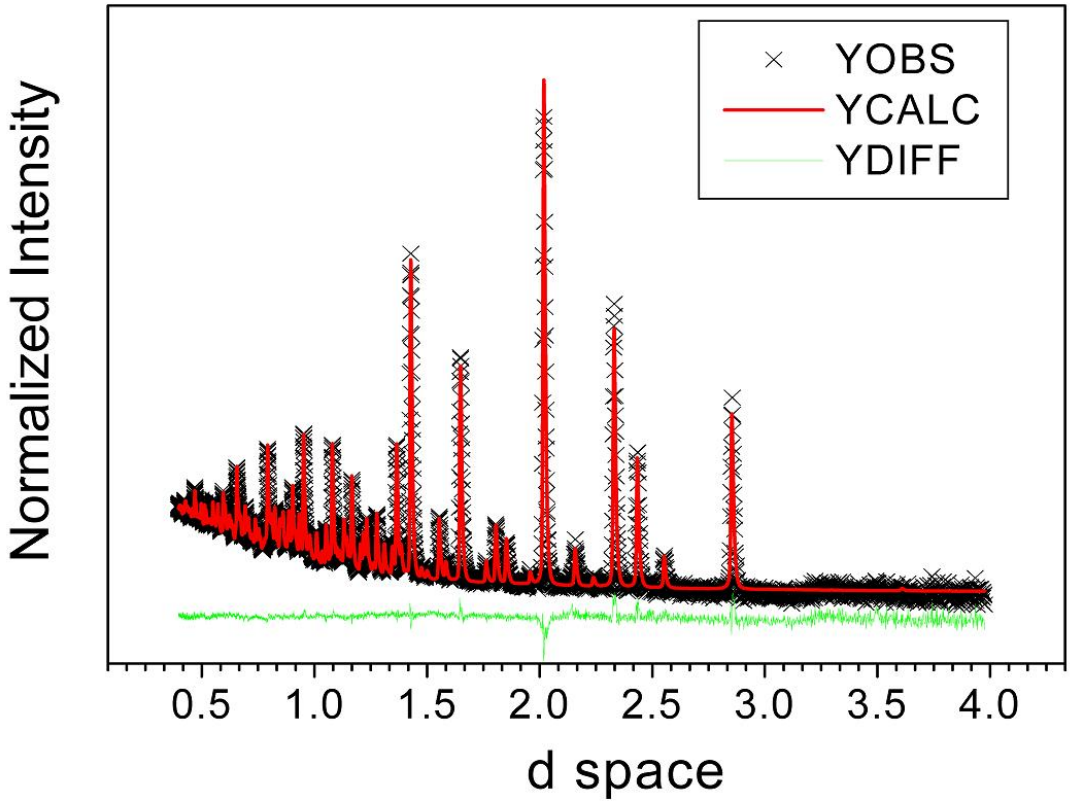

Figure 4.2 Rietveld fit from the NDP data of Sr_2InReO_6 at room temperature (black cross: observed, red line: calculated, green line: difference curve.

Table 4.2 Positional parameters of the crystal structure of Sr_2InReO_6 (X-ray diffraction: standard: upper; joint neutron diffraction data: below, in *italics*)

Atomic parameters						
Atom	**Site**	***x/a***	***y/b***	***z/c***	**sof**	**Beq *Ui*100***
Sr	4*e*	0.494(1) *0.4961(3)*	0.5238(2) *0.5247 (1)*	0.2443(8) *0.2546(4)*	1	1.1 *0.91*
In1	2*c*	0	1/2	0	0.967(5) *0.977(3)*	1.1 *0.61*
Re1	2*c*	0	1/2	0	0.033(5) *0.023(3)*	1.1 *0.61*
In2	2*d*	1/2	0	0	0.00(1) *0.0*	1.1 *0.14*
Re2	2*d*	1/2	0	0	1.00(1) *1.0*	1.1 *0.14*
O1	4*e*	0.3034(1) *0.3000(3)*	0.288(1) *0.2803(4)*	0.037(2) *0.02935(2)*	1	1.1 *1.23*
O2	4*e*	0.216(1) *0.2317(2)*	0.796(1) *0.7821(3)*	0.032(2) *0.0354(2)*	1	1.1 *0.4*
O3	4*e*	0.570(2) *0.5661(3)*	-0.013(2) *-0.0114(3)*	0.2413(7) *0.2361(3)*	1	1.1 *1.06*

Table 4.3 Selected Chemical bonds (*d*: atomic distance)

Atom 1	Atom 2	*d*(Å)
In	O1	2.1342(2)
	O2	2.1014(2)
	O3	2.1608(3)
Re	O1	1.9778(2)
	O2	1.9918(1)
	O3	1.9418(3)

4.3.2 Electronic structure

On the *GGA* level, Sr_2InReO_6 is a (half-)metal (c.f. Figure 4.3 (a)) irrespective of the crystal structure type, i.e. either cryolite or elpasolite. This result is mostly due to the absence of proper treatment of the on-site electron-electron interaction. On the other hand, already a Hubbard splitting of U = 2eV (*GGA* + *U*) opens up a band gap in case of the cryolite type structure model (c.f. Figure 4.3 (b)), while any computation based on the elpasolite structure type with considering a Hubbard splitting of U up to 3eV (*GGA* + *U*) and even spin-orbit coupling (*GGA* + *SOC*) leads to a (half-)metallic state. This finding is easily explained in terms of the high degeneracy in cubic symmetry, which results in large bandwidths and the metallic state due to $W > U$ in terms of the Hubbard model.

The bands close to the Fermi level are formed from the Re_*5d* and O_*2p* states. The original Re *5d* states form three bands, one above and two directly below the Fermi level. The latter ones formally accommodate two unpaired electrons, giving rise to a total momentum of approximately 2 μ_B. This situation corresponds to a localized state with two non-degenerate electrons on the Re^{5+} centers.

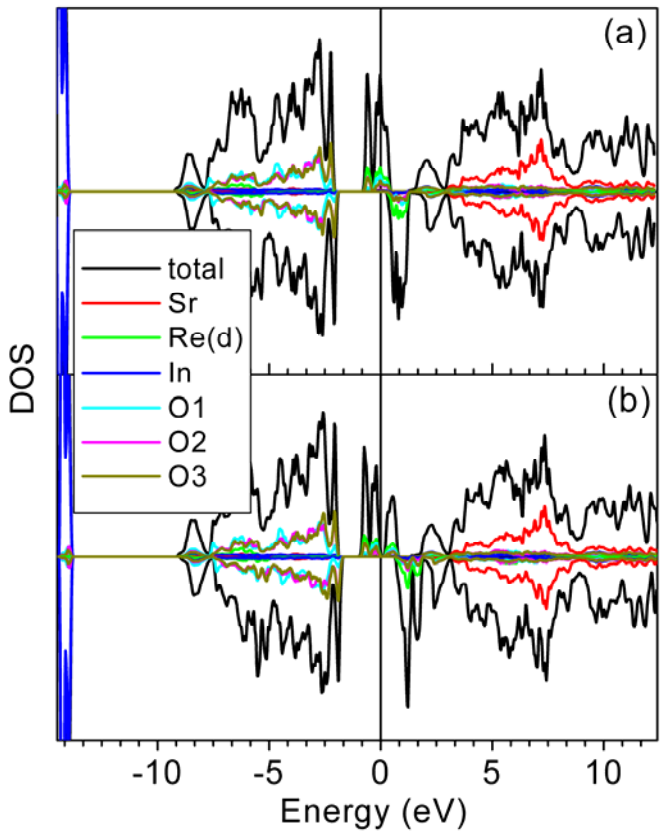

Figure 4.3 Density of states calculated for Sr_2InReO_6: (a) *GGA* method, (b) *GGA* + *U*(2eV), and only Re-*d* states is selected.

4.3.3 Conductivity measurement

The conductivity measurement was performed in the temperature range from 2–390 K. Due to the large resistivity of Sr_2InReO_6, the cooling measurement was interrupted at 132 K (c.f. Figure 4.4). The temperature-dependent electrical transport behavior of Sr_2InReO_6 fits to ln(ρ) vs. $T^{-1/4}$ (c.f. inset in Figure 4.4), indicating a variable range hopping (VRH) type of transport. This is in good agreement with the findings of the electronic structure investigations. The 5*d* electrons of the Re atoms are localized, the In atoms block the In–O–Re–O–In interaction pathway in Sr_2InReO_6 due to their close-shell configuration and the lack of or *d* states in an appropriate energy window and the tilting of the MO_6-octahedra hinders electron hopping from Re via O to the adjacent other metal ions. This resembles the situation reported for Sr_2MgReO_6 (Re, $5d^1$), a ferromagnetic insulator.[23] Therefore, Sr_2InReO_6 might be better described as a Mott-insulator like Ba_2NaOsO_6.[11]

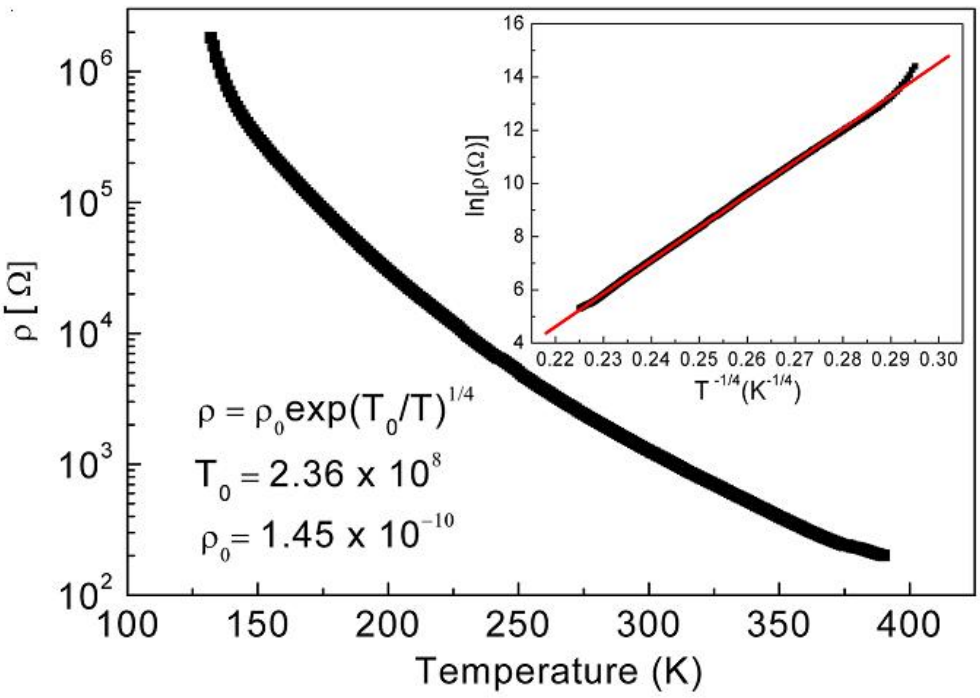

Figure 4.4 Temperature dependence of the resistivity of Sr_2InReO_6. The inset shows the VRH fit (black: experiment, red: fit).

4.3.4 Magnetic measurement

At a first glance, the magnetization measurement of Sr_2InReO_6 (c.f. Figure 4.5) appear to be a "Pauli-paramagnetic" behavior except a small hysteresis. However, this small hysteresis distinguishes Sr_2InReO_6 from simple Pauli-paramagnetic metals such as $SrMoO_3$[24, 25] and Sr_2VMoO_6.[26] Yet, the field cooled magnetization curve (FC) and the zero field cooled magnetization curve (ZFC) differ remarkably. The ZFC curve exhibits a cusp at around 40 K that turns less pronounced upon increasing field (c.f. Figure 4.5 (b)). According to a Curie–Weiss fit, the effective moment and the Weiss temperature are μ_{eff} = 1.5 μ_B and θ = -182 K, respectively. The effective moment is notably lower than the spin-only value (μ = 2.83 μ_B) due to spin-orbit coupling. Despite the strong antiferromagnetic interaction, as depicted by the high value of the Weiss temperature, Sr_2InReO_6 does not reach an antiferromagnetic state at temperatures above 5 K. *AC*-magnetometry data reveal no dependence of the susceptibility upon the frequency. Therefore, Sr_2InReO_6 is best described as a magnetically frustrated system lacking long range

order due to the *fcc* arrangement of the magnetic moments localized on the Re^{5+} cations. This situation is in line with the experimental data of Sr_2ScReO_6[16] and Sr_2YReO_6.[27]

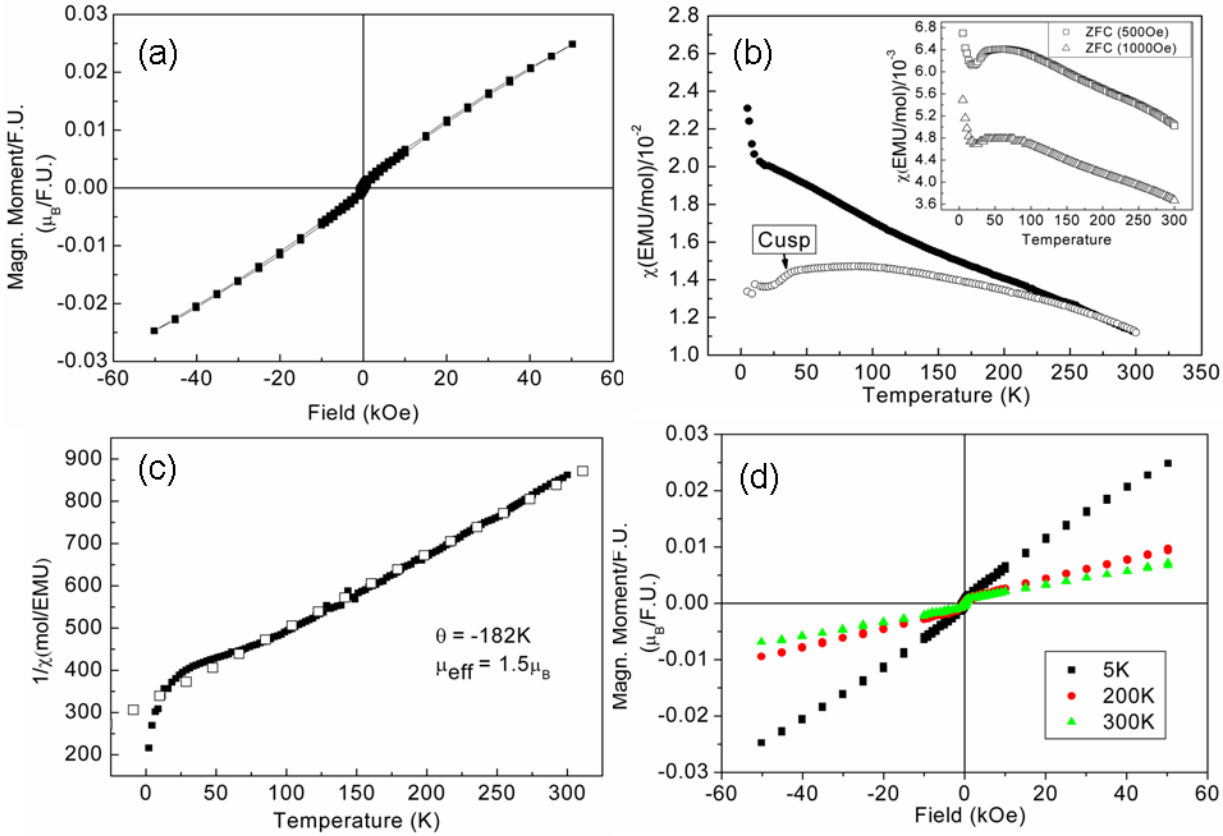

Figure 4.5 (a) *dc* magnetization measurement for Sr_2InReO_6 as a function of the applied field at T = 5 K, (b) *dc* magnetic susceptibility for H=100 Oe (inset: □ ZFC at H = 500 Oe, Δ ZFC at H = 1000 Oe), (c) ■ Inverse susceptibility (H = 1 T) vs. reciprocal temperature, □ linear fit of inverse susceptibility, (d) hysteresis at different temperatures. The data are well described by the Curie–Weiss law at high temperatures, $\chi = C/(T - \theta)$, where the Curie constant C is proportional to the square of the effective magnetic moment and the Weiss temperature θ is a measure of the strength and type of near-neighbor magnetic interaction. Deviations from this behavior occur only at low temperatures.

4.3.5 Heat capacity

The heat capacity of Sr_2InReO_6 (c.f. Figure 4.6) does not show any dependence on the applied external magnetic field. The low temperature data fit to $C_p(T) = \gamma \cdot T + \beta \cdot T^3$, with γT and βT^3

describing the electronic and the lattice contribution to the heat capacity, respectively.[28] Even if the electronic contribution is purely magnetic, the magnetic entropy at the vicinity of the cusp in the magnetic susceptibility is approx. $S_m = \int_0^T \frac{C_m}{T'} dT' \approx \gamma \cdot 40$ K = 0.9652 $Jmol^{-1}K^{-1}$, which is about 11% of the value expected for a spin-glass, i.e. $S_m = R \cdot \ln(2S+1) = 9.1344$ $Jmol^{-1}K^{-1}$. Thus, the *fcc* arrangement of Re^{5+} ($5d^2$) leads to a geometrically frustrated spin system and prevents long range magnetic order, but does not trigger the formation of a spin glass state.

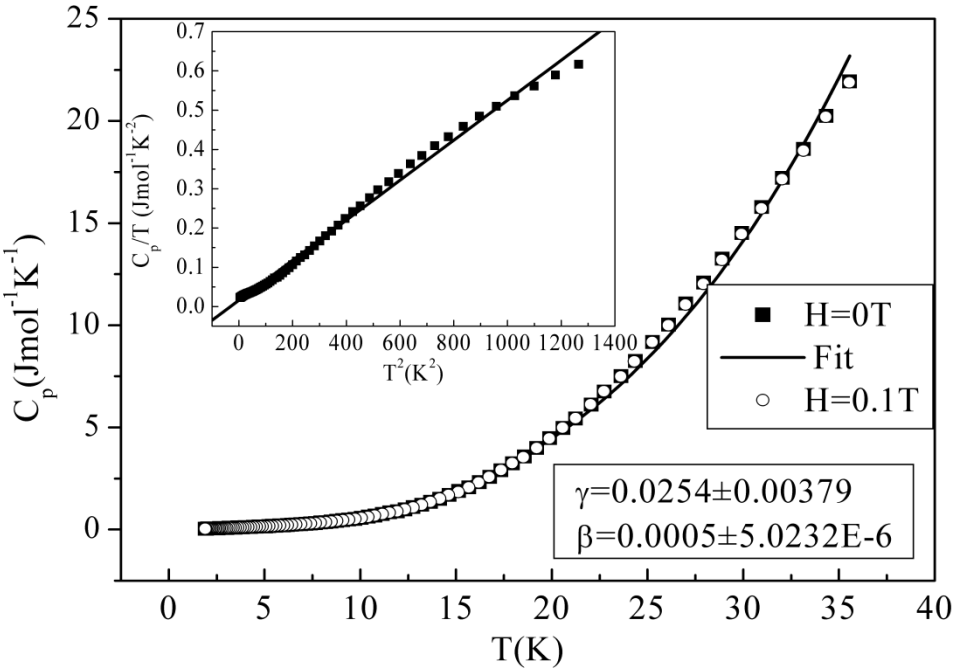

Figure 4.6 Heat capacity as a function of temperature and field for Sr_2InReO_6. The solid line is the best fit to $C_p = \gamma T + \beta T^3$, with $\gamma = 0.0254$ J/(K^2mol) and $\beta = 0.0005$ J/(K^4mol). The inset shows the same data and fit plotted as C_p/T.

4.4 Conclusion

The crystal structure of Sr_2InReO_6 has been carefully investigated and revised. The physical properties of Sr_2InReO_6 are studied with respect to the electronic structure, electrical transport properties, magnetism and low temperature heat capacity of the material. According to previously reported structure model of Sr_2InReO_6, all computations of the electronic structure predict a (half-)metallic state irrespective of the level of quality of computation. Electronic structure determination on the level of quality of the *GGA + U* approximation

converges to a Mott-insulator if the revised crystal structure model, i.e. the cryolite structure type, is taken into account. Sr_2InReO_6 exhibits a variable range type hopping transport behavior. The *fcc* arrangement of the Re^{5+} ions leads to geometrically frustrated spin system with complex magnetic behavior that lacks long range order but does not form a spin glass.

References

[1]W. E. Pickett, Phys. Rev. B **57**, 10613 (1998).

[2]R. E. Rudd, W. E. Pickett, Phys. Rev. B **57**, 557 (1998).

[3]H. Q. Yin, J. S. Zhou, J. P. Zhou, R. Dass, J. T. McDevitt, J. B. Goodenough, Appl. Phys. Lett. **75**, 2812 (1999).

[4]K. I. Kobayashi, T. Kimura, H. Sawada, K. Terakura, Y. Tokura, Nature **395**, 677 (1998).

[5]K. I. Kobayashi, T. Kimura, Y. Tomioka, H. Sawada, K. Terakura, Y. Tokura, Phys. Rev. B **59**, 11159 (1999).

[6]H. Kato, T. Okuda, Y. Okimoto, Y. Tomioka, Y. Takenoya, A. Ohkubo, M. Kawasaki, Y. Tokura, Appl. Phys. Lett. **81**, 328 (2002).

[7]J. M. De Teresa, D. Serrate, C. Ritter, J. Blasco, M. R. Ibarra, L. Morellon, W. Tokarz, Phys. Rev. B **71**, 092408 (2005).

[8]P. Majewski, S. Geprags, O. Sanganas, M. Opel, R. Gross, F. Wilhelm, A. Rogalev, L. Alff, Appl. Phys. Lett. **87**, 202503 (2005).

[9]Y. Krockenberger, M. Reehuis, M. Tovar, K. Mogare, M. Jansen, L. Alff, J. Magn. Magn. Mater. **310**, 1854 (2007).

[10]Y. Krockenberger, K. Mogare, M. Reehuis, M. Tovar, M. Jansen, G. Vaitheeswaran, V. Kanchana, F. Bultmark, A. Delin, F. Wilhelm, A. Rogalev, A. Winkler, L. Alff, Phys. Rev. B **75**, 020404 (2007).

[11]K. W. Lee, W. E. Pickett, EPL (Europhysics Letters) **80**, 37008 (2007).

[12]C. Azimonte, J. C. Cezar, E. Granado, Q. Huang, J. W. Lynn, J. C. P. Campoy, J. Gopalakrishnan, K. Ramesha, Phys. Rev. Lett. **98**, 017204 (2007).

[13]J. M. Michalik, J. M. D. Teresa, C. Ritter, J. Blasco, D. Serrate, M. R. Ibarra, C. Kapusta, J. Freudenberger, N. Kozlova, EPL (Europhysics Letters) **78**, 17006 (2007).

[14]J. M. D. Teresa, J. M. Michalik, J. Blasco, P. A. Algarabel, M. R. Ibarra, C. Kapusta, U. Zeitler, Appl. Phys. Lett. **90**, 252514 (2007).

[15]P. Majewski, S. Geprags, A. Boger, M. Opel, L. Alff, R. Gross, J. Magn. Magn. Mater. **290-291**, 1154 (2005).

[16]A. Winkler, N. Narayanan, D. Mikhailova, K. G. Bramnik, H. Ehrenberg, H. Fuess, G. Vaitheeswaran, V. Kanchana, F. Wilhelm, A. Rogalev, A. Kolchinskaya, L. Alff, New Journal of Physics **11**, 073047 (2009).

[17]A. Jung, I. Bonn, V. Ksenofontov, M. Panthofer, S. Reiman, C. Felser, W. Tremel, Phys. Rev. B **75**, 184409 (2007).

[18]A. Jung, V. Ksenofontov, S. Reiman, H. Therese, U. Kolb, C. Felser, W. Tremel, Phys. Rev. B **73**, 144414 (2006).

[19]A. Jung, I. Bonn, V. Ksenofontov, G. Melnyk, J. Ensling, C. Felser, W. Tremel, J. Mater. Chem. **15**, 1760 (2005).

[20]A. W. Sleight, J. Longo, R. Ward, Inorg. Chem. **1**, 245 (1962).

[21]A. Coelho, TOPAS Academic V1.0 (2004).

[22]M. W. Lufaso, P. W. Barnes, P. M. Woodward, Acta Crystallogr., Sect. B **62**, 397 (2006).

[23]J. B. Goodenough, Rep. Prog. Phys. **67**, 1915 (2004).

[24]G. H. Bouchard, M. J. Sienko, Inorg. Chem. **7**, 441 (1968).

[25]I. Nagai, N. Shirakawa, S.-i. Ikeda, R. Iwasaki, H. Nishimura, M. Kosaka, Appl. Phys. Lett. **87**, 024105 (2005).

[26]P. Karen, A. R. Moodenbaugh, J. Goldberger, P. N. Santhosh, P. M. Woodward, J. Solid State Chem. **179**, 2120 (2006).

[27]T. Aharen, J. E. Greedan, C. A. Bridges, A. A. Aczel, J. Rodriguez, G. MacDougall, G. M. Luke, V. K. Michaelis, S. Kroeker, C. R. Wiebe, H. Zhou, L. M. D. Cranswick, Phys. Rev. B **81**, 064436 (2010).

[28]M. Bieringer, J. E. Greedan, G. M. Luke, Phys. Rev. B **62**, 6521 (2000).

5 Sr_2GaReO_6: When Disorder Triggers Conductivity in an Intrinsic Insulator

5.1 Introduction

Oxides of the double perovskite type of $A_2MM'O_6$ (A = divalent cation or rare earth, *M/M′* = transition metal) have recently received much attention due to their intriguing physical properties and potential technological applications.[1-3] The two most prominent examples are Sr_2FeMoO_6[4] and Sr_2FeReO_6[5] with half-metallic ferrimagnetic behavior at room temperature, which makes them prospective magnetoelectronic compounds.

In order to elucidate the exchange mechanism between *M* and *M′* in double perovskites, some efforts were made to replace the variable-valence transition metal ions by rigid-valence elements, e.g. by substituting Fe with Zn and Re with Sb in Sr_2FeReO_6.[6, 7] Recently, disorder was found in Ga-substituted solid solutions $Sr_2Fe_{(1-x)}Ga_xReO_6$ due to size similarity between Ga^{3+}, Fe^{3+} and Re^{5+} cations, leading finally to a phase separation.[8] Although Sr_2GaReO_6, the end member of the solid solution series, does not contain any magnetic metals, such as Fe, Co and Ni, band structure calculations (*GGA*) predicted this material to be a half-metal with highly spin-polarized Re–O states and Ga *p* states situated above the Fermi-level.[8] However, the ordered Sr_2InReO_6 is found to be a Mott-insulator with spin frustration behavior, where the Re ions are isolated and no connectivity between one another. In contrast to three dimensional connections of Re in ReO_3, the adjacent Re ions in ordered Sr_2GaReO_6 are supposed to have a similar arrangement to those in Sr_2InReO_6. Whereas, Sr_2GaReO_6 is expected to be subject to a great amount of anti-disorder of Re/Ga, as found in $Sr_2Fe_{1-x}Ga_xReO_6$. This disorder effect would accordingly impact the properties of the material. Therefore, it is intriguing to fabricate and investigate Sr_2GaReO_6. Here, the synthesis and the characterizations are presented for Sr_2GaReO_6.

5.2 Experimental section

Synthesis: Sr_2GaReO_6 was synthesized by high temperature solid state reactions. The starting compounds SrO, Ga_2O_3, Re and Re_2O_7 (all purities above 99.9%) were weighed and mixed thoroughly inside a glovebox. In order to prevent an attack of SrO on the quartz tube, the pressed

pellets were transferred subsequently into corundum containers and finally sealed in evacuated quartz tubes. The samples were annealed for 50 hours at 1423 K. Thereafter, the ampoules containing the samples were either rapidly cooled to room temperature by quenching in a liquid nitrogen bath or cooled down naturally.

Characterization: X-ray diffraction measurement was performed on a Siemens D5000 powder diffractometer with a Braun M50 position sensitive detector and $CuK_{\alpha 1}$ radiation [Ge(220) monochromator]. Rietveld refinement was performed with TOPAS Academic V4.1[9] applying the fundamental parameter approach.

Neutron powder diffraction patterns were obtained on the high intensity powder diffractometer (HIPD) at the Lujan Neutron Scattering Center at the Los Alamos Neutron Science Center LANSCE. The refinement of the crystal structure was performed by the Rietveld method, using the GSAS refinement program for joint refinement of the X-ray- and the neutron-diffraction data.

Magnetometry was performed using the Quantum Design MPMS-XL SQUID magnetometer.

The electrical resistivity (ρ) measurement was carried out by using a PPMS (Quantum Design) device. For the measurement, a pellet was used. After pressed and re-heated (to make the pellet denser), the pellet was contacted with silver epoxy paste.

Band structure calculations: The band structure calculations were performed using the full-potential augmented plane-wave (FLAPW) within framework of the generalized gradient approximation (*GGA*) through the WIEN2k software package. The calculations were carried out by using the structural parameters obtained from the Rietveld refinements. The number of *k* points in the irreducible Brillouin Zone was 20, and the convergence criterion was fixed to 0.0001 Ry.

5.3 Results and discussion

5.3.1 Structural characterization

Sr_2GaReO_6 was previously reported by Sleigh *et al.* in 1960s. In their study, Sr_2GaReO_6 was thought to crystallize in the cubic double perovskite structure type (*cF*40, *Fm*-3*m*).[10] The X-ray diffraction pattern of the quenched samples and those samples cooled down naturally were

virtually identical. Therefore, all refinements were performed using an unquenched sample. Weak Bragg intensities (see Figure 5.1) at *1/d* ≈ 0.217 and *1/d* = 0.253 clearly indicate the presence of an ordered superstructure variant of the so called double perovskite type. All reflections can be indexed according to the cubic elpasolite type (a = 7.8484(2) Å). The observed reflection profiles are slightly asymmetric but do not show any hints towards a reflection splitting corresponding to a tetragonal distortion. In order to ascertain the correct symmetry, Rietveld refinements were performed according to idealized starting models of Sr_2GaReO_6 (using SPuDS[11]) in the Elpasolite-structure type (*cF*10), the Sr_2CuWO_6 structure type (*tI*10) and the Cryolite structure type (*mP*10). All refinements were carried out using TOPAS Academic V4.1,[9] applying the fundamental parameter approach. Already at early stages of the refinement, it became clear that (i) corrections for strain had to be applied irrespective of the crystal system, (ii) there was a pronounced anti-site disorder of Re and Ga and (iii) the ratio of Re to Ga was approximately 1.1 / 0.9. The parameter data of X-ray refinement are presented in Table 5.1.

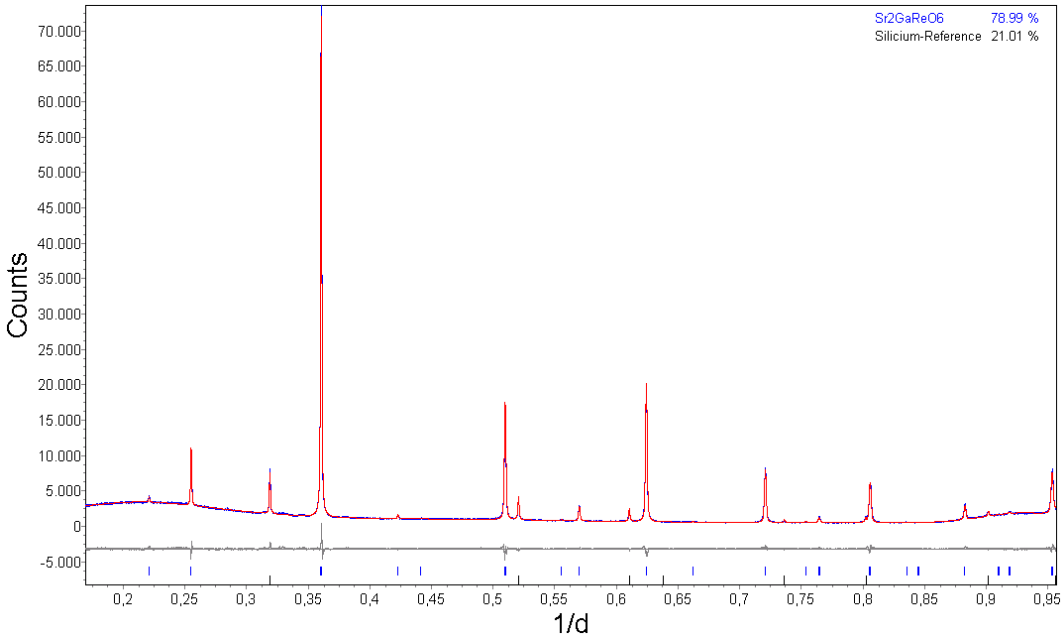

Figure 5.1 X-ray powder diffraction pattern of Sr_2GaReO_6 at ambient conditions (blue: experiment, red: fit from Rietveld-refinement, grey: difference curve, blue tics indicate the Bragg reflections positions, all intensities are in square root scale in order to emphasize the weak reflections)

Considering the number of parameters, the number of reflections, and the final residuals (R_{wp}) and goodness of fit (*gof*), the elpasolite structure type model (R_{wp} = 4.751; *gof* = 1.829; 29 Parameters; 23 Bragg reflections) and the Sr_2CuWO_6 structure type model (*Rwp* = 4,583; *gof* = 1.825; 32 parameters; 65 Bragg reflections) are virtually at the same level of quality, while the Cryolite structure type model (R_{wp} = 4.453; *gof* = 1.775; 44 parameters, 225 reflections) does not lead to a significantly improved refinement and may be ruled out from consideration. Due to the problem of handling very different numbers of overlapping reflections in powder diffraction, the significance tests according to Hamilton[12] were not able to help to select the better fit from both the elpasolite structure type and the Sr_2CuWO_6 structure type. On the other hand, the Sr_2CuWO_6 structure model refines only to chemically meaningful *M*–O distances if bond length restraints (GRS series on O–O interaction)[9] are taken into account. Thus, the elpasolite structure type is the most reasonable structure model according to the present data.

Table 5.1 Positional parameters: X-ray Diffraction at room temperature, space group: *Fm*-3*m*, *a* = 7.8484(2) Å, refined composition $Sr_2Ga_{0.90}Re_{1.10}O_6$.

Atomic parameters					
Atom	**Site**	***x/a***	***y/b***	***z/c***	***sof***
Sr	4e	0.25	0.25	1	1
Ga1	2c	0	0	0	0.5863(3)
Re1	2c	0	0	0	0.4137(3)
Ga2	2d	0.5	0	0	0.3102(3)
Re2	2d	0.5	0	0	0.6898(3)
O	4e	0.24987(7)	0	0	1

The structure exhibits a considerable amount of anti-site disorder, which is close to (but still distinguishable from) an entirely statistical distribution of Ga^{3+} and Re^{5+} cations on the *M* and *M′* cations sites. Accordingly, the Ga–O and Re–O bond-lengths in Sr_2GaReO_6 are virtually identical (1.961(6) Å and 1.963(6) Å, respectively)

The neutron diffraction structural refinements are shown in Figure 5.2 and structural parameters are summarized in Table 5.2 and Table 5.3 respectively for 495 K and 5 K. At 5 K,

this material is found to crystallize in the Sr_2CuWO_6 tetragonal structure type with a space group *I*4/*m*. The low temperature structure is in contrast to the X-ray diffraction results as well as high temperature neutron diffraction. In the high temperature neutron data, Sr_2GaReO_6 is found to be a cubic phase with a space group *Fm*-3*m*. A comparison between LT-PND and HT-PND is shown in inset in Figure 5.2 (b). The LT-PND measurement does not exhibit any indications for a magnetic ordering. All structural characterizations suggested a chemical composition $Sr_2Ga_{0.92}Re_{1.08}O_6$, a bit different from ideal Sr_2GaReO_6.

Table 5.2 Positional parameters: Neutron Diffraction at 5 K, space group: *I*4/*m*, *a* = 5.52887(6) Å, *b* = 5.52887(6) Å, *c* = 7.84294(2) Å, refined composition $Sr_2Ga_{0.92}Re_{1.08}O_6$.

Atomic parameters					
Atom	**Site**	**x/a**	**y/b**	**z/c**	**sof**
Sr	4d	0	0.5	0.25	1.00(0)
Ga1	2a	0	0	0	0.600(9)
Re1	2a	0	0	0	0.399(1)
Ga2	2b	0	0	0.5	0.320(1)
Re2	2b	0	0	0.5	0.679(9)
O1	4e	0	0	0.2557(6)	1.00(0)
O2	8h	0.2737(8)	0.2338(7)	0	1.00(0)

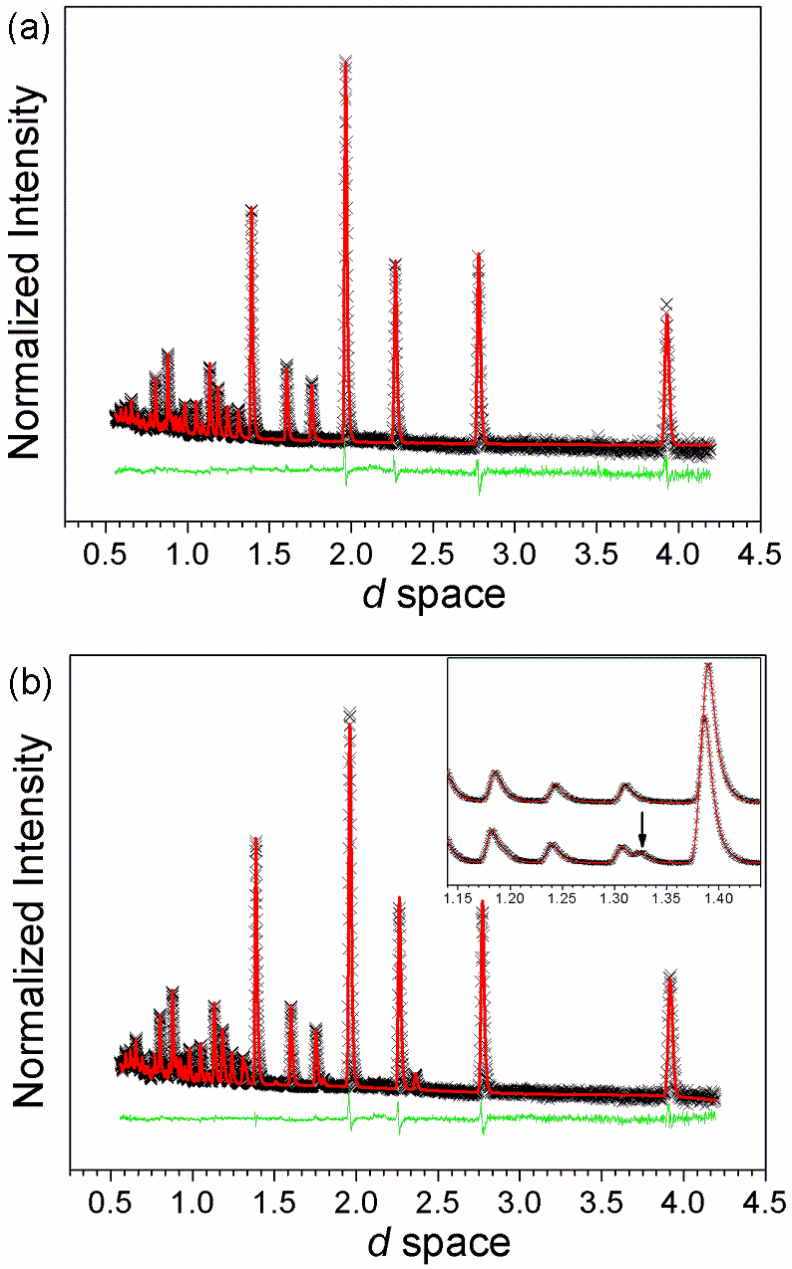

Figure 5.2 Rietveld fit from the NDP data of Sr_2GaReO_6 (black cross: observed, red line: calculated, green line: difference curve): (a) at 495 K and (b) at 5 K; inset is the highlight at range 1.15 – 1.45 Å for 495 K (upper) and 5 K (below).

5.3.2 Conductivity measurement

The conductivity measurement was performed in the temperature range from 2–400 K. The temperature-dependent electrical transport behavior of Sr_2GaReO_6 indicates that this material is a

semiconductor. The conductivity of Sr_2GaReO_6 obeys neither a variable range hopping model nor an Arrhenius-like model. The anomaly around 225 K arose from an experimental artifact and did no imply any intrinsic physical properties of the material (Figure 5.3). The local distortion might always exist within the temperature range but just locally.[16] Therefore, no corresponding temperature-dependent physical properties were detected with respect to transport or magnetism in spite of a structural change from 5 K to room temperature.

The electrical transport properties might be explained by electron hopping between the Re^{5+} sites. If there is no anti-site disorder in Sr_2GaReO_6, there is neither a Re–O–Re path nor a Re–O–Ga–O–Re path available. In this case, electron hopping is only possible directly between the Re^{5+} cations along the face diagonal of the cubic unit cell.[8] As the 5*d* orbitals of Re are not diffuse, the corresponding overlap is low. Thus, electron hopping requires a comparably high activation energy. This corresponds to the situation observed in the Mott-insulator Sr_2InReO_6. Taking the amount of anti-site disorder into account and assuming a binomial distribution, one finds that more than half of the Re^{5+} cations in Sr_2GaReO_6 are surrounded by $\{O_6Re\}$- and $\{O_6Ga\}$- units, respectively, instead of exactly six $\{O_6Ga\}$-units. As a result, electron hopping can take place between Re^{5+} cations on neighboring *M* and *M′* sites in a way close to a completely disordered simple perovskite $SrGa_{½}Re_{½}O_3$.

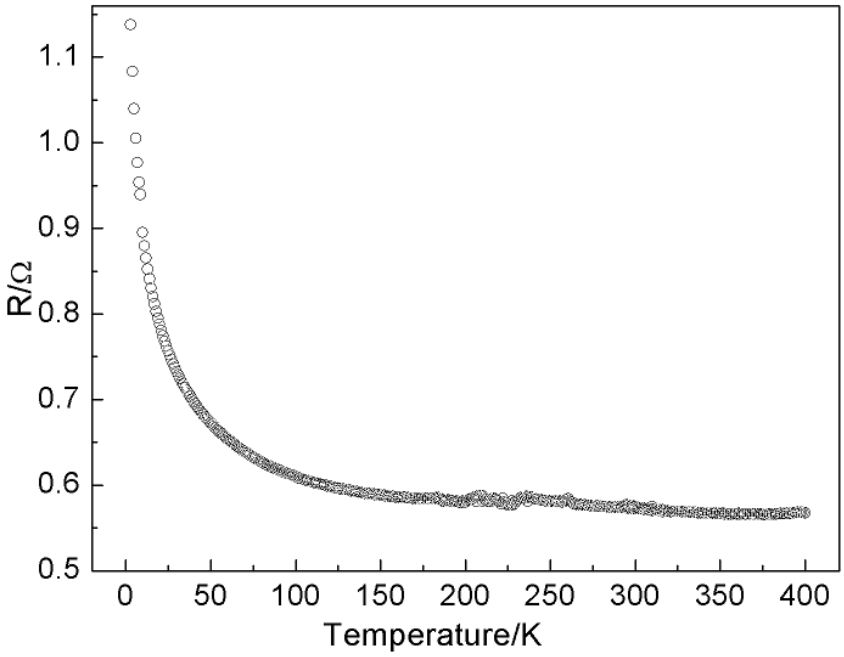

Figure 5.3 Resistivity of Sr_2GaReO_6 versus temperature

5.3.3 Magnetic measurement

The magnetic susceptibility for Sr_2GaReO_6 was measured under magnetic fields of 100 Oe and 1000 Oe. No long-range order is observed. However, hysteresis behavior and FC/ZFC divergence was found. This is more prominent in the 100 Oe data. And the data do not show the typical maximum in susceptibility versus temperature for antiferromagnetic long-range ordering (see Figure 5.4 (a) and (b)).The magnetization measurement indicates that no saturation of the magnetization is reached at 5 K. A small hysteresis is observed in the field-dependent data (see Figure 5.4 (c)). Reciprocal susceptibility at H = 0.1 T suggests Curie–Weiss behavior: Weiss temperature θ = -183 K and effective moment (μ_{eff}) = 0.96 μ_B (Figure 5.4 (d)). The large and negative Weiss temperature is indicative of strong antiferromagnetic interactions.

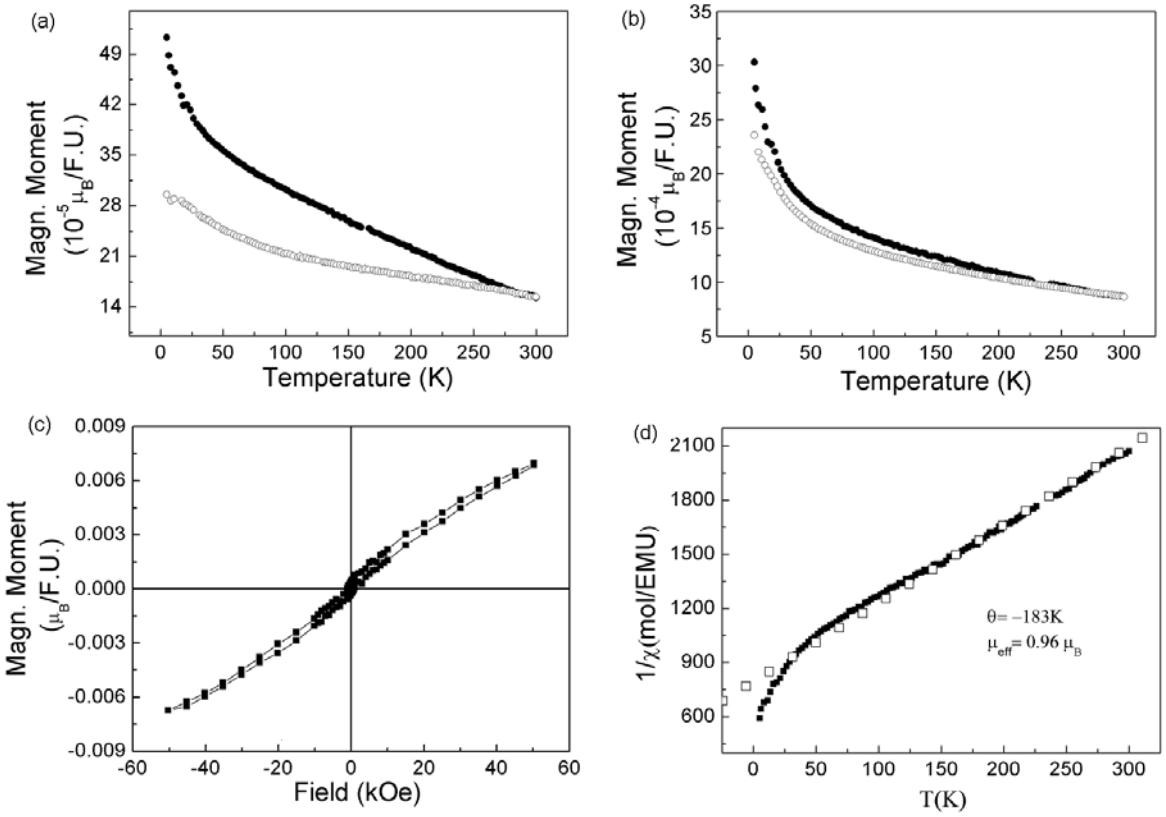

Figure 5.4 (a) *dc* magnetic susceptibility for H =100 Oe (inset H = 500 Oe), (b) *dc* magnetic susceptibility for H = 1000 Oe, ● FC curve and ○ZFC curve, (c) *dc* magnetization measurement for Sr_2GaReO_6 as a function of the applied field at T = 5 K, (d) ■ Inverse susceptibility (H = 0.1 T) vs. reciprocal temperature, □ linear fit of inverse susceptibility. The data are well described by the Curie–Weiss law at high temperatures, $\chi = C/(T-\theta)$, where the Curie constant C is proportional to the square of the effective magnetic moment and the Weiss temperature θ is a measure of the strength and type of near-neighbor magnetic interaction.

A hysteresis relaxation measurement was carried out at 10 K, 50 K, and 100 K. The sample was cooled in the absence of a magnetic field and, after switching on an external magnetic field of 1 T, magnetic susceptibility data were collected over a time of approximately 200 minutes. At 10 K and 50 K, a bi-exponential saturation behaviour is observed, whereas at 100 K no saturation can be seen. The absence of magnetic saturation at 100 K suggested a cooperative magnetism below 100 K. The *dc*-magnetic relaxation measurement is shown in Figure 5.5.

The divergence between ZFC and FC[17] and magnetization relaxation suggest that a spin frustration may exist in Sr_2GaReO_6, arising from the ordering residues Re–O–Ga–O–Re, where Re^{5+} species carry a spin moment, forming a quasi *fcc* tetragonal configuration.[18, 19] The analogous magnetic properties were reported in Sr_2InReO_6,[20] Sr_2CaReO_6[14] and Sr_2MgReO_6.[15] However, these *M/M′* ordered compounds are all insulators like Sr_2MgReO_6.[21]

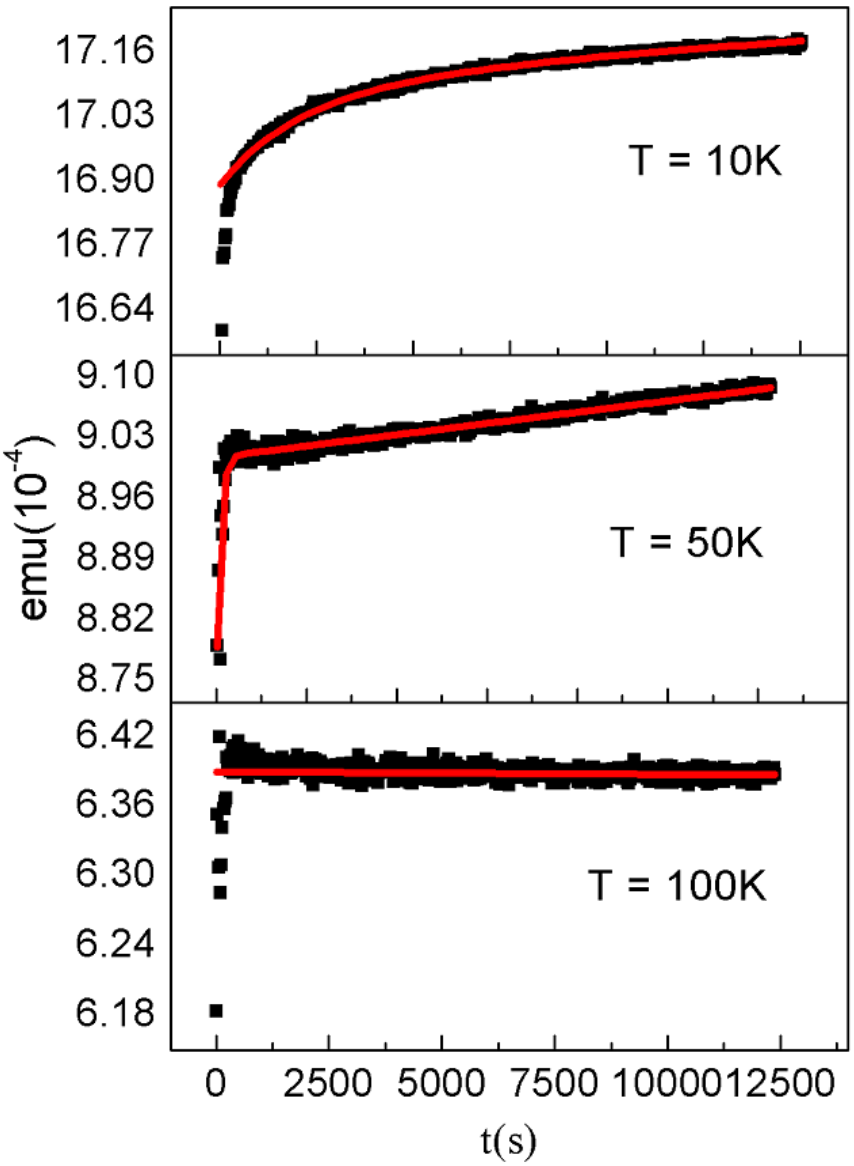

Figure 5.5 Magnetization relaxation measurement at 10 K, 50 K, and 100 K using an external magnetic field of H = 1 T. The data sets acquired are fitted using a bi-exponential relaxation function (black: experiment, red: fit).

5.3.4 Band structure

The study on Sr_2InReO_6 in last chapter indicates that the isolated Re in Sr_2MReO_6 gives rise to an Mott-insulating state within the framework of ordered Sr_2MReO_6.[22] In addition, the temperature dependence of the conductivity of Sr_2GaReO_6 shows a semiconducting feature. Therefore, the ordered Sr_2GaReO_6 is supposed to be a semiconductor or Mott-insulator like Sr_2InReO_6. The band structure calculation for Sr_2GaReO_6 was therefore performed based on the crystal structures model data obtained from structure analysis. In order to simplify the calculation, an ordered and ideal structure was explored, i.e. Ga/Re was 1:1 and 100% ordered. The band structure was computed based on tetragonal and cubic structure respectively. Both calculations gave rise to a very similar band structure. In general, the *GGA*, *GGA* + Hubbard *U*(3eV), and *GGA* + *SOC* (spin orbit coupling) all give rise to a metal and fail to produce a semiconducting band structure (not shown). These results are basically analogous to Jung's calculation.[8] However, when *GGA* + *SOC* + *U* was applied, a band gap was opened up in original t_{2g} degenerated band, indicative of semiconducting/insulating nature for Sr_2GaReO_6. A magnetic moment of 1.96 μ_B per unit cell was found, which is carried on Re. The band structure based tetragonal structure is shown in Figure 5.6.

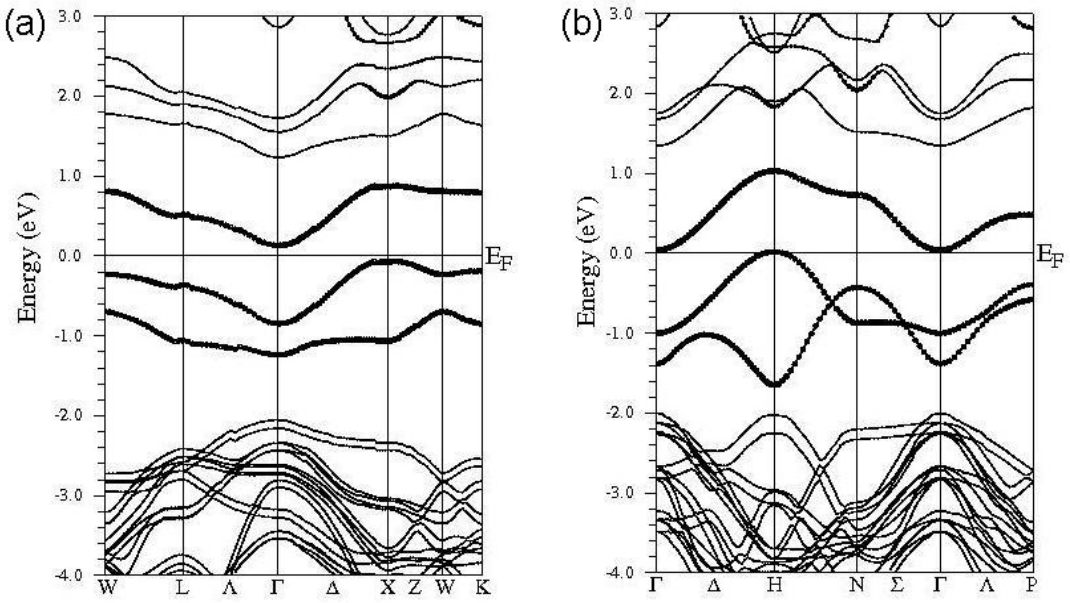

Figure 5.6 Band structure of Sr_2GaReO_6: (a) based on cubic structure, (b) based on tetragonal structure; both performed using method of *GGA* + *SOC* + *U*(3eV). The bands near E_F are highlighted in bold. In tetragonal structure two bands near below E_F are not completely split.

5.4 Conclusion

The study on Sr_2GaReO_6 indicates that this material crystallizes in two structures at different temperatures: cubic at 5 K and tetragonal at(above) room temperature. Sr_2GaReO_6 is subject to a significant disorder due to the similar cationic radii between Ga^{3+} and Re^{5+}. Such disorder leads to an increased conductivity in Sr_2GaReO_6. The locally ordered Ga/Re residues give rise to a spin frustration due to an *fcc* Re^{5+}-tetrahedral geometry configuration. The band structure calculation based on the structural results reproduces the intrinsic semiconducting nature for Sr_2GaReO_6 and suggests that overall magnetic moment in Sr_2GaReO_6 is from Re. This result supports the magnetic measurement, in which the antiferromagnetic interaction is found in this material.

References

[1]W. E. Pickett, Phys. Rev. B **57**, 10613 (1998).

[2]R. E. Rudd, W. E. Pickett, Phys. Rev. B **57**, 557 (1998).

[3]H. Q. Yin, J. S. Zhou, J. P. Zhou, R. Dass, J. T. McDevitt, J. B. Goodenough, Appl. Phys. Lett. **75**, 2812 (1999).

[4]K. I. Kobayashi, T. Kimura, H. Sawada, K. Terakura, Y. Tokura, Nature **395**, 677 (1998).

[5]K. I. Kobayashi, T. Kimura, Y. Tomioka, H. Sawada, K. Terakura, Y. Tokura, Phys. Rev. B **59**, 11159 (1999).

[6]A. Jung, V. Ksenofontov, S. Reiman, H. Therese, U. Kolb, C. Felser, W. Tremel, Phys. Rev. B **73**, 144414 (2006).

[7]A. Jung, I. Bonn, V. Ksenofontov, G. Melnyk, J. Ensling, C. Felser, W. Tremel, J. Mater. Chem. **15**, 1760 (2005).

[8]A. Jung, I. Bonn, V. Ksenofontov, M. Panthofer, S. Reiman, C. Felser, W. Tremel, Phys. Rev. B **75**, 184409 (2007).

[9]A. Coelho, TOPAS Academic V1.0 (2004).

[10]A. W. Sleight, J. Longo, R. Ward, Inorg. Chem. **1**, 245 (1962).

[11]M. W. Lufaso, P. W. Barnes, P. M. Woodward, Acta Crystallogr., Sect. B **62**, 397 (2006).

[12]A. Whitaker, J. W. Jeffery, Acta Crystallogr. **23**, 984 (1967).

[13]M. Bieringer, J. E. Greedan, G. M. Luke, Phys. Rev. B **62**, 6521 (2000).

[14]C. R. Wiebe, J. E. Greedan, G. M. Luke, J. S. Gardner, Phys. Rev. B **65**, 144413 (2002).

[15]C. R. Wiebe, J. E. Greedan, P. P. Kyriakou, G. M. Luke, J. S. Gardner, A. Fukaya, I. M. Gat-Malureanu, P. L. Russo, A. T. Savici, Y. J. Uemura, Phys. Rev. B **68**, 134410 (2003).

[16]E. S. Božin, M. Schmidt, A. J. DeConinck, G. Paglia, J. F. Mitchell, T. Chatterji, P. G. Radaelli, T. Proffen, S. J. L. Billinge, Phys. Rev. Lett. **98**, 137203 (2007).

[17]J. Winterlik, G. H. Fecher, C. Felser, C. Muhle, M. Jansen, J. Am. Chem. Soc. **129**, 6990 (2007).

[18]A. P. Ramirez, Annu. Rev. Mater. Sci. **24**, 453 (1994).

[19]J. E. Greedan, J. Mater. Chem. **11**, 37 (2001).

[20]H. Gao, M. Panthoefer, W. Tremel, 2010).

[21]A. Ferretti, D. B. Rogers, J. B. Goodenough, J. Phys. Chem. Solids **26**, 2007 (1965).

[22]H. Gao, A. Llobet, J. Barth, J. Winterlik, C. Felser, M. Panthoefer, W. Tremel, (to be submitted).

6 Half Metallic Double Perovskites, to Be or Not to Be?

6.1 Introduction

Double perovskites $A_2MM'O_6$ compounds (A = divalent cation or rare earth, *M/M′* = transition metal) have recently attracted much attention due to their novel physical properties and potential technological applications.[1-3] The two most prominent examples are Sr_2FeMoO_6[4] and Sr_2FeReO_6[5] with half-metallic ferrimagnetic behavior at room temperature, which makes them prospective magnetoelectronic compounds. For the polycrystalline materials low-field intergrain tunneling magnetoresistance (TMR) has been reported at room temperature.[1– 4] The conceptual basis for the observed half-metallic ferromagnetism is a large density of states of one spin direction at the Fermi level while the other spin direction is insulating.[6, 7]

People made many efforts to improve the TMR effect and to investigate the double exchange mechanism.[8] Quite a few reports have recently emerged that Fe and Re(Mo) in $Sr_2FeRe(Mo)O_6$ were substituted by closed-shell ions, such as $Sr_2FeMo_{(1-x)}Ta_xO_6$,[9] $Sr_2Fe_{(1-x)}Mg_xMoO_6$,[10] $Sr_2Fe_{(1-x)}Sc_xReO_6$,[11] $Sr2Fe_{(1-x)}Zn_xReO_6$,[12] $Sr_2Fe_{(1-x)}Ga_xReO_6$,[13] $Sr_2FeRe_{(1-x)}Sb_xO_6$[14] and $Sr_2FeRe_{(1-x)}Nb_xO_6$.[15] Some of the end members of the above solid solutions were also studied. The disordered Sr_2FeTaO_6 was reported as a spin glass material.[16] Sr_2FeSbO_6 was reported to be a insulator[14] with type I magnetic structure.[16] Whereas Sr_2GaReO_6 was surprisingly predicted to be a half-metallic magnet.[13] This type of materials contains only one transition element with partially filled *d* orbitals on either *M* or *M′* position and has a formula of A_2CMO_6, where A is the alkali earth metal, C signifies closed-shell elements and M stands for 4*d*/5*d* transition elements. Therefore, these compounds can be called *Double Perovskites Containing Unique Open-Shell Transition Ions*. There are many candidates such as Ba_2YMoO_6 ($4d^1$),[17] Ba_2YWO_6 ($5d^1$),[18] A_2MgReO_6 ($5d^1$),[19, 20] Ba_2CaReO_6 ($5d^1$),[21] Sr_2YReO_6 ($5d^2$),[22] Sr_2GaReO_6 ($5d^2$),[23] Ba_2NaOsO_6 ($5d^1$),[24, 25] Ba_2LiOsO_6 ($5d^1$),[25] Ba_2DySbO_6[26]. This series of compounds have some common features: (i) they are structurally ordered and the octahedra of open-shell elements form *fcc* tetrahedra; (ii) they are all semiconductors or Mott-insulators; (iii) they tend to be sujected to spin-frustration due to *fcc* geometry,[27, 28] except that Ba_2NaOsO_6 and Ba_2LiOsO_6 are magnetic insulators[24, 25] (iv) electronic structure of these materials are easily calculated to be half metals.

As matter of fact, to predict a half-metal turned out to be a challenge, if some detailed treatment is not carefully conducted. For instance, it was suggested that Rb_4O_6 should be a half-metallic ferromagnet with the magnetic moment carried by the hyperoxide anions and a Curie temperature above room temperature.[29] However the experimental data demonstrated that Rb_4O_6 is actually a magnetically frustrated system.[30] $Ca_3Co_2O_6$ was also computed to be a ferromagnetic half-metal at the beginning,[31] but Wu *et al*.[32] pointed out that $Ca_3Co_2O_6$ should be a Mott-insulator with Ising-like magnetism. Another Mott-insulator (ferromagnetic) Ba_2NaOsO_6 was readily calculated to be a half-metal without proper treatment of the parameters.[33]

Of all the diverse materials, A_2CMO_6 double perovskite compounds are highlighted and their electronic structures are investigated in the present study. Although these materials are mostly characterized to be semiconductors/insulators, their electronic structures unexceptionally exhibit half-metallic features whatever by means of generalized gradient approximation (*GGA*) calculations, *GGA* + *Hubbard U* or *GGA* + *SOC* (spin orbit coupling). Until *GGA* + *SOC* + *U* is applied,[34] the reasonable electronic structures are produced. Herein, it is demonstrated that the approach of *GGA* + *SOC* + *U* is necessary to calculate the reasonable electronic structure for the most of A_2CMO_6 type of double perovskites. In addition, a comparison is made between A_2CMO_6 with M = 4*d*/5*d*/*f* ions and A_2CMO_6 with M = 3*d* elements such as Sr_2MnSbO_6 ($3d^4$)[35, 36] and A_2CrSbO_6 (A = Sr, Ca: $3d^3$).[37] A great difference is demonstrated between the lighter 3*d* metals and heavier metals (4*d*/5*d*/*f*) within the framework of A_2CMO_6.

6.2 Computational details

Our first-principle *DFT* band structure calculations were performed by using the full-potential augmented plane wave plus local orbital method as implemented in the WIEN2k code.[38] The expansion in spherical harmonic of the radial wave functions was taken up to l = 10. The value of $R_{MT}^{\min} K_{\max}$ was set to 7. The number of k points in the irreducible Brillouin zone was 20 for all calculations. Four computational procedures were tested in order to reach the reasonable solution. The preliminary tests were always started with a full-potential generalized gradient approximation (*GGA*).[39] Thereafter, the approaches were applied in a sequence of *GGA* plus Hubarrd *U* (*GGA* + *U*),[40] *GGA* plus spin-orbit coupling (*GGA* + *SOC*),[32, 41] and *GGA* plus Hubarrd *U* plus spin-orbit coupling (*GGA* + *SOC* + *U*).[34] The experimental data given in Table 6.1 were explored. The convergence criterion was fixed to 0.0001 Ry.

6.3 Results and discussion

The discussion is started with Table 6.1. The measured crystal structures and lattice constants given in Table 6.1 were adopted in the calculations. According to the type of unfilled orbitals as well as number of electrons in these orbitals, the compounds are classified as following:

$4d^1$: Ba_2YMoO_6;

$4d^2$: Sr_2GaTcO_6;

$5d^1$:Ba_2YWO_6, Ba_2MgReO_6, Ba_2CaReO_6, Ba_2NaOsO_6;

$5d^2$: Ba_2CaOsO_6, Ba_2YIrO_6 (low spin);

$5d^3$: Ba_2YRuO_6, Ba_2InOsO_6;

4*f*: Ba_2DySbO_6, Ba_2HoSbO_6, Ba_2SmSbO_6, Ba_2EuSbO_6, Ba_2GdSbO_6, Ba_2TbNbO_6, Ba_2ErSbO_6;

5*f*: Ba_2InUO_6;

3*d*: Sr_2MnSbO_6, A_2CrSbO_6, (A=Sr and Ca).

For the 5*d* series compounds with $5d^1$, $5d^2$ and $5d^3$ electrons, the calculated magnetic moment increases with the number of electrons in unfilled orbitals (Table 6.1), and the calculated values are in fair agreement with measured. These results indicate that 5*d* electrons are located in A_2CMO_6 setting. The same observation is found for 4*f* and 3*d* open-shell compounds, namely Ba_2DySbO_6 Sr_2MnSbO_6, and A_2CrSbO_6. This phenomenon suggests that electrons in unfilled orbitals of transition ions are usually localized in the geometry of A_2CMO_6. According to the electronic structures by *GGA* and *GGA + U*, these compounds can be further divided into three types (Table 6.2).

As shown in Figure 6.1, Ba_2YMoO_6, Ba_2MgReO_6, Sr_2GaTcO_6, Ba_2CaOsO_6, Ba_2YIrO_6, and Ba_2DySbO_6 exhibit half metallicity in the preliminary *GGA* calculations. This type of materials belongs to type I. In the spin-up direction, the DOS of type I is metallic, comprising unfilled t_{2g}-states or *f*-states. The insulating spin-down states reveal a band gap of about 1 eV. Due to lack of *d* orbitals, the ions at *C* positions (Y, Mg, Ga, Ca and Sb) do not participate in the DOS near E_F. High spin polarization (100%) takes place in hybridized *d/f-O* states. The type I include also Ba_2DySbO_6, Ba_2SmSbO_6,[45] Ba_2ErSbO_6, and Ba_2HoSbO_6. Ba_2InUO_6 (5*f* compound) was also found to be a half metal with polarized *f-O* states and a broader DOS diffuse around E_F (not shown), so it also belongs to type I.

Table 6.1 Experimental data for the double perovskite compounds. M_{tot}^{calc} stands for the calculated magnetic moment (μ_B per formula moment).

Compound	Symmetry	Lattice constant (Å)	Type	M_{tot}^{calc}
Ba_2YMoO_6[17]	*Fm*-3*m*	*a*=8.39091(8)	magnetic frustration	0.99703
Ba_2YWO_6[18]	*Fm*-3*m*	*a*=8.378	magnetic frustration	0.97437
Ba_2GaTcO_6*	*Fm*-3*m*	*a*=7.918(9)	unknown	1.9988
Ba_2MgReO_6[19]	*Fm*-3*m*	*a*= 8.0847(1)	magnetic frustration	0.94729
Ba_2CaReO_6[42]	*Fm*-3*m*	*a*= 5.8961(1) *b*= 8.375(1)	magnetic frustration	1.01010
Sr_2MgReO_6[20]	*Fm*-3*m*	*a*=5.5350(6) *b*=7.9724(9)	magnetic frustration	1.00530
Sr_2GaReO_6[43]	*Fm*-3*m*	*a*= 7.843(3)	magnetic frustration	1.91841
Ba_2CaOsO_6[42]	*Fm*-3*m*	*a*= 8.344(5)	unknown	1.93269
Ba_2YIrO_6[44]	*Fm*-3*m*	*a*= 8.35032(9)	unknown	1.73576
Ba_2YRuO_6[45]	*Fm*-3*m*	*a*= 8.3390(5)	unknown	2.99299
Ba_2InOsO_6[23]	*Fm*-3*m*	*a*=8.378	unknown	3.00020
Ba_2DySbO_6[26]	*Fm*-3*m*	*a*=8.4247(1)	magnetic frustration	4.97248
Ba_2HoSbO_6[26]	*Fm*-3*m*	*a*=8.4119(1)	unknown	3.99935
Ba_2SmSbO_6[46]	*Fm*-3*m*	*a*= 8.50908(8)	unknown	5.00212
Ba_2EuSbO_6[47]	*Fm*-3*m*	*a*= 8.489(1)	unknown	5.72518
Ba_2GdSbO_6[48]	*Fm*-3*m*	*a*= 8.475(1)	unknown	6.93173
Ba_2TbNbO_6[49]	*I*4/*m*	*a*= 5.9816(1) *b*= 8.4757(2)	unknown	5.85604
Ba_2ErSbO_6[49]	*Fm*-3*m*	*a*= 8.3960(1)	unknown	3.00348
Ba_2InUO_6[50]	*Fm*-3*m*	*a*= 8.521	unknown	1.00007
Sr_2MnSbO_6[35, 36]	*I*4/*m*	*a*= 5.5313(4) *b*= 8.0832(7)	ferromagnetic due to disorder	4.01307
Sr_2CrSbO_6[37]	$P2_1n$	*a*= 5.762 (2) *b*= 5.5541(2) *c*= 7.8474(4)	Antiferromagmetic	3.00009

***** assumed values

Table 6.2 Three types of compounds of A_2CMO_6

Type	Characteristic	Example
I	Half metallic by *GGA*, and *GGA+ U*	Ba_2YMoO_6, Ba_2DySbO_6
II	Metallic by *GGA*, Half metallic by *GGA + U*	Ba_2YWO_6, Ba_2CaReO_6
III	Insulating by *GGA*	Ba_2YRuO_6, Ba_2GdSbO_6

For the $5d^1$ series of compounds (except Ba_2MgReO_6), the *GGA* calculations indicate that these materials are not 100% spin polarized. *GGA* depicts them to be metals (Figure 6.2). When the *GGA* + Hubbard *U* scheme is applied, as shown, these compounds become half-metals like the compounds in Figure 6.1. It is worthy noted that, in this series of compounds, the $5d$-t_{2g} and O-*p* states are sitting around E_F and highly hybridized. The overall DOS across E_F is almost equally distributed on both the 5*d* and O-*p* orbitals. This situation fits the feature of 5*d* heavy metal natures.[24, 34] In addition, Ba_2EuSbO_6, one of the *f*-element containing compounds, belongs to this type of material (not shown). *GGA* makes Ba_2EuSbO_6 be a metal, and it becomes a half-metal when using *GGA + U*(3eV). To differentiate this series of compounds from type I, in which the simple *GGA* makes them half-metals, this series is classified as type II.

When this study was extended to $4d^3/5d^3$ as well as $4f^7/4f^8$ compounds such as Ba_2YRuO_6 Ba_2InOsO_6, Ba_2GdSbO_6 and Ba_2TbNbO_6 (not shown), one found that *GGA* calculations make these compounds neither a metal nor a half metal (Figure 6.3). *GGA* gives rise to reasonable electronic structures for this type of materials. For $4d^3/5d^3$, the band gaps exist naturally between t_{2g} and e_g according to the octahedral crystal field splitting, because the t_{2g} sub-orbitals are fully filled. For the *f*-elements containing samples, E_F is sitting exactly above the *f-O* covalence band due to the fully-filled *f* orbitals. Whereas upon increasing the number of *f* electrons from Tb on, such as Ba_2DySbO_6 ($4f^9$), Ba_2HoSbO_6 ($4f^{10}$), and Ba_2ErSbO_6 ($4f^{11}$), they become half-metals by *GGA* calculations like their other sister compounds such as Ba_2SmSbO_6 ($4f^5$), and Ba_2EuSbO_6 ($4f^6$, *GGA + U*) with unfilled *f*-orbitals. This kind of compounds can be called type III. Although the symmetry is much lower than the $4d^3/5d^3$ compounds, the $3d^3$ compound (Ca_2CrSbO_6) was also investigated. The insulating state of Ca_2CrSbO_6 is also perfectly reflected in *GGA* calculation. Interestingly, the combination of the results on Ba_2InOsO_6 and Ca_2CrSbO_6 supports

perfectly the argument that Sr_2CrOsO_6 is at the end of spin-polarized metal insulator transition.[51] The individual Cr^{3+} as well as Os^{5+} ions in octahedral surrounding respectively has an energy gap due to the completely filling of their t_{2g} sub-orbitals. The insulating nature of Sr_2CrOsO_6 may be ascribed to this collective effect rather than the insulating nature on Os site alone. Kübler *et al.* recently predicted Sr_2FeRuO_6 to be an antiferromagnetic insulator by means of *LDA* + *U* calculations.[7] The present calculation on Ba_2YRuO_6 also indicates that, even if the close-shell ions Y^{3+} is replaced by an open-shell ion Fe^{3+}, the interaction between Fe^{3+} and Ru^{5+} does not bring about the electron hopping via bridge oxygen across these two ions. This situation is similar to that of Sr_2CrOsO_6. This finding is in striking contrast to Ba_2FeMoO_6 and Sr_2FeReO_6, in which when Fe^{3+} replaces respectively Y^{3+} in Sr_2YMoO_6 and Ga^{3+} in Sr_2GaReO_6, Mott-insulators with spin frustration, the resultant compounds become half metallic magnets. However, the feature of these two cases is that the original frustrated-spin is switched to a spin-ordering due to the magnetic induction of magnetic ions Fe^{3+} through the double exchange.

It can be summarized that the compounds of $4d^1$, $4d^2$, $5d^2$ as well as partially-filled *f* orbitals (except $4f^8$) are readily predicted to be half-metals. This result implies that the unfilled sub-*d* states (e.g. t_{2g}) should be taken special care to reproduce the reasonable electronic structure.

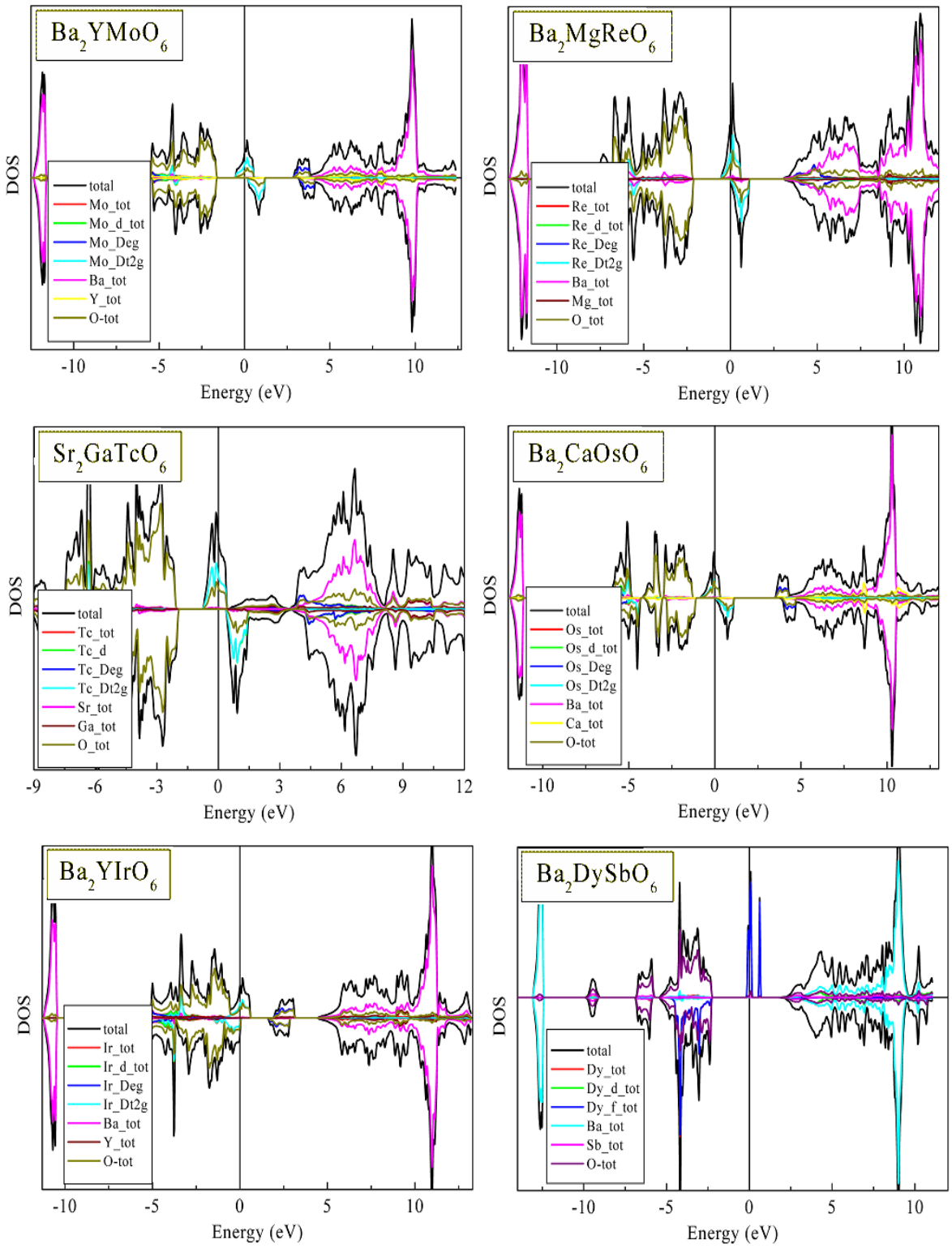

Figure 6.1 *GGA* calculations for type I compounds: Ba_2YMoO_6, Ba_2MgReO_6, Sr_2GaTcO_6, Ba_2CaOsO_6, Ba_2YIrO_6, and Ba_2DySbO_6.

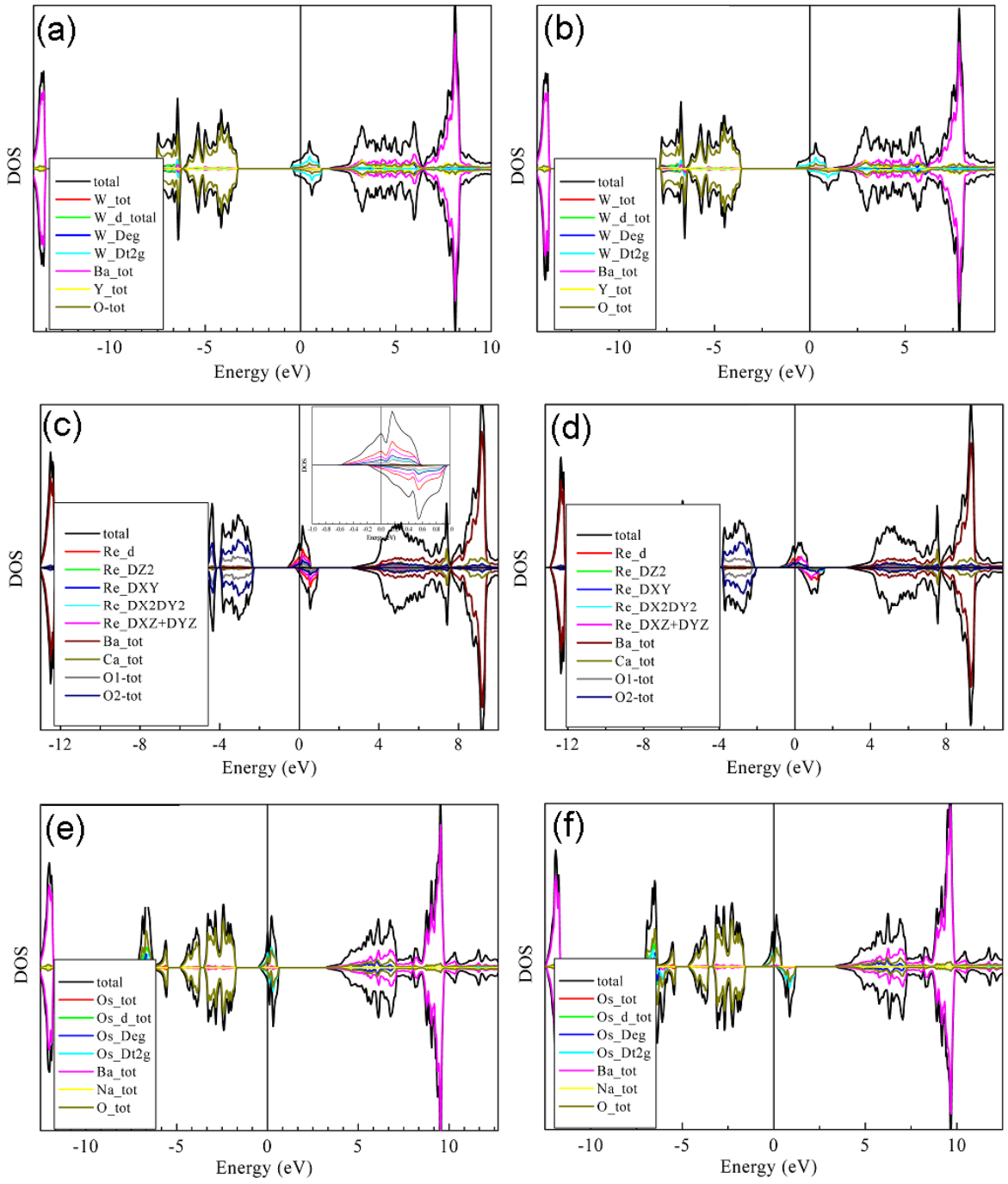

Figure 6.2 *GGA* and *GGA + U* calculations for type II compounds: (a) and (b) for Ba_2YWoO_6; (c) and (d) for Ba_2CaReO_6; (e) and (f) for Ba_2NaOsO_6.

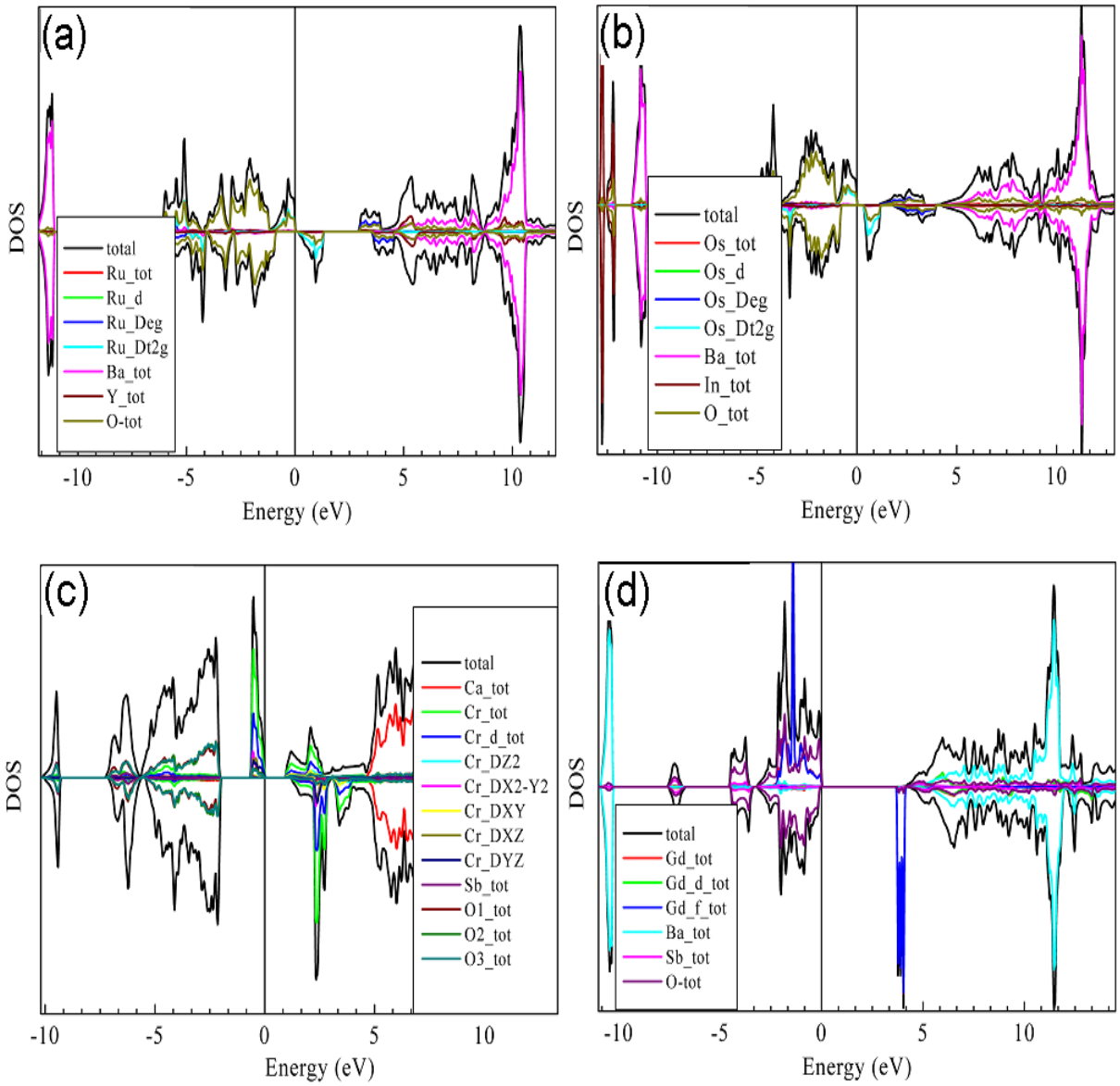

Figure 6.3 *GGA* calculations for type III compounds: (a) Ba_2YRuO_6, (b) Ba_2InOsO_6, (c) Ca_2CrSbO_6, and (d) Ba_2GdSbO_6.

In order to calculate the reasonable band structures of type I and type II compounds, some further tests were undertaken such as *GGA* + Hubbard *U*, *GGA* + *SOC* (spin orbit coupling). These efforts do not lead to an insulating/semiconducting state. However, when on-site repulsion effect is combined with spin-orbit coupling,[32, 34] the Mott-insulating feature is produced. Following, Ba_2YMoO_6 is selected as an example to demonstrate how to proceed.

As shown in Figure 6.4, *GGA*, *GGA* + *U*(2eV and 3eV), and *GGA* + *SOC* (*SOC*: spin orbit coupling) fail to give rise to the reasonable electronic structure for Ba_2YMoO_6, since *GGA* calculation gives a half-metallic electronic structure. Nonetheless, the results of these calculations indicated that electron correlation increases the exchange splitting, while *SOC* splits the narrow conduction bands consisting of the hybridized Mo-4*d* states and O-2*p* states. This finding gives a clue to consider a cooperative effect of electron correlation and spin orbit coupling. Therefore, in the next step, the correlation energy was taken into account (*GGA* + *SOC* + *U*), which have been successful in explaining the electronic structure of Ba_2NaOsO_6[34] and $Ca_3Co_2O_6$.[32] A continuous increase of *U* to 2 eV leads to a complete splitting of the narrow conduction band and opens up a band gap between the Mo-O valence band below E_F and the conduction band above E_F. After applying *SOC* (quantization along [1 1 1]), the originally degenerate t_{2g} band undergoes non-degenerate transition. Upon adding *U*(1eV), the t_{2g} band grows larger, and is still hybridized with Oxygen. Finally in *GGA* + *SOC* + *U*(2eV) calculation (Figure 6.4), the reasonable electronic structure for Ba_2YMoO_6 was reproduced. One found that partial states of O-2*p* weigh almost equal to that of Mo-4*d* and z^2 states are hybridized with Oxygen *p* states and accommodate the one 4*d* electron from Mo. The total moment per formula unit is calculated to be about 0.97 μ_B, which is very close to the spin-only value of 1 μ_B.

Although the *U* values vary in given cases, the above procedure can be extended to both type I and type II compounds, which is shown respectively in Figure 6.5 and Figure 6.6. In Figure 6.6, by the comparison between *GGA* + *SOC* and *GGA* + *SOC* + *U*, it is clearly demonstrated how cooperative effect of electron correlation in association with spin-orbit coupling makes success. As for Ba_2NaOsO_6 in the type II family, its calculation was not shown, since Whangbo *et al.* has already discussed.[34]

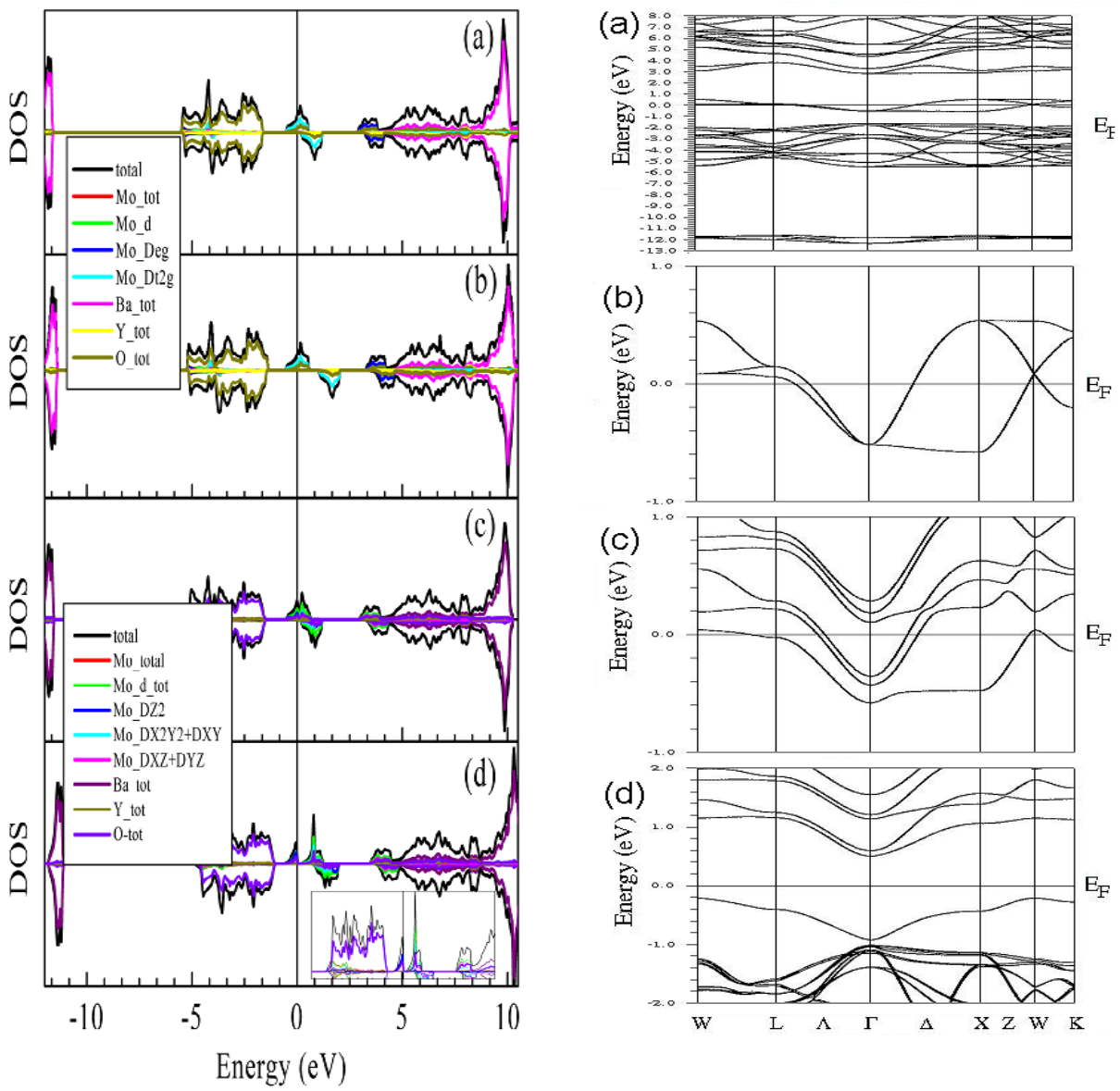

Figure 6.4 DOS and band structures calculated for Ba_2YMoO_6: (a) *GGA*, (b) *GGA* + *U*(4eV), (c) *GGA* + *SOC*, and (d) *GGA* + *SOC* + *U*(2eV), in (a) and (b) only the spin-up bands are shown respectively.

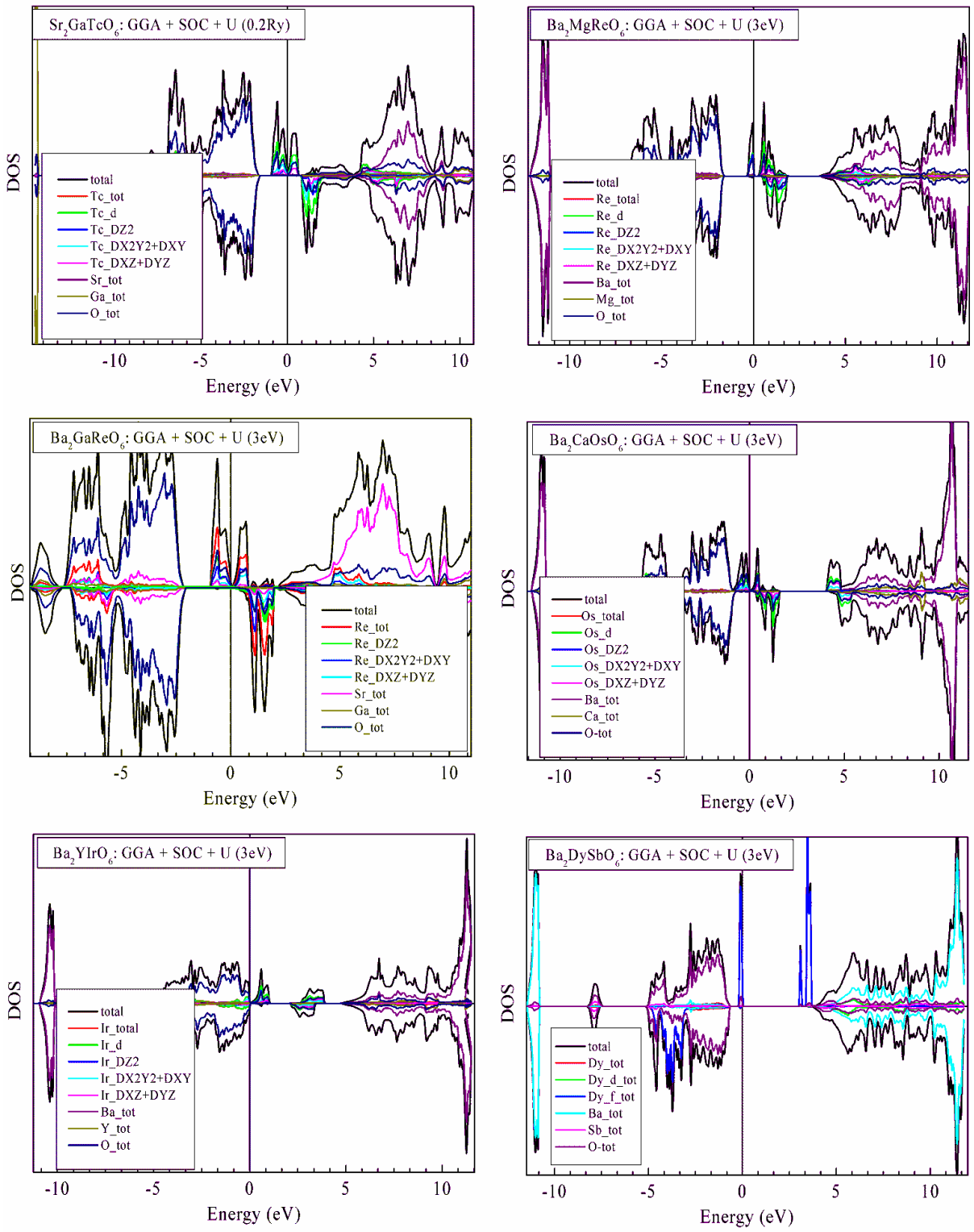

Figure 6.5 DOS produced by cooperative effect of electron correlation and spin-orbit coupling for type I compounds: Ba_2GaTcO_6, Ba_2MgReO_6, Sr_2GaReO_6, Ba_2CaOsO_6, Ba_2YIrO_6 and Ba_2DySbO_6.

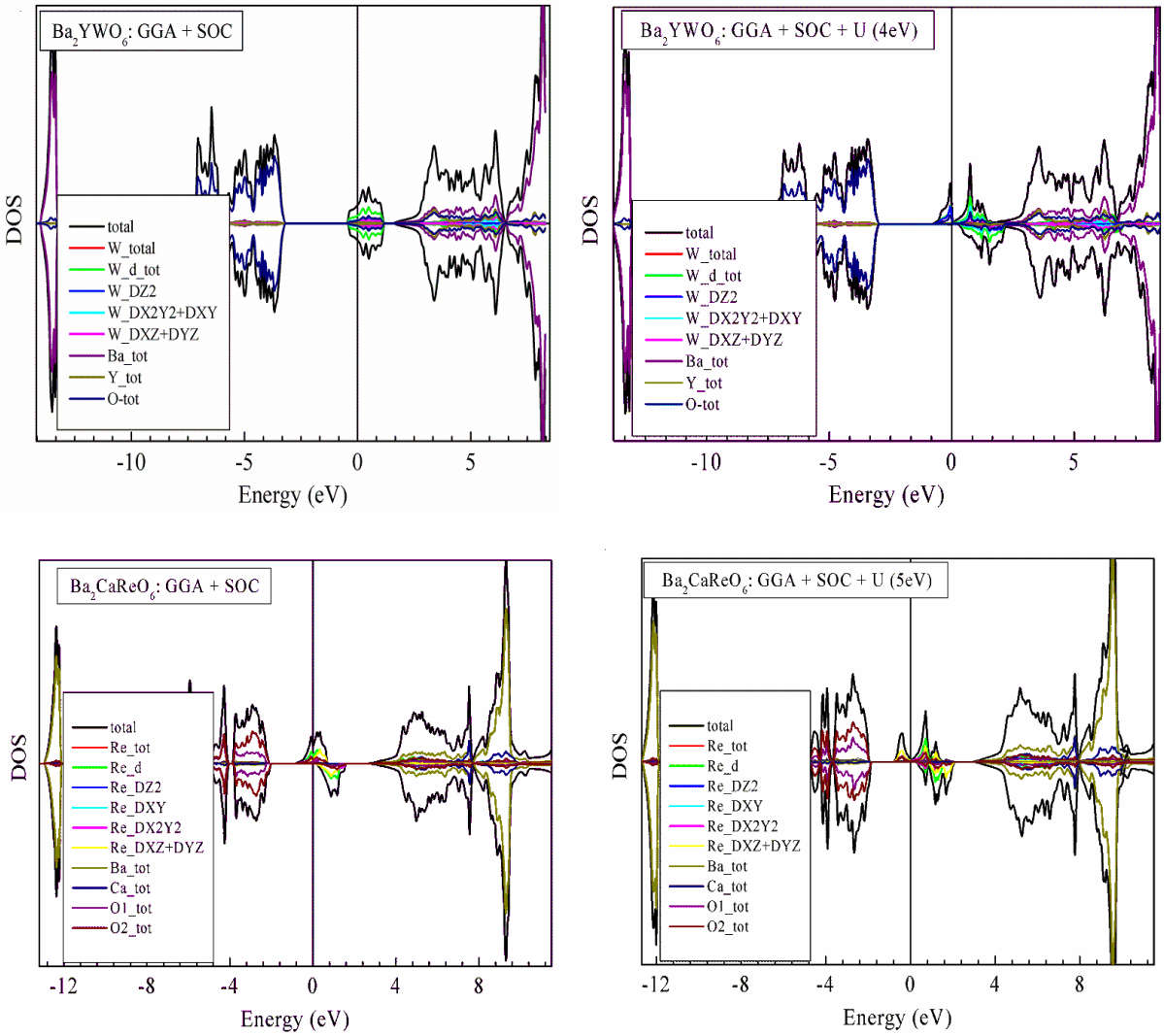

Figure 6.6 DOS of GGA plus spin orbit coupling (right) and of cooperative effect of electron correlation and spin-orbit coupling for type II compounds: Ba_2YWO_6, Sr_2CaReO_6.

In order to make a comparison between light metals and heavy metals in A_2CMO_6, a 3*d* compound, Sr_2MnSbO_6 was investigated. This material contains a bit of Mn/Sb anti-site disorder, however in order to simplify the calculations, one can assume that it is an ordered compound. The results in Figure 6.7 shows that, like type I and type II, Sr_2MnSbO_6 is also a half metal by *GGA*. It is clearly shown that the z^2 state is not completely split up. The band gap is growing as function of *U*. Therefore, Sr_2MnSbO_6 can be considered as a correlated insulator.[52] This finding is similar to the case of $Ca_3Co_2O_6$, which used to be wrongly predicted as a half metal until Wu *et al*. came up with a Mott-insulator electronic configuration.[32] In contrast to the type I and type II

compounds, only increase of Hubbard *U* for Sr_2MnSbO_6 is able to produce an insulating state. This reflects the difference between 3*d* elements and heavier transition metals. Another notable feature of Sr_2MnSbO_6 is that the degree of *d*-*p*(O) hybridization is not so remarkable compared to that of 4*d*/5*d*/*f* elements containing materials. The fact indicates that spin-orbit coupling does not indeed plays an important role due to the relatively smaller atomic size of 3*d* ions and not so dispersive open-shell orbitals.

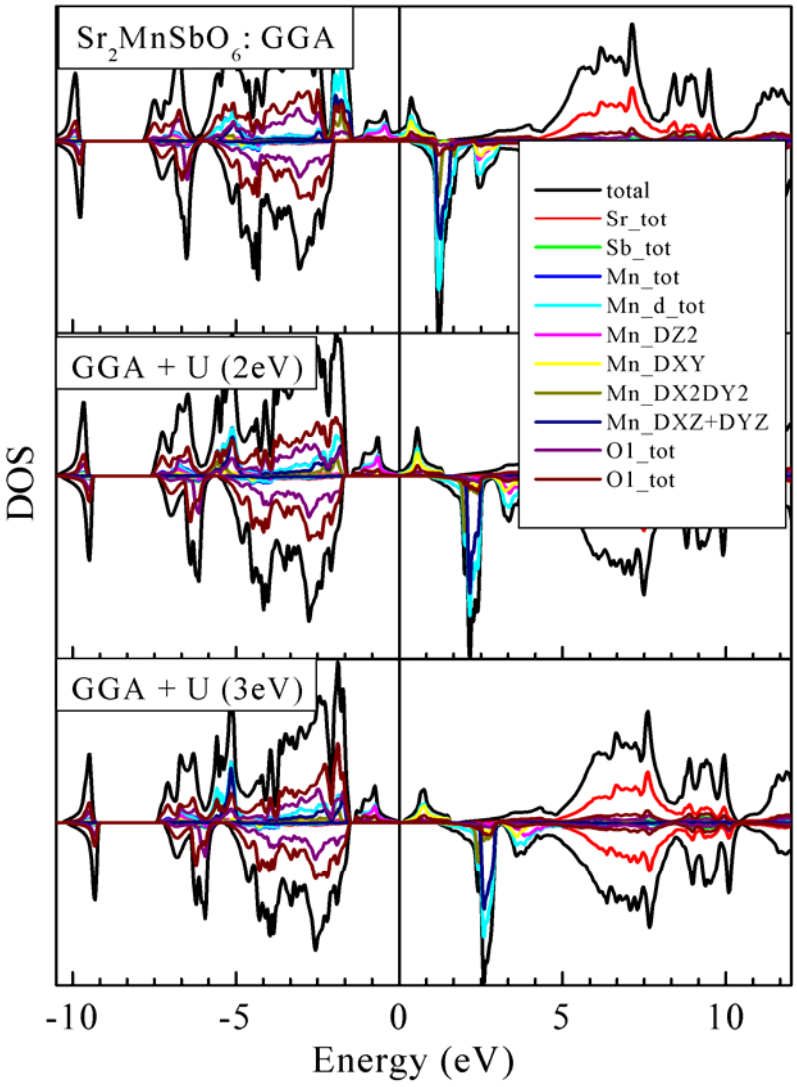

Figure 6.7 DOS calculated for ordered Sr_2MnSbO_6.

6.4 Conclusion

The electronic structures of the A_2CMO_6 type double perovskites are surveyed and discussed. These materials are mostly predicted as a half metal without proper treatment, which are characterized experimentally to be either a magnetic or a spin-frustrated insulator/semiconductor. The cooperative effect of combination spin-orbit coupling with on-site repulsion energy is a good solution to produce reasonable electronic structures for most of A_2CMO_6 compounds. By contrast, spin-orbit coupling is not so important for light 3*d* transition metals in A_2CMO_6 setting. In the octahedral configuration, the fully filled sub-band e.g. t_{2g}, gives only the insulating state due to the crystal fielding splitting. The study on the individual 4*d*/5*d* elements in A_2CMO_6 setting indicates that spin-orbit coupling is a significant factor to compute the reasonable electronic structure of the intensively-studied half-metal candidates such as Sr_2FeMoO_6, Sr_2FeReO_6, Sr_2CrReO_6, and Sr_2CrWO_6 etc.

References

[1]W. E. Pickett, Phys. Rev. B **57**, 10613 (1998).

[2]R. E. Rudd, W. E. Pickett, Phys. Rev. B **57**, 557 (1998).

[3]H. Q. Yin, J. S. Zhou, J. P. Zhou, R. Dass, J. T. McDevitt, J. B. Goodenough, Appl. Phys. Lett. **75**, 2812 (1999).

[4]K. I. Kobayashi, T. Kimura, H. Sawada, K. Terakura, Y. Tokura, Nature **395**, 677 (1998).

[5]K. I. Kobayashi, T. Kimura, Y. Tomioka, H. Sawada, K. Terakura, Y. Tokura, Phys. Rev. B **59**, 11159 (1999).

[6]R. A. de Groot, F. M. Mueller, P. G. v. Engen, K. H. J. Buschow, Phys. Rev. Lett. **50**, 2024 (1983).

[7]T. K. Mandal, C. Felser, M. Greenblatt, J. Kubler, Phys. Rev. B **78**, 134431 (2008).

[8]C. Zener, Phys. Rev. **82**, 403 (1951).

[9]J. Lindén, T. Yamamoto, J. Nakamura, H. Yamauchi, M. Karppinen, Phys. Rev. B **66**, 184408 (2002).

[10]F. Sher, A. Venimadhav, M. G. Blamire, B. Dabrowski, S. Kolesnik, J. P. Attfield, Solid State Sci. **7**, 912 (2005).

[11]T. H. Jose Julio Blanco, Lide M. Rodriguez-Martinez, Maite Insausti, Jose Manuel Barandiaran, Jean-Marc Greneche and Teofilo Rojo, J. Mater. Chem. **11**, 253 (2001).

[12]A. Jung, I. Bonn, V. Ksenofontov, G. Melnyk, J. Ensling, C. Felser, W. Tremel, J. Mater. Chem. **15**, 1760 (2005).

[13]A. Jung, I. Bonn, V. Ksenofontov, M. Panthofer, S. Reiman, C. Felser, W. Tremel, Phys. Rev. B **75**, 184409 (2007).

[14]A. Jung, V. Ksenofontov, S. Reiman, H. Therese, U. Kolb, C. Felser, W. Tremel, Phys. Rev. B **73**, 144414 (2006).

[15]J. J. Blanco, M. Insausti, L. Lezama, J. P. Chapman, I. Gil de Muro, T. Rojo, J. Solid State Chem. **177**, 2749 (2004).

[16]E. J. V. Cussen, Jaap F.; Battle, Peter D.;and Gibb, C. Terence, J.Mater.Chem. **7**, 459 (1997).

[17]E. J. Cussen, D. R. Lynham, J. Rogers, Chem. Mater. **18**, 2855 (2006).

[18]K. Y. Kamata, Masahiro; Nakamura, Tetsuroand Sata,Toshiyuki Chem. Lett. **1** 1201 (1972).

[19]K. G. Bramnik, H. Ehrenberg, J. K. Dehn, H. Fuess, Solid State Sci. **5**, 235 (2003).

[20]C. R. Wiebe, J. E. Greedan, P. P. Kyriakou, G. M. Luke, J. S. Gardner, A. Fukaya, I. M. Gat-Malureanu, P. L. Russo, A. T. Savici, Y. J. Uemura, Phys. Rev. B **68**, 134410 (2003).

[21]C. R. Wiebe, J. E. Greedan, G. M. Luke, J. S. Gardner, Phys. Rev. B **65**, 144413 (2002).

[22]Y. Sasaki, Y. Doi, Y. Hinatsu, J. Mater. Chem. **12**, 2361 (2002).

[23]A. W. Sleight, J. Longo, R. Ward, Inorg. Chem. **1**, 245 (1962).

[24]A. S. Erickson, S. Misra, G. J. Miller, R. R. Gupta, Z. Schlesinger, W. A. Harrison, J. M. Kim, I. R. Fisher, Phys. Rev. Lett. **99**, 016404 (2007).

[25]K. E. Stitzer, M. D. Smith, H.-C. zur Loye, Solid State Sci. **4**, 311 (2002).

[26]H. Karunadasa, Q. Huang, B. G. Ueland, P. Schiffer, R. J. Cava, Proc. Natl. Acad. Sci. U. S. A., Early Ed. **100**, 8097 (2003).

[27]J. E. Greedan, J. Mater. Chem. **11**, 37 (2001).

[28]A. P. Ramirez, Annu. Rev. Mater. Sci. **24**, 453 (1994).

[29]J. J. Attema, G. A. de Wijs, G. R. Blake, R. A. de Groot, J. Am. Chem. Soc. **127**, 16325 (2005).

[30]J. Winterlik, G. H. Fecher, C. Felser, C. Muhle, M. Jansen, J. Am. Chem. Soc. **129**, 6990 (2007).

[31]R. Vidya, P. Ravindran, H. Fjellvåg, A. Kjekshus, O. Eriksson, Phys. Rev. Lett. **91**, 186404 (2003).

[32]H. Wu, M. W. Haverkort, Z. Hu, D. I. Khomskii, L. H. Tjeng, Phys. Rev. Lett. **95**, 186401 (2005).

[33]K. W. Lee, W. E. Pickett, EPL (Europhysics Letters) **80**, 37008 (2007).

[34]H. J. Xiang, M. H. Whangbo, Phys. Rev. B **75**, 052407 (2007).

[35]M. Cheah, P. J. Saines, B. J. Kennedy, J. Solid State Chem. **179**, 1775 (2006).

[36]T. K. Mandal, V. V. Poltavets, M. Croft, M. Greenblatt, J. Solid State Chem. **181**, 2325 (2008).

[37]M. Retuerto, M. Garcia-Hernandez, M. J. Martinez-Lope, M. T. Fernandez-Diaz, J. P. Attfield, J. A. Alonso, J. Mater. Chem. **17**, 3555 (2007).

[38]P. Blaha, K. Schwartz, G. K. H. Madsen, D. Kvasnicka, J. Luitz, *Wien2K,An Augmented Plane Wave+Local Orbitals Program for Calculating Crystal Properties* ((Techn. Universität Wien, Austria,2001).

[39]U. v. Barth, L. Hedin, J. Phys. C: Solid State Phys. **5**, 1629 (1972).

[40]V. I. Anisimov, J. Zaanen, O. K. Andersen, Phys. Rev. B **44**, 943 (1991).

[41]J. Kuneš, P. Novák, M. Diviš, P. M. Oppeneer, Phys. Rev. B **63**, 205111 (2001).

[42]K. Yamamura, M. Wakeshima, Y. Hinatsu, J. Solid State Chem. **179**, 605 (2006).

[43]A. W. Sleight, J. Longo, R. Ward, Inorg. Chem. **1**, 245 (1962).

[44]W. T. Fu, D. J. W. Ijdo, J. Alloys Compd. **394**, L5 (2005).

[45]P. D. Battle, C. W. Jones, J. Solid State Chem. **78**, 108 (1989).

[46]W. T. Fu, D. J. W. Ijdo, J. Solid State Chem. **178**, 2363 (2005).

[47]A. M. I. R. P. García Casado, Z. Anorg. Allg. Chem. **510**, 194 (1984).

[48]G. R. S. K.-S. U. Wittmann, Z. Anorg. Allg. Chem. **482**, 143 (1981).

[49]P. J. Saines, B. J. Kennedy, M. M. Elcombe, J. Solid State Chem. **180**, 401 (2007).

[50]A. W. Sleight, R. Ward, Inorg. Chem. **1**, 790 (1962).

[51]Y. Krockenberger, K. Mogare, M. Reehuis, M. Tovar, M. Jansen, G. Vaitheeswaran, V. Kanchana, F. Bultmark, A. Delin, F. Wilhelm, A. Rogalev, A. Winkler, L. Alff, Phys. Rev. B **75**, 020404 (2007).

[52]J. Zaanen, G. A. Sawatzky, J. W. Allen, Phys. Rev. Lett. **55**, 418 (1985).

7 Ba_2MnReO_6: from "a Pseudo Half-metal" to "a Real Magnetic Insulator"

7.1 Introduction

Double perovskites $A_2MM'O_6$ compounds (A = divalent cation or rare earth, *M*/*M*′= transition metal) have recently attracted much attention due to their novel physical properties and potential for technological applications.[1-3] The two most prominent examples are Sr_2FeMoO_6[4] and Sr_2FeReO_6[5] that exhibit half-metallic ferrimagnetic behavior at room temperature. This makes them prospective magnetoelectronic compounds. For the polycrystalline materials low-field intergrain tunneling magnetoresistance (TMR) has been reported at room temperature.[1–4] The conceptual basis for the observed half-metallic ferromagnetism is a large density of states of one spin direction at the Fermi level while the other spin direction is insulating.[6, 7]

As matter of fact, to predict a half-metal turned out to be a challenge if some appropriate treatment is not carefully conducted. For instance, It has been suggested that Rb_4O_6 should be a half-metallic ferromagnet with the magnetic moment carried by the hyperoxide anions and a Curie temperature above room temperature.[8] However the experimental data demonstrated that Rb_4O_6 is actually a magnetically frustrated system.[9] $Ca_3Co_2O_6$ was also computed to be a ferromagnetic half-metal at the beginning,[10] but Wu *et al.*[11] pointed out that $Ca_3Co_2O_6$ should be a Mott-insulator with Ising-like magnetism. Another Mott-insulator (ferromagnetic) Ba_2NaOsO_6 was readily calculated to be a half-metal without proper treatment of the parameters.[12]

Ba_2MnReO_6 (Figure 7.1) was firstly reported to be a magnetic insulator in the early 1970s.[13] Due to intensive studies on Re-based double perovskites, people came to pay attention to this compound. Since Mn is close to Fe, the Mn^{2+}/Re^{6+} configuration in Ba_2MnReO_6[14] seems to be metallic as found for Fe^{3+}/Mo^{5+} in Sr_2FeMoO_6. In addition, Ba_2MnReO_6 is also seemingly very close to its sister compound Ba_2FeReO_6 (Fe^{3+}/Re^{5+}), except that Ba_2MnReO_6 has one more 5*d* electrons on Re. Many experimental characterizations however indicate that, in contrast to other Re-double perovskits, Ba_2MnReO_6 is an magnetic insulator.[14-16] Whereas, Kübler and his co-workers recently showed that Ba_2MnReO_6 was a half metallic magnet.[7] The experimentally measured conductivity of Ba_2MnReO_6 is in striking contrast to Kübler's calculation despite the calculated Curie temperature in fair agreement with the measured value. Although Yang *et al*.

obtained a narrow band gap for Ba_2MnReO_6, a pretty large Hubbard *U* was applied on both Mn(6eV) and Re(4eV). In this study, a reasonable band structure and a corresponding detailed discussion are presented for Ba_2MnReO_6.

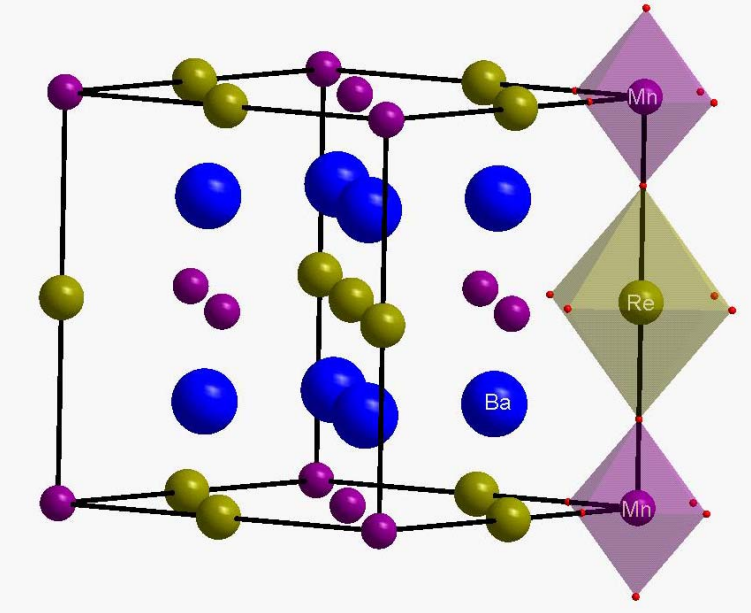

Figure 7.1 Structure of Ba_2MnReO_6: MnO_6 and ReO_6 octahedra are highlighted in purple and light brown colors.

7.2 Computational details

The electronic structure calculation was performed by the full potential linearized augmented plane wave method as implemented in WIEN2K.[17] The exchange-correlations functional was taken within the generalized gradient approximation (*GGA*).[18] Local density approximation including Coulomb correlations (*LDA + U*) was exploited to examine the on-site repulsion on the transition elements.[19, 20] Since Re is a heavy element, spin orbit coupling should be taken into account.[19] The muffin-tin radii are respectively 3.3, 2.15, 1.91 and 1.7 a.u. for Ba, Mn, Re and O. The lattice parameters were explored from the work of Popov *et al*.[14] The plane wave expansion cutoffs are 7.0 for expanding the wave function. In the complete Brillouin zone, 1000 *k* points were applied.

7.3 Results and discussion

7.3.1 *GGA* gives a half metallic property; *GGA + U* gives a metal.

Preliminary *GGA* and *GGA* plus Hubbard *U* calculations are shown in Figure 7.2. The calculations indicate that the local magnetic moment on Mn is 4.19 μ_B and that on Re is -0.40 μ_B. This result suggests an antiferromagnetic coupling between Mn and Re. an overall magnetic moment (per molecular unit) of 3.98 μ_B is calculated in Ba_2MnReO_6. In spin up channel, the Re *d* states are sitting high above the Fermi Energy (E_F), shown in Figure 7.2(a) and a band gap is left between Mn_e_g and Re_t_{2g} states. In spin down channel, Re_t_{2g} bands are dispersive around E_F, shown in Figure 7.2(b′). In spin up channel, Mn_e_g are below E_F and touch E_F at L point, shown in Figure 7.2(a′). However, in spin down state, the overall Mn *d* bands are elevated above Re_t_{2g} bands around E_F. This overall electronic structure, in agreement with Kübler's calculations,[7] satisfies the criterions of a half-metal: in spin up, the material is a semiconductor; whereas it is a metal in spin down state.[6] However, this result is not consistent with the experimental measurement, namely, a magnetic insulator. The DOS of Ba_2MnReO_6 in Figure 7.3 demonstrates that the Re *d* orbitals are highly hybridized with oxygen *p* orbitals (Figure 7.3), a feature of 5*d* heavy orbitals such as in Ba_2NaOsO_6.[12, 21] After the application of *GGA + U*(3eV) on Re, the Re_t_{2g} bands in spin up is lowered down to E_F, and the previous band gap in *GGA* is now closed. In spin down state, the previous Re_t_{2g} bands in *GGA* are slightly lifted but still diffuse around E_F. As a result, Ba_2MnReO_6 is transformed by *GGA + U* from a "half metal" by *GGA* to a "metal". Continuously increasing *U* to 7 eV, the band structures remains almost unchanged (not shown).

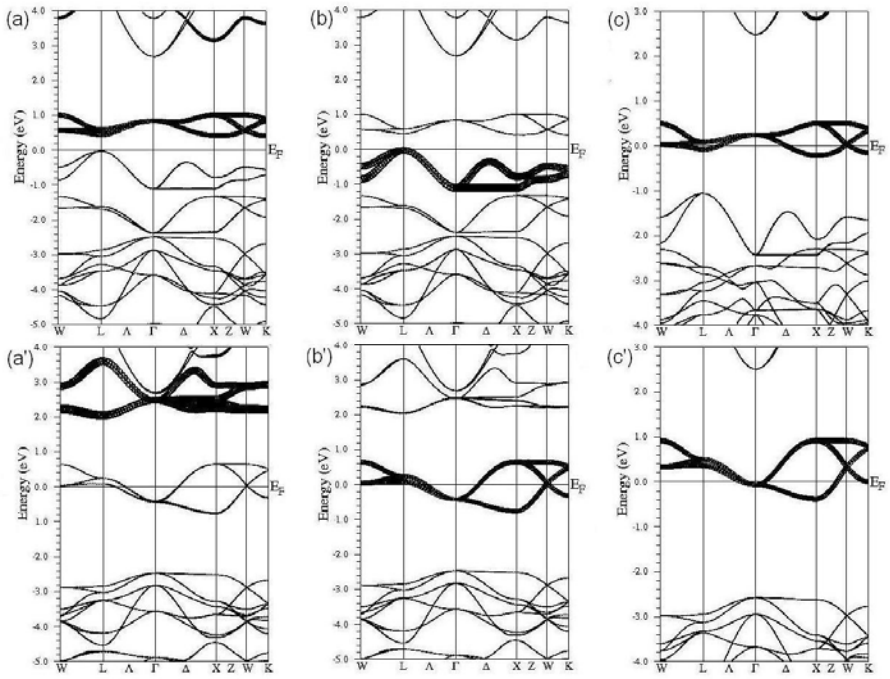

Figure 7.2 Band structure of Ba_2MnReO_6: (a) *GGA* spin up Re *d* bands; (a′) *GGA* spin down Mn *d* bands; (b) *GGA* spin up Mn *d* bands; (b′) *GGA* spin down Re *d* bands; (c) *GGA* + U_{Re}(3eV) spin up; (c′) *GGA* + U_{Re}(3eV) spin down.

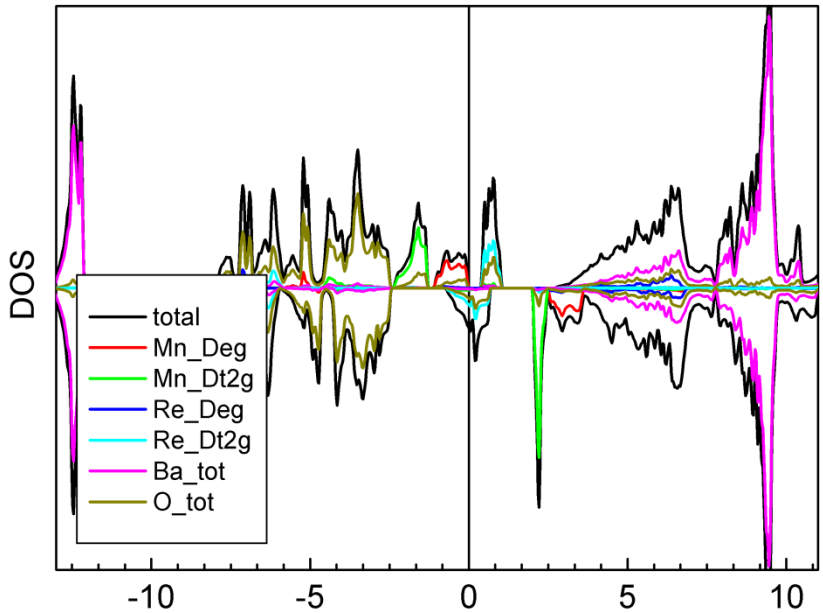

Figure 7.3 DOS of *GGA* calculation of Ba_2MnReO_6.Total DOS: black; Mn_e_g: red; Mn_e_g: green; Re_e_g: blue; Re_t_{2g}: cyan; Ba: megneta; O: dark yellow.

7.3.2 *GGA + SOC + U_{Re}* is not able to open up the band gap

Recently people found evidences of an orbital magnetic moment at Re in Re-based double perovskites.[22-24] It is reasonable to consider spin orbit coupling (*SOC*) on Re. In *GGA + SOC* (Figure 7.4), the magnetic configuration of Ba_2MnReO_6 remains not significantly changed. Mn *d* spin up states (Figure 7.4 (a)) are slightly lifted above E_F at L, and Re_t_{2g} spin down bands appear to start splitting (Figure 7.4 (a′)). Upon application of 3 eV Hubbard *U* along with *SOC* on Re (Figure 7.4 (b′)), Re *d*_t_{2g} spin down bands are completely split despite of one part of the split bands touching E_F , and Mn *d* spin up bands are however further lifted towards E_F (Figure 7.4 (b)). Continuously increasing *U* to 5 eV finally opens a gap with respect to Re *d* spin down bands (Figure 7.4 (c′)). Whereas, Mn *d* spin up bands are considerably diffuse around E_F. Cooperative effect of *SOC* and Hubbard *U* on Re lead to a band gap in Re *d* bands but make previous band gap closed between Mn_t_{2g} bands and Re_t_{2g} bands in spin up state by *GGA*.

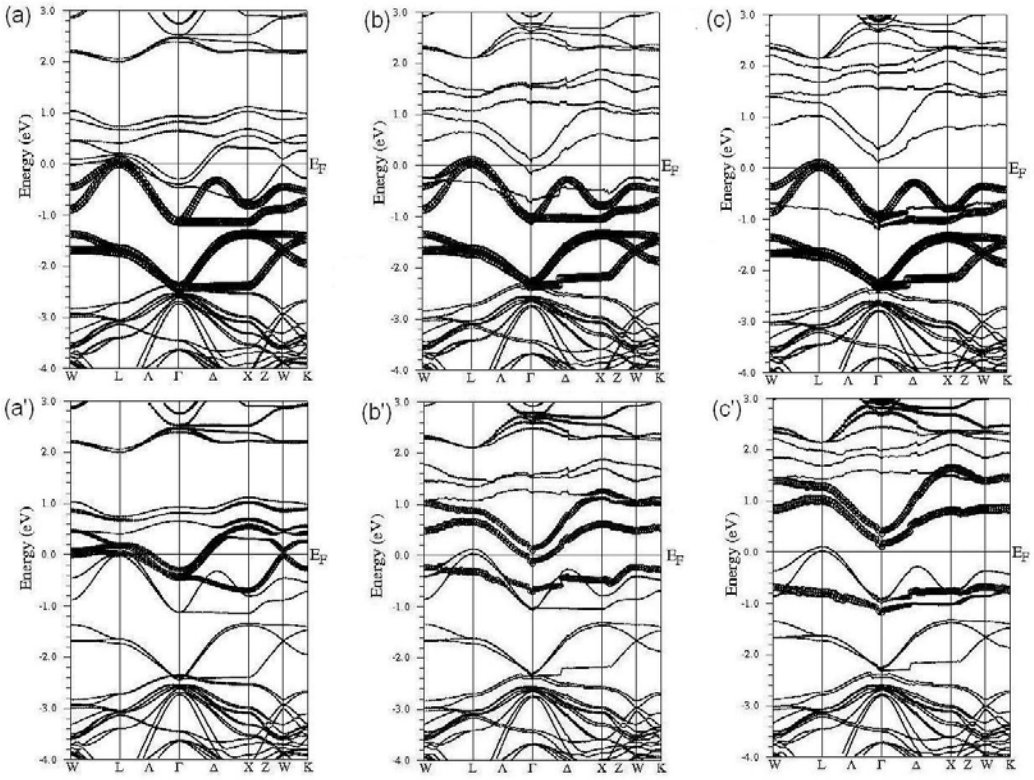

Figure 7.4 Band structure of Ba_2MnReO_6: (a) *GGA + SOC* spin up Mn *d* bands; (a′) *GGA + SOC* spin down Re *d* bands; (b) *GGA + SOC* + U_{Re}(3eV) spin up Mn *d* bands; (b′) *GGA + SOC* + U_{Re}(3eV) spin down Re *d* bands; (c) *GGA + SOC* + U_{Re}(5eV) spin up Mn *d* bands; (c′) *GGA + SOC* + U_{Re}(5eV) spin down Re *d* bands.

7.3.3 Combination of *GGA* + U_{Mn} + *SOC* + U_{Re} produces the insulating state

In order to lower Mn *d* bands away from E_F and simultaneously to keep the Re *d* bands open, the cooperative treatments of *GGA* + U_{Mn} + *SOC* + U_{Re} is carried out. As demonstrated above that U_{Re} = 5 eV is a critical value to open a gap in the previous Re_t_{2g} bands, the first attempt is to keep U_{Re} = 5 eV and apply U_{Mn} = 2 eV. As shown in Figure 7.5 (a) and (a′), *GGA* + U_{Mn}(2eV) + *SOC* + U_{Re}(5eV) completely opens up a band gap around 1.2 eV. In comparison with the treatment without U_{Mn}(2eV), namely, *GGA* + *SOC* + U_{Re}(5eV), Mn *d* bands at spin up is shifted down below E_F and the gap of Re *d* bands remains open. The calculated data suggest that the overall magnetism of Ba_2MnReO_6 is increased to 4.0 μ_B. The increase of the magnetic moment is exclusively due to the increased magnetic moment on Mn and no changes on Re. Summarily, this treatment is able to reproduce the magnetic insulator nature of Ba_2MnReO_6.

7.3.4 In *GGA* + U_{Mn} + *SOC* + U_{Re}, the minimal U_{Re} = 2 eV

In the work of Yang *et al.*, they exploited *LSDA* + *U* respectively both on Mn(6eV) and Re(4eV) to open a band gap.[25] However, it is pointed out in their study that *U* was too large for the two transition elements. In the present study, U_{Re} is gradually reduced with U_{Mn} fixed at 2 eV at first. It is found that the band gap stays open until U_{Re} = 2 eV. When U_{Re} is reduced to 1 eV, the band gap becomes closed again, because Re *d* bands cannot be separated around E_F (Figure 7.5 (b), (b′), (c) and (c′)). Interestingly, Mn *d* bands at spin up state are shifted below from E_F with U_{Re} decreasing. The test on variation of U_{Re} suggests that U_{Re} = 2 eV is a boundary for a band gap.

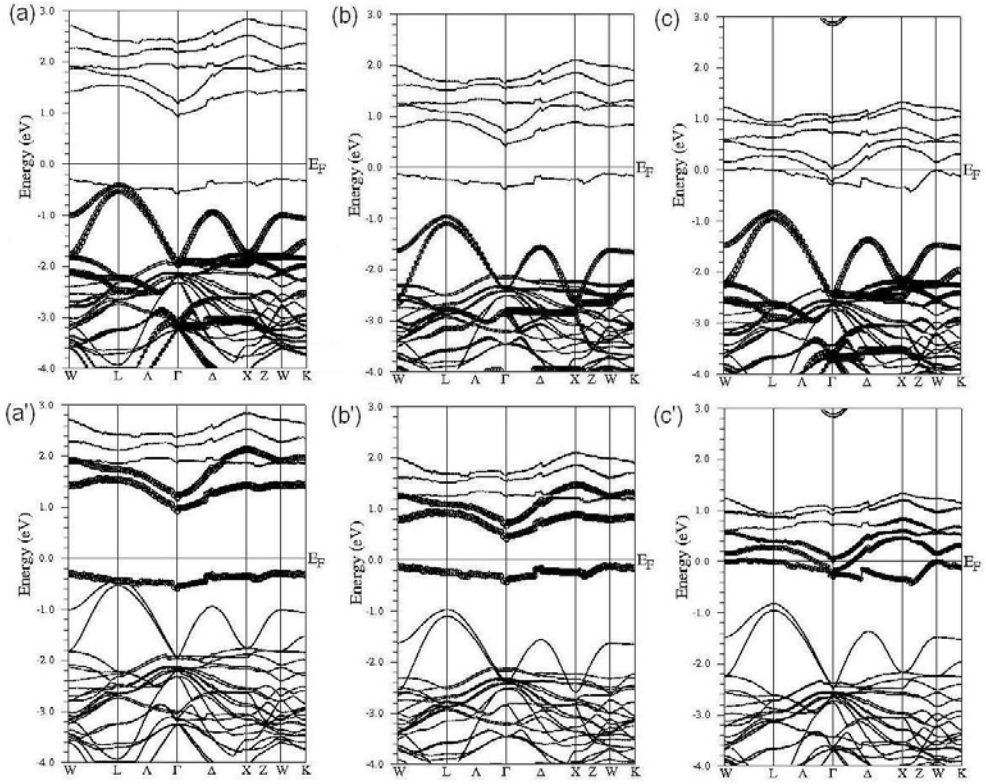

Figure 7.5 Band structure of Ba_2MnReO_6: (a) *GGA* + U_{Mn}(2eV) + *SOC* + U_{Re}(5eV) spin up Mn *d* bands; (a′) *GGA* + U_{Mn}(2eV) + *SOC* + U_{Re}(5eV) spin down Re *d* bands; (b) *GGA* + U_{Mn}(2eV) + *SOC* + U_{Re}(2eV) spin up Mn *d* bands; (b′) *GGA* + U_{Mn}(2eV) + *SOC* + U_{Re}(2eV) spin down Re *d* bands; (c) *GGA* + U_{Mn}(2eV) + *SOC* + U_{Re}(1eV) spin up Mn *d* bands; (c′) *GGA* + U_{Mn}(2eV) + *SOC* + U_{Re}(1eV) spin down Re *d* bands.

7.3.5 In *GGA* + U_{Mn} + *SOC* + U_{Re}, the minimal U_{Mn} = 0.5 eV

When U_{Mn} is reduced with U_{Re} fixed at 5 eV, Mn *d* bands at spin up state are lifted upward until touching E_F when U_{Mn} = 0.5 eV (Figure 7.6). If U_{Mn} is further decreased to zero, this situation then becomes the case of *GGA* + *SOC* + U_{Re}(5eV). As shown in Figure 7.3 (c), U_{Mn} = 0 eV makes Mn_e_g bands dispersed around E_F and Ba_2MnReO_6 gets back again to a metal. Although U_{Re} is set at a rigid value, Re *d* bands above E_F are lowered toward E_F. As an overall effect, reducing U_{Mn} causes both Mn spin up *d* bands and Re spin down *d* bands to approach E_F, and band gap is consequently reduced, e.g. band gap is 0.4 eV when U_{Mn} = 0.5 eV. This series data provides a clue that U_{Mn} should be ≥ 0.5 eV to keep a band gap open.

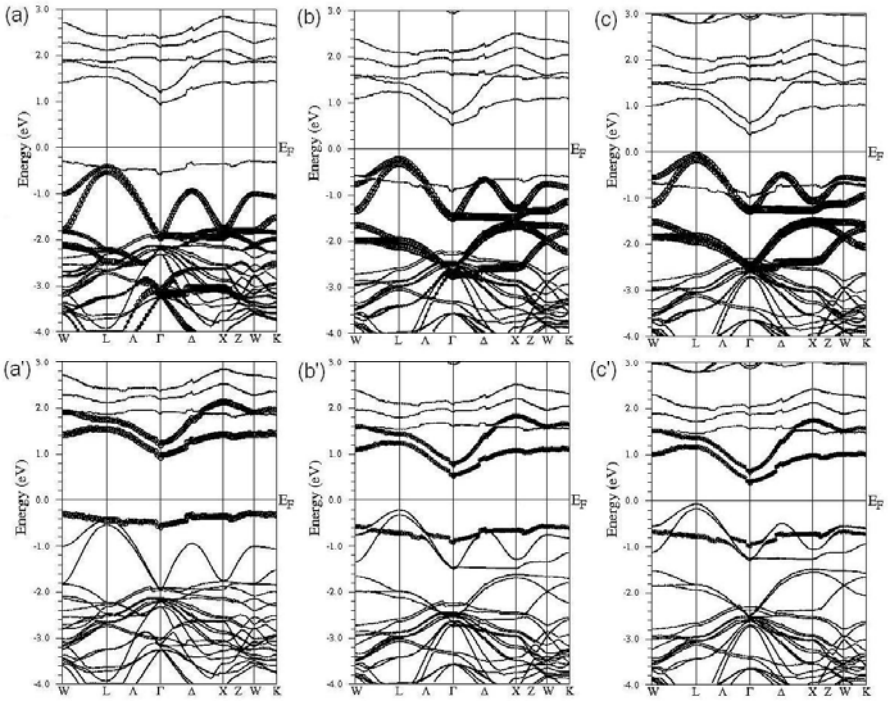

Figure 7.6 Band structure of Ba_2MnReO_6: (a) *GGA* + U_{Mn}(2eV) + *SOC* + U_{Re}(5eV) spin up Mn *d* bands; (a′) *GGA* + U_{Mn}(2eV) + *SOC* + U_{Re}(5eV) spin down Re *d* bands; (b) *GGA* + U_{Mn}(1eV) + *SOC* + U_{Re}(5eV) spin up Mn *d* bands; (b′) *GGA* + U_{Mn}(1eV) + *SOC* + U_{Re}(5eV) spin down Re *d* bands; (c) *GGA* + U_{Mn}(0.5eV) + *SOC* + U_{Re}(5eV) spin up Mn *d* bands; (c′) *GGA* + U_{Mn}(0.5eV) + *SOC* + U_{Re}(5eV) spin down Re *d* bands.

7.3.6 In *GGA* + U_{Mn} + *SOC* + U_{Re}, the minimal U_{Mn} + U_{Re} = 4 eV

Since the boundary condition is found to be $U_{Re} \geq 2$ eV and for $U_{Re} \geq 0.5$ eV, the combination of *GGA* + U_{Mn}(0.5eV) + *SOC* + U_{Re}(2eV) is therefore tested, where both critical values are applied. It turns out that this treatment is not able to open the band gap (Figure 7.7 (a) and (a′)). Although Mn *d* bands do not change, Re *d* bands are not split and diffuse around E_F. The calculations point to a correlation between U_{Mn} and U_{Re}. One can speculate that there might be a critical value of U_{Mn} + U_{Re} to keep a band gap. Considering *GGA* + U_{Mn}(2eV) + *SOC* + U_{Re}(2eV) having a band gap, one could think that U_{Mn} + U_{Re} might be 4 eV. Following this clue, the computations are performed with *GGA* + U_{Mn}(1eV) + *SOC* + U_{Re}(3eV) and *GGA* + U_{Mn}(0.5eV) + *SOC* + U_{Re}(3.5eV). Indeed, band gaps are obtained. As a disapproval, *GGA* + U_{Mn}(1eV) + *SOC* + U_{Re}(2eV) (not shown) and *GGA* + U_{Mn}(0.5eV) + *SOC* + U_{Re}(3eV) (not

shown) are all not able to open the band gaps. That means merely increasing U_{Mn} or U_{Re} without fulfilling $U_{Mn} + U_{Re} = 4$ eV is not able to produce the insulating state.

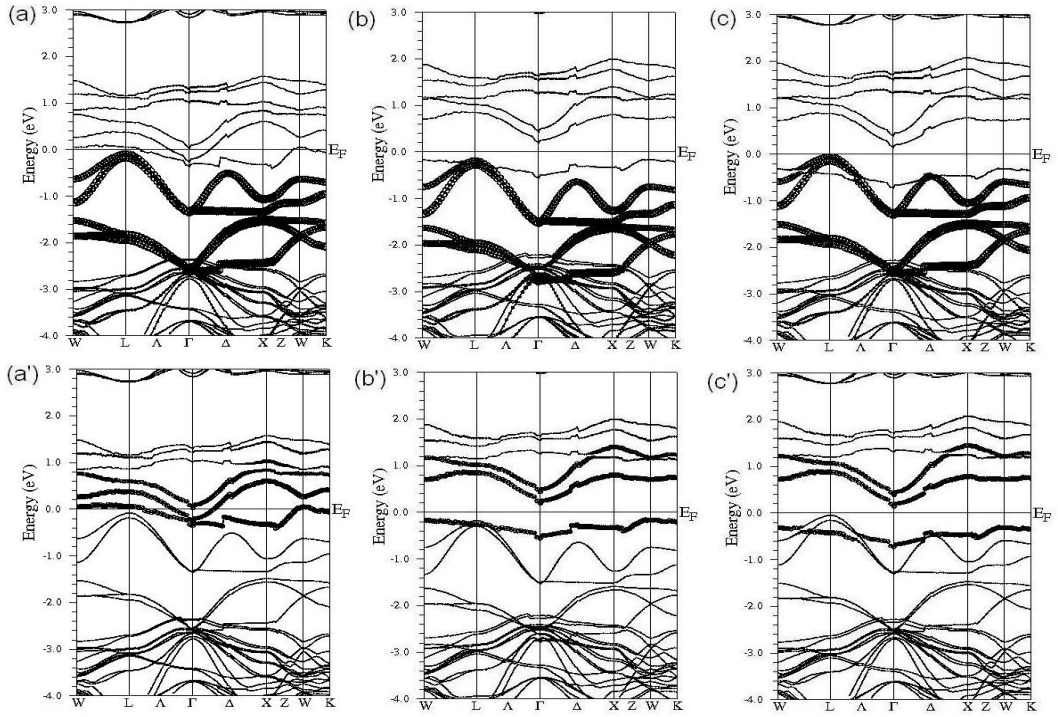

Figure 7.7 Band structure of Ba_2MnReO_6: (a) *GGA* + U_{Mn}(0.5eV) + *SOC* + U_{Re}(2eV) spin up Mn *d* bands; (a′) *GGA* + U_{Mn}(0.5eV) + *SOC* + U_{Re}(2eV) spin down Re *d* bands; (b) *GGA* + U_{Mn}(1eV) + *SOC* + U_{Re}(3eV) spin up Mn *d* bands; (b′) *GGA* + U_{Mn}(1eV) + *SOC* + U_{Re}(3eV) spin down Re *d* bands; (c) *GGA* + U_{Mn}(0.5eV) + *SOC* + U_{Re}(3.5eV) spin up Mn *d* bands; (c′) *GGA* + U_{Mn}(0.5eV) + *SOC* + U_{Re}(3.5eV) spin down Re *d* bands.

7.3.7 U_{Re} essentially influences the band gap; Ba_2MnReO_6 is a correlated insulator

In order to check the effect of U_{Mn} and that of U_{Re} respectively, the U_{Re} is firstly fixed to 2 eV and a comparison is made between U_{Mn}(2eV)/U_{Re}(2eV), (namely, *GGA* + U_{Mn}(2eV) + *SOC* + U_{Re}(2eV)), U_{Mn}(5eV)/U_{Re}(2eV) and U_{Mn}(7eV)/U_{Re}(2eV). It is found that with increasing U_{Mn} band gaps are not changed significantly, despite a slight greater opening (seen Figure 7.8 (a), (b) and (c)). This slight change might be ascribed to the correlation between $U_{Mn} + U_{Re}$, as discussed above. The only difference between these band structures is the positions of the Mn *d* states, which are shifted below Re *d* states and stay farther away from E_F with increasing U_{Mn}. And with U_{Mn} above 2 eV, Re *d* bands is dominating around E_F. Secondly, U_{Mn} is fixed at 2 eV to check

the effect of U_{Re}. By contrast, the comparison between U_{Mn}(2eV)/U_{Re}(2eV), U_{Mn}(2eV)/U_{Re}(5eV) and U_{Mn}(2eV)/U_{Re}(7eV) reveals that the band gaps grow strikingly with U_{Re} increasing and reach maximum at 1.6 eV with U_{Re} = 7 eV. It is worthy noted that at U_{Re} = 7 eV, the covalent Re *d* bands are shifted below Mn *d* bands. In this case, if one wants a larger band gap, one has to increase U_{Mn} to push Mn *d* bands down. The size of band gap depends on U_{Mn} and U_{Re}, but U_{Re} influences more significantly on the band gap. Like Ca_3CoO_6,[11] Ba_2MnReO_6 may also considered as a correlated insulator.[26] Since the experimental value of the band gap of Ba_2MnReO_6 is not given because the practical measurement limits in the literatures,[14-16] the values of U_{Mn} and U_{Re} cannot be definitely selected in this present study.

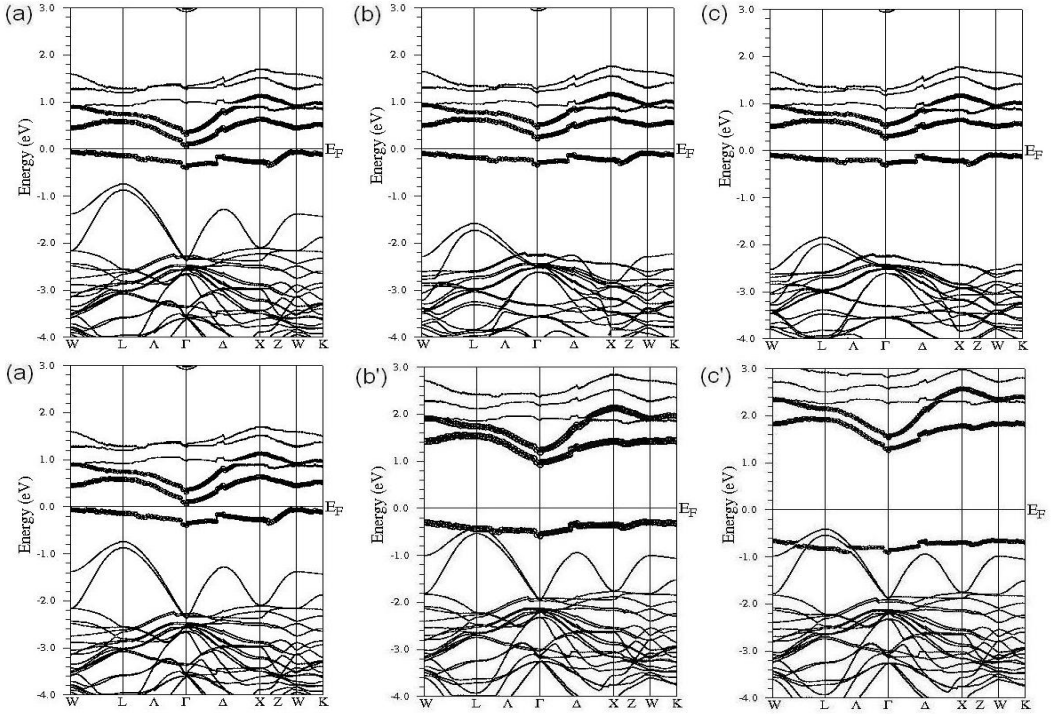

Figure 7.8 Band structure of Ba_2MnReO_6: (a) spin up and (a′) spin down for *GGA* + U_{Mn}(2eV) + *SOC* + U_{Re}(2eV); (b) spin up and (b′) spin down for *GGA* + U_{Mn}(5eV) + *SOC* + U_{Re}(2eV); (c) spin up and (c′) spin down for *GGA* + U_{Mn}(7eV) + *SOC* + U_{Re}(2eV).

7.4 Conclusion

The band structure is computed for Ba_2MnReO_6. In contrast to the previously study,[25] a more reasonable and much smaller Hubbard *U* is exploited on the transitional metals of Mn and Re with taking account of spin-orbit coupling. It is concluded as following:

1) Proper treatment of electron correlations respectively on Mn and Re in conjunction with spin-orbit coupling on Re is able to reproduce the magnetic insulating property of Ba_2MnReO_6;

2) In such a treatment, there exist boundary values for both transitional metals: $U_{Mn} \geq 0.5$ eV and $U_{Re} \geq 2$ eV;

3) In addition to 2), $U_{Mn} + U_{Re} \geq 4$ eV;

4) U_{Mn} and U_{Re} are correlated: changing U_{Mn} also influences Re *d* bands and vice versa;

5) U_{Re} has more effective impact on the size of band gap;

6) Ba_2MnReO_6 is a correlated insulator, since its band gap depends on sum of Hubbard *U* on both transitional metals.

7) References

[1]W. E. Pickett, Phys. Rev. B **57**, 10613 (1998).

[2]R. E. Rudd, W. E. Pickett, Phys. Rev. B **57**, 557 (1998).

[3]H. Q. Yin, J. S. Zhou, J. P. Zhou, R. Dass, J. T. McDevitt, J. B. Goodenough, Appl. Phys. Lett. **75**, 2812 (1999).

[4]K. I. Kobayashi, T. Kimura, H. Sawada, K. Terakura, Y. Tokura, Nature **395**, 677 (1998).

[5]K. I. Kobayashi, T. Kimura, Y. Tomioka, H. Sawada, K. Terakura, Y. Tokura, Phys. Rev. B **59**, 11159 (1999).

[6]R. A. de Groot, F. M. Mueller, P. G. v. Engen, K. H. J. Buschow, Phys. Rev. Lett. **50**, 2024 (1983).

[7]T. K. Mandal, C. Felser, M. Greenblatt, J. Kubler, Phys. Rev. B **78**, 134431 (2008).

[8]J. J. Attema, G. A. de Wijs, G. R. Blake, R. A. de Groot, J. Am. Chem. Soc. **127**, 16325 (2005).

[9]J. Winterlik, G. H. Fecher, C. Felser, C. Muhle, M. Jansen, J. Am. Chem. Soc. **129**, 6990 (2007).

[10]R. Vidya, P. Ravindran, H. Fjellvåg, A. Kjekshus, O. Eriksson, Phys. Rev. Lett. **91**, 186404 (2003).

[11]H. Wu, M. W. Haverkort, Z. Hu, D. I. Khomskii, L. H. Tjeng, Phys. Rev. Lett. **95**, 186401 (2005).

[12]K. W. Lee, W. E. Pickett, EPL (Europhysics Letters) **80**, 37008 (2007).

[13]A. W. Sleight, J. F. Weiher, J. Phys. Chem. Solids **33**, 679 (1972).

[14]G. Popov, M. Greenblatt, M. Croft, Phys. Rev. B **67**, 024406 (2003).

[15]B. Fisher, J. Genossar, K. B. Chashka, L. Patlagan, G. M. Reisner, Curr. Appl. Phys. **7**, 151 (2007).

[16]B. Fisher, J. Genossar, K. B. Chashka, A. Knizhnik, L. Patlagan, G. M. Reisner, J. Appl. Phys. **104**, 033716 (2008).

[17]P. Blaha, K. Schwartz, G. K. H. Madsen, D. Kvasnicka, J. Luitz, *Wien2K,An Augmented Plane Wave+Local Orbitals Program for Calculating Crystal Properties* ((Techn. Universität Wien, Austria,2001).

[18]J. P. Perdew, K. Burke, M. Ernzerhof, Phys. Rev. Lett. **77**, 3865 (1996).

[19]V. I. Anisimov, J. Zaanen, O. K. Andersen, Phys. Rev. B **44**, 943 (1991).

[20]A. I. Liechtenstein, V. I. Anisimov, J. Zaanen, Phys. Rev. B **52**, R5467 (1995).

[21]H. J. Xiang, M. H. Whangbo, Phys. Rev. B **75**, 052407 (2007).

[22]M. Sikora, C. Kapusta, M. Borowiec, C. J. Oates, V. Prochazka, D. Rybicki, D. Zajac, J. M. De Teresa, C. Marquina, M. R. Ibarra, Appl. Phys. Lett. **89**, 062509 (2006).

[23]C. Azimonte, J. C. Cezar, E. Granado, Q. Huang, J. W. Lynn, J. C. P. Campoy, J. Gopalakrishnan, K. Ramesha, Phys. Rev. Lett. **98**, 017204 (2007).

[24]D. Serrate, J.Phys.:Condense.Matter **19**, 023201 (2007).

[25]J. Cheng, Z. Q. Yang, Phys. Stat. Sol. (b) **243**, 1151 (2006).

[26]J. Zaanen, G. A. Sawatzky, J. W. Allen, Phys. Rev. Lett. **55**, 418 (1985)

8 Conclusion

Oxides of double perovskite type, $A_2MM'O_6$ (A = divalent cation or rare earth, *M*/*M*′ = transition metal), were investigated experimentally and theoretically based on parent compound, Sr_2FeReO_6. Cation-substitutions were performed at *M* or *M*′ sites, respectively. Some electronic structure studies were performed to predict or rationalize physical properties of some double perovskites.

Substitutions of Re in Sr_2FeReO_6 were carried out with Ga and Fe respectively, forming solid solutions $Sr_2FeRe_{1-x}M'_xO_6$ (*M*′ = Ga/Fe, $0 \leq x \leq 0.5$). In $Sr_2FeRe_{1-x}Ga_xO_6$, the parent compound, Sr_2FeReO_6, (x = 0) is ordered, a perfect double perovskite. Whereas, the solid solution immediately starts to be disordered upon substitution with Ga, and the disorder becomes severe with substitution increasing. Ga^{3+} is intermediate in size between Fe^{3+} and Re^{5+}. This effect catalytically causes re-distribution of cations over the *M*/*M*′ sites, eventually leading to a high disorder system in $Sr_2FeRe_{1-x}Ga_xO_6$. Generally, the *M* site is favourite for Fe, and the *M*′ site favourite for Re. Ga prefers to occupy the *M* site at low level substitution, but Ga is forced to enter the *M*′ sites above x = 0.4 due to the inter-charge repulsion pressure, making the *M*′ site become slight more favourite for Ga. Along with the striking anti-site disorder, a magnetic transition takes place from a ferro/ferrimagnetic ordering to an antiferromagnetic ordering. Mössbauer spectra suggest that the valence of Fe increases from the initial 2.7+ to 3+ and remains stable. And then, Re becomes the redox buffer to compensate the charge deficiency of cations due to hole-doping effect.

An electron-doping on the *M*′ sites was implemented in $Sr_2FeRe_{1-x}Fe_xO_6$. The series of compounds undergo a structural transition from the ordered parent phase (x = 0) to the disordered phases upon increasing degree of substitution. This situation is similar to that observed in $Sr_2FeRe_{1-x}Ga_xO_6$. Fe-substituted solid solutions undergo magnetic transitions from ferro/ferri-magnetic to antiferromagnetic ordering, suggesting an increased amount of Fe–O–Fe units introduced by Fe-substitution. Another substitution effect is that the solid solutions are transformed from an initial (half-) metal (x = 0) to semiconductors ($x \geq 0.1$). Mössbauer spectroscopy confirms the anti-site disorder and indicates, a similar result to that of $Sr_2FeRe_{1-x}Ga_xO_6$, i.e., the oxidation state of Fe increases gradually from 2.7+ to 3+, and then remains constant while Re acts as a valence buffer. In addition, both Ga-substitution and Fe-

substitution lead to an electrical transport change from an initial metal (x = 0) to a semiconductor upon substitution (x = 0.1).

Replacing Fe in Sr_2FeReO_6 with main group IIIA cations leads to entirely different effects. In^{3+} is larger than Ga^{3+} (in similar size to Fe^{3+}). Hence, Sr_2InReO_6 is ordered but crystallizes in monoclinic structure (cryolite type, $P2_1/n$). Double exchange path, Fe–O–Re–O–Fe in Sr_2FeReO_6, is accordingly changed to In–O–Re–O–In in Sr_2InReO_6. Thus, the close-shelled In^{3+} completely blocks the electron itinerancy between *M* and *M′* sites. As a result, Sr_2InReO_6 is characterized as a Mott insulator. Magnetometry indicates that there exists an antiferromagnetic ordering in Sr_2InReO_6 and two electrons on Re^{5+} in Sr_2InReO_6 are unpaired and localized. Due to the *fcc* geometrical arrangement of Re^{5+} in Sr_2InReO_6, the long-range magnetic ordering is broken and the electron spins are subject to frustration. Another interesting finding is that the effect of tilted octahedra in double perovskite compounds plays important role in structural determination. This effect is hard to discern, so that some of analogous double perovskites oxides used to be readily solved in a structure with a high symmetry. In addition, this effect influences band structure calculation. A structure rectified with taking account of the tilted octahedra immediately gives rise to a Mott insulating state without any complex treatments for Sr_2InReO_6. Whereas, the high symmetry structural solution without taking account of this effect always leads to a half-metal state.

In contrast to the ordered and insulating Sr_2InReO_6, Sr_2GaReO_6 exhibits a very high anti-site Ga/Re disorder (40%) arising from a small size difference between Ga^{3+} and Re^{5+}. Interestingly, the anti-site disorder however triggers conductivity in Sr_2GaReO_6. The disorder breaks down the blocking effect in Sr_2InReO_6 and makes electron locally hopping in a pathway like Re–O–Re–O–Re. Magnetometry reveals an antiferromagnetic ordering and a spin-frustration in Sr_2GaReO_6, and the frustration is thought to arise from the ordered remnant of Ga–O–Re–O–Re.

The previous study indicated that a special type of double perovskite oxides tended to be mis-predicted as half-metals. These materials are virtually either semiconductors or insulators. It turns out to be a challenge to predict these materials as a half metal (or not). Typically, these materials have a general formula of A_2CMO_6, where A stands for the alkali earth metals, *C* for closed shell elements and *M* for 4*d*/5*d* transition elements. These materials usually have a high symmetry and contain heavy transition metals with *d/f* orbital partially filled. The heavy metal atoms are structurally isolated by closed shell metals, making an (almost) *fcc* configuration. *GGA* method,

GGA plus Hubbard potential *U*, and *GGA* + *SOC* (spin orbit coupling) all fail to realize the insulating/semiconducting state for these materials. However, the insulating/semiconducting state can be reproduced, when the cooperative effect of electron correlation and spin-orbit coupling is applied. Therefore, *GGA* + *SOC* + *U* can be taken as one of general approaches to test or to reproduce the band structures of some materials of this type.

Some double perovskites contain both transition metals at *M*/*M′* sites, e.g. Ba_2MnReO_6. These materials were also experimentally characterized to be insulators/semiconductors. However, the insulating/semiconducting state of these materials is hardly reproduced using *GGA*, *GGA* + *U*, and *GGA* + *SOC*. The treatment for Ba_2MnReO_6 is in contrast to A_2CMO_6, where just an application of *SOC* and *U* on heavy transition metals is able to open a band gap. For Ba_2MnReO_6, Hubbard *U* needs to be applied on both transition metals (Mn and Re) in addition to *SOC* on the heavy metal Re. The band gap of Ba_2MnReO_6 is dependent on sum of *U* applied on both transition metals, and there exists a limit of the sum of $U_{Mn} + U_{Re}$ to open a band gap, meaning that if the U_{sum} is small, the band gap cannot be open. In this sense, Ba_2MnReO_6 is a correlated insulator.

As a conclusive summary, this PhD work presents:

(1) For the parent compound, Sr_2FeReO_6, two 5*d* electrons on Re is inherently unpaired and localized. These two 5*d* electrons become itinerant due to magnetic induction by adjacent Fe neighbours through double exchange mechanism, giving rise to a half metal state in Sr_2FeReO_6.

(2) When the original double exchange path is completely blocked, a spin frustration takes place and an insulating state is produced, e.g. in ordered Sr_2InReO_6.

(3) When the electron hopping path is just partially blocked, e.g. in highly disordered Sr_2GaReO_6, a partial and local spin frustration is retained, and the electron hopping persists, leading to a significant conductivity for Sr_2GaReO_6 compared to that of Sr_2InReO_6.

(4) The effect of tilted octahedra in double perovskite oxides is always readily neglected but plays a subtle and important role in structural determinations. Accordingly, the correctly solved crystal structure leads to a reasonable band structure without any special and complex treatments.

(5) The *M*–*M′* ordering, a prerequisite to form ordered double perovskites ($A_2MM'O_6$), can be broken by introducing an intermediate cation, e.g. Ga with an intermediate size between that of

Fe and of Re in $Sr_2FeRe_{1-x}Ga_xO_6$. As a result, the order-breaking leads to a statistical cations-redistribution over the *M/M′* sites.

(6) Electron-doping does not work to improve the half metallic properties, e.g. like in $Sr_2FeRe_{1-x}Fe_xO_6$. This supports the previous study. Electron-doping induced by substitution of Re with Fe produces an insulating/semiconducting state and deteriorates magnetic properties. In addition, the solid solutions undergo magnetic transitions from original ferro/ferrimagnetism to antiferromagnetism. Fe and Re alternately serve as redox buffers. The redox buffer is Fe at low level substitution, and is Re at high level substitution.

(7) The cooperative effect of electron correlation and spin-orbit coupling (*SOC* + *U*) can be taken as a general approach to compute a reasonable band structure for "pseudo-half-metal" double perovskite containing heavy transition metals with partially filled *d/f* orbital.

(8) For the insulating double perovskites, e.g. Ba_2MnReO_6, containing transition metals on both *M* and *M′* sites, the combination of Hubbard *U* on *M* (light transition metal) and *SOC* + *U* on *M′* (heavy transition metal with unfilled *d* orbitals) is able to open the band gap. And the band gap of the material is correlated to the sum of U_M and $U_{M'}$.

(9) This PhD work suggests that it is necessary to re-test the band structures of the current half metals candidates of double perovskites. The effect of spin orbit coupling on heavy metals e.g. on Re in Sr_2FeReO_6, is not neglectable to rationalize physical properties and to perform band structure calculations.

9 List of figures

10 List of tables